論文 / 著書情報
Article / Book Information

題目(和文)	
Title(English)	Control of Microdroplet Deformation and Dispersion in The Non-Isothermal Field by Laser Heating
著者(和文)	Mu'minGea Fardias
Author(English)	Gea Fardias Mumin
出典(和文)	学位:博士（工学）, 学位授与機関:東京工業大学, 報告番号:甲第12072号, 授与年月日:2021年9月24日, 学位の種別:課程博士, 審査員:齊藤 卓志,花村 克悟,野﨑 智洋,伏信 一慶,田中 智久,西迫 貴志
Citation(English)	Degree:Doctor (Engineering), Conferring organization: Tokyo Institute of Technology, Report number:甲第12072号, Conferred date:2021/9/24, Degree Type:Course doctor, Examiner:,,,,,
学位種別(和文)	博士論文
Type(English)	Doctoral Thesis

Control of Microdroplet Deformation and Dispersion in The Non-Isothermal Field by Laser Heating

A DISSERTATION

SUBMITTED TO THE FACULTY OF SCHOOL OF ENGINEERING,

GRADUATE MAJOR OF MECHANICAL ENGINEERING

OF TOKYO INSTITUTE OF TECHNOLOGY

BY

Gea Fardias Mu'min

IN PARTIAL FULFILLMENT OF THE REQUIREMENTS
FOR THE DEGREE OF
DOCTOR OF ENGINEERING

Supervisor:

Associate Professor Takushi Saito

March 2021

Acknowledgment

I would like to express my sincere gratitude to my academic supervisor Assoc. Prof. Takushi Saito, for his genuine encouragement, advice, supervision, and guidance during my research years. I also would like to thank Asst. Prof. Tatsuya Kawaguchi for his valuable discussion and suggestion for this research work.

This work would not be possible without the financial support from The Ministry of Finance of The Republic of Indonesia for allowing me the opportunity to pursue the doctoral degree through The Indonesia Endowment Fund for Education (LPDP). I am very grateful and honored to be one of the selected few for the scholarship.

I express my greatest appreciation to my fellow Indonesian students at Tokyo Institute of Technology for giving numerous help and life support to my family and me during my study period.

For my wife, Windy Iriana, whom herself was also a doctoral student while still being a mother to our wonderful son and daughter. Without her endless love, support, patience, and sacrifice, I would never be reached this point. Finally, I want to give my thanks and gratitude to my parents and dedicated this work to my late father, Zaenal Alimin, the man with the big heart who never hesitate to put the interest of other way above his own.

Tokyo, March 2021

Gea Fardias Mu'min

Table of Contents

List of Figure

List of Table

1. Chapter 1: Introduction

1.1. Immiscible Blend

Many engineering or industrial process involves a fluid system that constitutes of different components. Common examples of such a fluid system and its application are emulsions in food processing, cosmetics, agrochemical, and polymer blends **[1]**. Specifically, in polymer processing, mixing different polymer substance types is widely implemented due to its simplicity, versatility, and economic benefit compared to the actual material synthesizing **[2-4]**. However, mixing different substances into a blended system must consider the components type, concentration, and interfacial feature, for it can fulfill the requirement related to their specific applications.

Interfacial characteristic determines the compatibility aspect between the blend constituent, i.e., affecting each blend component's affinity for it can be thoroughly combined to form a homogenous solution. This interfacial characteristic is quantified physically as the interfacial tension value between the component of the mixed fluid. A mixed fluid system with a high degree of compatibility (i.e., having a very small or negligible interfacial tension) is called a miscible blend; an example of the miscible state is diluting ethanol into water. On the other hand, a blend showing some degree of incompatibility is known as an immiscible blend; an example of the immiscible state is water and oil solution, as illustrated in Figure 1-1.

A certain level of interfacial tension is usually present in many blends. Therefore, many blends are commonly founded in the immiscible state, although the degree of immiscibility will differ depending on the order of the interfacial tension value.

Figure 1-1. Immiscible blend formation by mixing oil into water **[5]**.

1.2. Morphology of Immiscible Fluid

Typical structural morphologies of the immiscible systems are droplets dispersed in a matrix (i.e., emulsion) **[6]**, although fibrillar and co-continuous structures are also possible **[2-4, 8, 9]**, as illustrated in Figure 1-2 **[9]**. This morphology holds a significant role in the application of the immiscible blend. For example, in the case of polymer, the droplet phase's dispersion determines the final properties of the blended polymer materials **[10,11]**. Whereas in the case of food processing, a fine dispersion of flavor oil in beverage products is employed as a controlled release of flavor **[12]**. An additional process in the form of flow or stirring may be involved in processing the immiscible fluids. This applied flow or stirring can affect or change the morphology of the immiscible blend. Therefore, a careful arrangement should be in place for the resulting morphology can fulfill their specific applications.

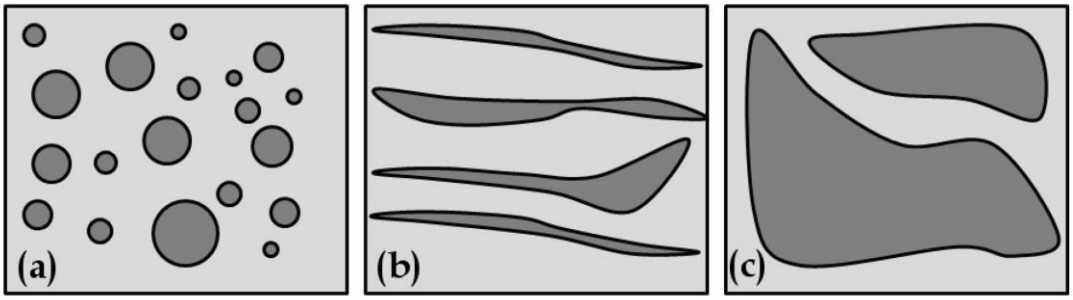

Figure 1-2. Morphologies in immiscible blends (a) droplet dispersed in matrix (b) elongated fibrils (c) co-continuous structure **[9]**.

The investigation of the morphological evolution of the immiscible blend, in the form of droplet emulsion and subjected to shear flow, is initially started by Taylor **[13-14]**. However, the groundwork of droplet deformation by Taylor was restricted only to small deformation on Newtonian fluids. Today, the general understanding of morphological evolution in simple blends and shear flow has been relatively well established and understood. The microstructural changes in blend morphologies include droplet deformation and breakup, droplet coalescence, and droplet retraction **[7]**. Relevant theoretical and experimental work in morphological evolution in simple blends and shear flow is well summarized **[15-17]**.

Two dimensionless parameters mainly describe the morphological evolution for the immiscible blend: viscosity ratio (p) and capillary numbers (Ca). Viscosity ratio defines the ratio of viscosity between droplet (η_d) and matrix phase (η_m) of the blend. Whereas Ca is defined as the ratio between the hydrodynamic and interfacial stresses when the blend is subjected to flow. The following equations express the viscosity ratio and the capillary number:

$$p = \frac{\eta_d}{\eta_m} \tag{1-1}$$

$$\mathrm{Ca} = \frac{\eta_m \dot{\gamma} R}{\sigma} \tag{1-2}$$

Hydrodynamics stress in capillary numbers is the result of the matrix viscosity (η_m) at the applied shear rate ($\dot{\gamma}$). While interfacial stress (σ/R) representation is obtained from the interfacial tension (σ) between the droplet and matrix phase at the corresponding droplet radius (R). When the immiscible blend is subjected to flow, the droplet phase will be experiencing some degree of deformation due to the hydrodynamic stresses. The degree of deformation from hydrodynamic stresses is affected by the blend viscosity ratio and the restoring interfacial forces countering the hydrodynamic stresses indicated by the capillary number.

Guido and Villone conducted an experimental investigation and three-dimensional visualization of the droplet deformation mechanism under simple shear flow **[18]**. The experimental results of Guide and Vilone are in good agreement with numerical simulations from Uijtewal and Nijhof **[19]**. The results were also consistent with Taylor's theory of deformation at a small value of the capillary number.

The applied external flow to the mixing process, however, is not only affecting the droplet deformation. When the applied flow is strong enough (i.e., resulting in a high capillary number), the applied flow may eventually lead to the droplet breakup. However, the droplet phase's breakup only occurs if the capillary number (Ca) exceeds a specific limiting value, known as the critical capillary number (Ca_c). Additionally, there is a maximum value of viscosity ratio *p,* where the shear flow cannot cause any breakup regardless of the degree of applied shear rate or Ca **[20].** Grace had provided a systematical relation between Ca_c and *p* **[21]**, as shown in Figure 1-3. From the figure, the Ca_c requirement is known at a minimum when the *p* value is in the region near one.

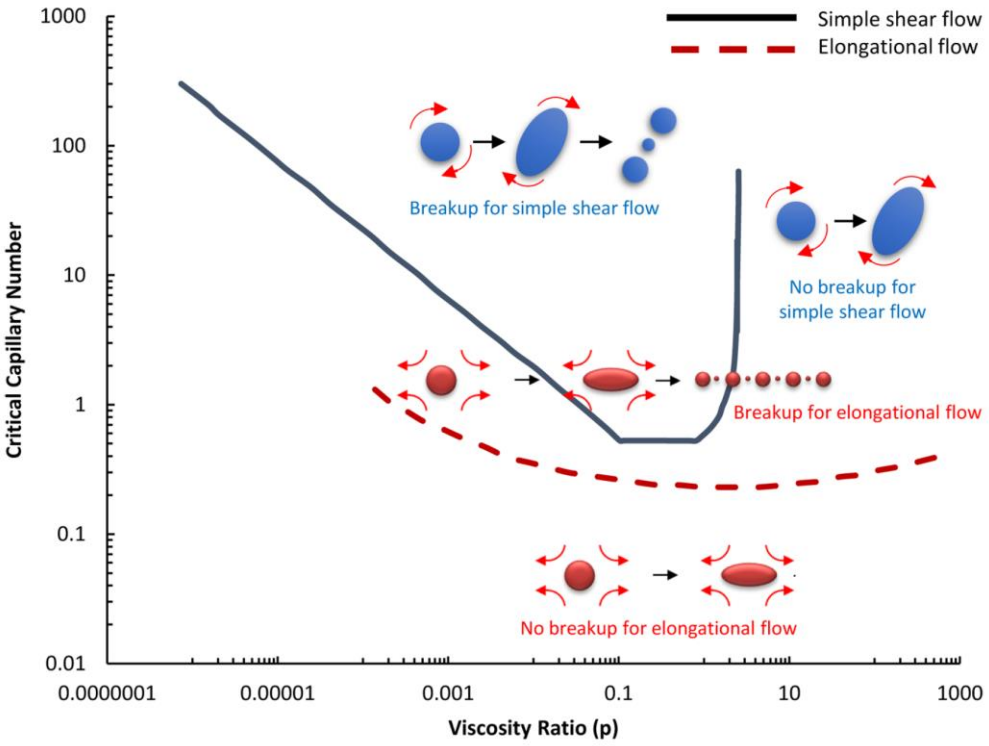

Figure 1-3. Schematic of droplet deformation for simple shear and elongational flow as a function of the capillary number and viscosity ratio from Mehrabian et al. **[22]** adapted from data by Grace **[21].**

The mechanism of droplet breakup can follow several different modes. The breakup process is delayed if a relatively fast flow is given to the biphasic fluid systems. However, if the capillary number is adequately large, the droplet will break into multiple smaller droplets after initially extended into a long thread **[7]**. Mighri and Huneault investigated the visualization of droplet dispersion and its mechanism at different viscosity ratios **[23]**. Furthermore, the numerical analyses for a more complex system of long filament structure are investigated by Tjahjadi et al. **[24]** and Janssen and Meijer **[25]**.

While the morphology in the form of the microdroplet suspended in a matrix fluid is considered the most optimal form, preserving such a morphology during processing can be

difficult for a particular blend system as thermodynamic stability drives the droplets to coalesce **[7]**. An additional stabilizing agent can then be introduced to maintain or promote a better level of dispersion in the blend **[26]**. The agent, also commonly known as surfactant, works by reduces interfacial tension between the blend component.

An example of a stabilizing agent can be found in the field of polymer processing. The additional agent for the polymer blend application, commonly called compatibilizer, is usually a block copolymer placed in the polymer blend constituent interface. The compatibilizer has two compatible arms, one arm compatibles with the dispersed phase and the other compatibles with the matrix phase. A reactive polymer can also be added to the blend components to form an in-situ block copolymer during melt blending **[27,28]**. The former process is known as physical compatibilization, while the latter is defined as chemical compatibilization.

The addition of a dispersing agent, however, affects the droplet deformation and breakup. The presence of compatibilizer material in the interface is causing a complex condition that could no longer be defined by merely interfacial tension **[7, 29]**. Additionally, the dispersing agent can only start to work once the dispersed phase is on a microscale **[3]**. It is also reported that the effect of the dispersing agent diminishes sharply along with the increase of the viscosity ratio **[30]**.

1.3. Advancement in Science and Application of Immiscible System

It was mentioned that an immiscible blend with microdroplet structure could be found in many engineering applications, with polymer blending as the most common example. Meanwhile, in the recent decade, interest in microfluid systems has driven development for building a laboratory in a chip **[31]**. The selection of multicomponent fluids in such a system, especially in chemical or bio-chemical technology, is not uncommon **[32]**. The multiphase droplet-matrix flow

in the microsystem is implemented in micro-encapsulation, micro-mixing, and micro-reaction **[33]**. Therefore, the advancement of knowledge in the science of immiscible droplet-matrix systems is necessary for both bulk and microsystem applications.

For accommodating the vast range application of the immiscible microdroplet blend, the research of such system has expanded to include the effect of compatibilization for droplet deformation and coalescence **[34]**, the effect of elongational flow on Newtonian and viscoelastic immiscible blend **[35]**, the behavior of viscoelastic droplet in a Newtonian matrix **[36]**. Investigation in confined shear flow is summarized by Van Puyvelde et al. **[37]**, while the study from the combination of both compatibilization and viscoelasticity effect in confined geometry is discussed by Cardinaels et al. **[38]**.

1.4. Selective Heating by Laser Irradiation

However, the aforementioned fundamental and expanded work in droplet deformation under shear flows is only considered the isothermal temperature condition of the immiscible blend constituent. The thought for realizing a non-uniform temperature comes from the fact that viscosity is a temperature-dependent property. If each component's temperature could be modified independently, it opens the possibility to customize the blend's viscosity ratio into a targeted desirable range. One way to realize a non-uniform temperature field in the immiscible microdroplet system is by exploiting the difference in heat absorption for the droplet and matrix components. The viscosity ratio then will change proportionally according to the temperature distribution (Figure 1-4 (a)). Laser irradiation is proposed as the external heat source for realizing such a non-uniform temperature field (Figure 1-4 (b)).

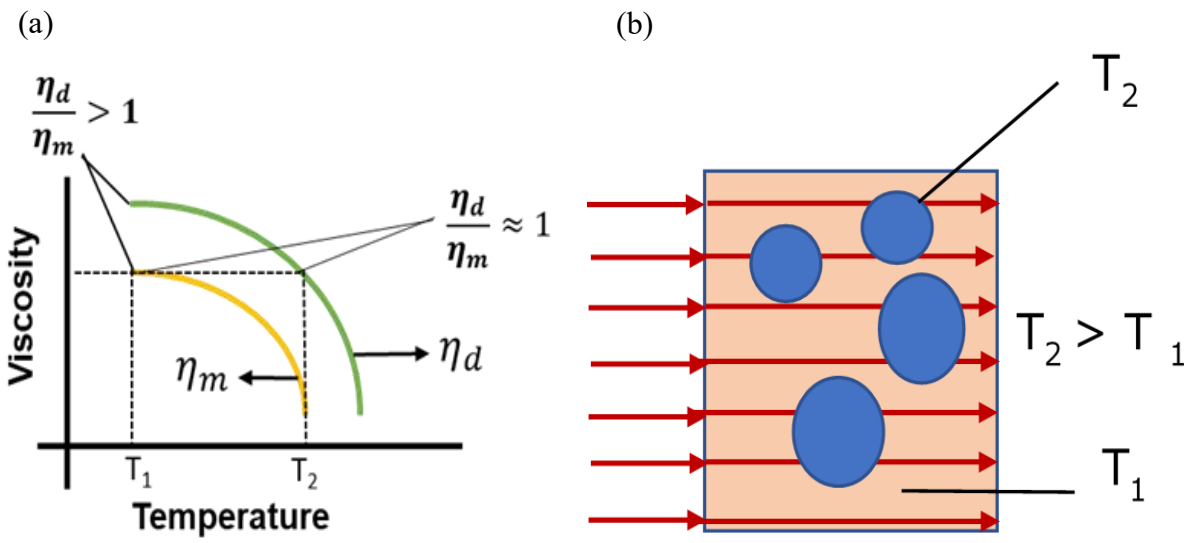

Figure 1-4. (a) Viscosity ratio adjustment between droplet phase and matrix due to non-homogenous temperature field in the immiscible blend system, (b) Forming of a non-homogenous field in blend system by heat irradiation from an external source, with T_1 represents the temperature of the matrix phase and T_2 the temperature of droplet phase in the immiscible blend.

A general concept of selective radiation heating is shown in Figure 1-5. The proposed method of selective heating method is highly beneficial as it will be able to improve and modify the degree of droplet dispersion by employing viscosity modification without the need to change the molecular weight of the blend component. Moreover, the droplet dispersion modification is independently achieved from outside the system, unlike the conventional method involving an additional substance that controls the droplet in-situ, thus requiring a specific and complicated arrangement of the blend and its dispersing agent.

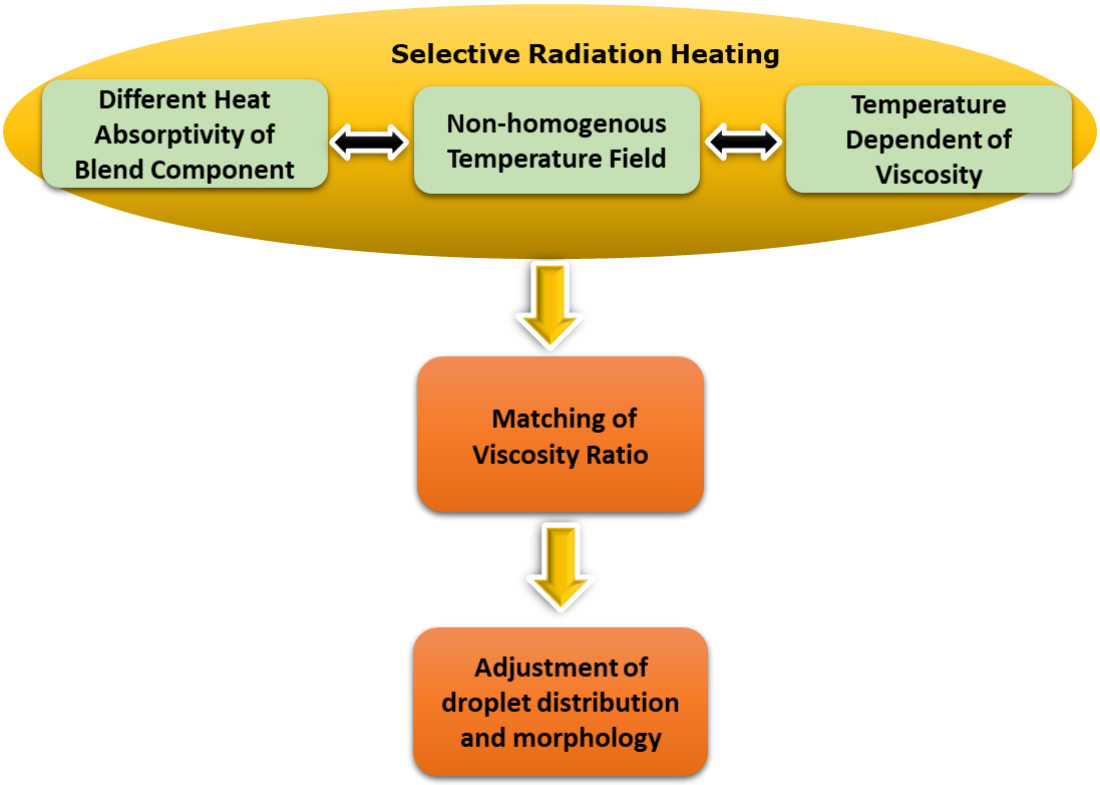

Figure 1-5. Schematic of selective radiation heating on dispersion control of droplet in the immiscible blend.

Saito et al. **[39]** had initiated an investigation of selective radiation heating for achieving dispersion control on polymer blends. The selected polymer blend was Polyethylene (PE) as the droplet phase and Polystyrene (PS) as the matrix phase. The PE droplet phase was added by carbon black to enhance its heat absorption. The polymer blend was extruded into a small channel with a 4 mm dimension in width and 2 mm in depth, Nd:YAG laser at 1.06 μm was used as a radiation energy source. The extruded samples were then observed under the Scanning Electron Microscope (SEM). This initial work showed that the distribution of droplet size was improved after radiation heating was applied, as shown in Figure 1-6. Based on this initial work, the proposed selective radiation technique showed promising potential as a method to enhance droplet dispersion in an immiscible blend.

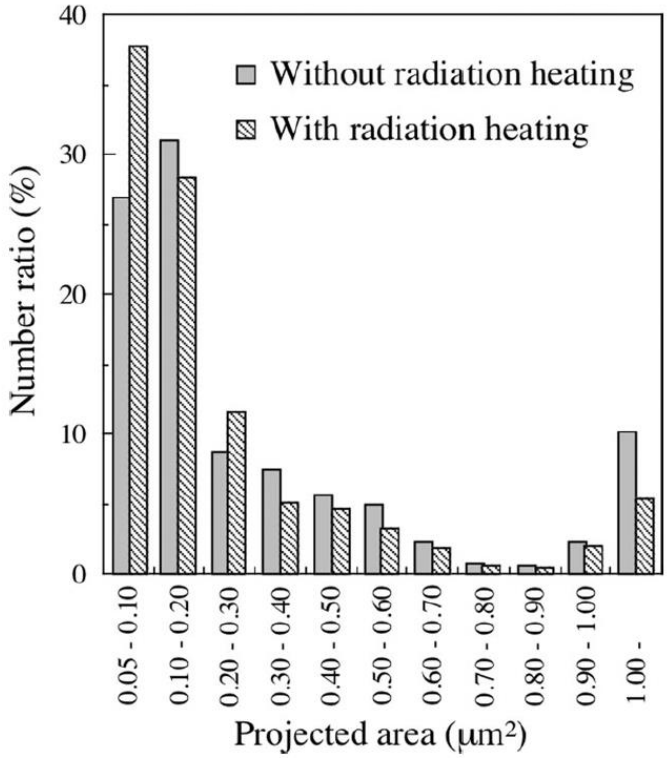

Figure 1-6. Laser irradiation effect on the diameter distribution of the dispersed droplet phase **[39]**.

However, the analysis approach of the mentioned initial work was limited only to describe the final droplet condition under radiation heating and droplet dispersion without selective radiation heating. The discussion for the morphological changes during the selective radiation process was still absent. The knowledge of the morphological changes on the non-homogenous temperature of immiscible emulsion systems is essential for thoroughly understanding the selective radiation heating technique. The comprehensive discussion can also lead to the possibility for the expansion of selective heating techniques to other micro-fluid or biochemical systems, not limited only to the polymer mixing process.

1.5.Scope and Objective

This study aims to conduct a systematic investigation on the droplet morphology in an immiscible system under the selective radiation method as a means to control droplet dispersion. This work is expected to provide an experimental visualization of droplet evolution under the selective heating process. Furthermore, this study also discusses the relevant parameter in the mechanism of droplet deformation and dispersion in non-homogenous temperatures from selective heating. The flow, however, is limited only to simple shear flow, and the droplet-matrix system representing the immiscible blend is considered to show the properties of the Newtonian fluid system at the selected range of shear flow. The simple shear flow is emulated by using a concentric counter-rotating transparent Couette-cylinder device. The detailed arrangement of the Couette-cylinder device will be provided later in Chapter 3.

Furthermore, a numerical simulation to estimate the temperature distribution due to the selective radiation heating will also be carried out. The estimated temperature is then used as a basis to predict the viscosity ratio modification as reflected in the droplet deformation in the experimental work.

1.6.Outline of this Thesis

The structure of this thesis is divided into five chapters, which are:

1. Chapter 1 introduces the concept of immiscibility, immiscible blend, and morphology, including their relevant parameters. The concept of the selective radiation method to control droplet dispersion is also introduced in this chapter.
2. Chapter 2 describes the viscosity ratio tuning for the droplet system by implementing selective radiation heating. This chapter will discuss the feasibility and mechanism of

viscosity adjustment by exploiting temperature dependence. This part will then use the background stage and give a quantitative prediction on viscosity ratio adjustment from a non-homogeneous temperature field. Part of this chapter has been presented at *the 12th Pacific Symposium on Flow Visualization and Image Processing, 19th – 22nd November 2019, New Taipei City, Taiwan*.

3. Chapter 3 provides a comparative discussion for the evolution of droplet morphology in both homogenous and non-homogenous temperature fields from selective radiation methods. The discussion is then extended to discuss droplet deformation in a fluid system with a non-homogeneous temperature field. Part of this chapter is published as *G. F. Mu'min, T. Kawaguchi, and T. Saito, "Study on droplet deformation of an immiscible fluid system by selective radiation heat using infrared laser," Polymer Engineering and Science, 61, 1232 (2021). DOI 10.1002/pen.25674*.
4. Chapter 4 highlight the breakup of the dispersed phase by selective radiation. The discussion starts from the numerical approach of the non-isothermal temperature distribution realized from the selective radiation method. Relevant discussion about the estimation of the modified viscosity ratio, the formation of the critical capillary number, and droplet breakup will be covered in this chapter. The proposed application of selective radiation heating in an immiscible system is also briefly provided. Part of this chapter is published as *G. F. Mu'min, T. Kawaguchi, and T. Saito, "Droplet breakup of a high-viscosity-ratio system in non-uniform temperature field under laser irradiation," Physics of Fluids, 33, 073108 (2021). DOI:10.1063/5.0055235.*
5. Chapter 5 is the conclusive summary and recommendation for future works.

1.7. References

1. Tadros, T. F., "Fundamental Principles of Emulsion Rheology and Their Applications," Colloids and Surfaces A: Physicochemical and Engineering Aspects, 91, 39 (1994).
2. Utracki, L.A., "Commercial Polymer Blends," Chapman and Hall, London (1998).
3. Utracki, L.A., "Polymer Blends Handbook," Kluwer Academic, Dordecht (2003).
4. Utracki, L.A., "Polymer Alloys and Blends: Thermodynamics and Rheology," Hanser Publisher, Munich/New York (1989).
5. https://www.shutterstock.com/image-photo/physics-immiscible-fluids-oil-being-poured-689465653 (accessed December 2020).
6. Muratoglu, O.K., Argon, A.S., Cohen, R.E., and Weinberg, M., "Toughening Mechanism of Rubber-Modified Polyamides," Polymer, 36, 921 (1995).
7. Van Puyvelde, P. and Moldenaers, P., "Rheology and Morphology Development in Immiscible Polymer Blends," Rheology Reviews, The British Society of Rheology, 101, (2005).
8. Pötschke, P. and Paul, D.R., "Formation of Co-Continuous Structure in Melt Mixed Immiscible Polymer Blends.," Journal of Macromolecule Science Part C: Polymer Review, 43, 87 (2003).
9. Grosso, M. and Maffettone, P.L., "Fourier Transform Rheology: A New Tool to Characterize Material Properties, Fourier Transforms – New Analytical Approaches and FTIR Strategies, Goran Nikolic (Ed.)," Intech, Rijeka (2011).
10. Mouzakis, D., Papke, N., Wu, J.S., and Karger-Kocsis, J., "Fracture Toughness Assessment of Poly(ethylene terephthalate) Blends with Glycidyl Methacrylate Modified Polyolefin Elastomer Using Essential Work of Fracture Method," Journal of Polymer Sciences, 79, 842 (2001).

11. Sivaraman, P., Chandrasekhar, L, Mishra, V.S., Chakraborty, B.C., and Varghese, T.O., "Fracture Toughness of Thermoplastic Co-poly(ether ester) Elastomer – Acrylonitrile Butadiene Styrene Terpolymer Blends," Polymer Testing, 25, 562 (2006).
12. Given Jr., P. S., "Encapsulation of Flavors in Emulsions for Beverages" Current Opinion in Colloid and Interface Science, 14, 43 (2009).
13. Taylor, G.I., "The Viscosity of a Fluid Containing Small Drops of Another Fluid," Proceedings of The Royal Society of London. Series A, Containing Papers of Mathematical and Physical Character, 138, 41 (1932).
14. Taylor, G.I., "The Formation of Emulsions in Definable Fields Flow, Proceedings of The Royal Society of London. Series A, Containing Papers of Mathematical and Physical Character," 146, 501 (1934).
15. Tucker III, C.L and Moldenaers, P., "Microstructural Evolution in Polymer Blends," Annual Review of Fluid Mechanics, 34, 177 (2002).
16. Ottino, J.M., DeRoussel, P., Hansen, S., and Khakhar, D.V., "Mixing and Dispersion of Viscous Liquids and Powered Solids," Advances in Chemical Engineering, 25, 105 (1999).
17. Guido, S. and Greco, F., "Dynamics of a Liquid Drop in a Flowing Immiscible Liquid," Rheology Reviews, The British Society of Rheology, 99, (2004).
18. Guido, S. and Villone, M., "Three-Dimensional Shape of a Drop Under Simple Shear Flow," Journal of Rheology, 42, 395 (1998).
19. Uijttewal, W.S.J. and Nijhof, E.J, "The Motion of a Droplet Subjected to Linear Shear Flow Including The Presence of a Plane Wall," Journal of Fluid Mechanics, 302, 45 (1995).

20. Utracki, L. A. and Shi, Z. H., "Development of Polymer Blend Morphology During Compounding in a Twin‐Screw Extruder. Part I: Droplet Dispersion and Coalescence—a review," Polymer Engineering and Science, 32, 1824 (1992).
21. Grace, H.P., "Dispersion Phenomena in High Viscosity Immiscible Fluid Systems and Application of Static Mixers as Dispersion Devices in Such Systems," Chemical Engineering Communication, 14, 225 (1982).
22. Mehrabian, S., Acosta, E., and Bussmann, M., "Oil-Particle Separation in a Falling Sphere Configuration: Effect of Oil Film Thickness," Energy & Fuels, 30, 8776 (2016).
23. Mighri, F. and Huneault, M.A., "Dispersion Visualization of Model Fluids in a Transparent Couette Flow Cell," Journal of Rheology, 45, 783 (2001).
24. Tjahjadi, M., Stone, H.A., and Ottino, J.M., "Satellite and Subsatellite formation in Capillary Breakup," Journal of Fluid Mechanics, 243, 297 (1992).
25. Janssen, J.M.H. and Meijer, H.E.H., "Droplet Breakup Mechanisms: Stepwise Equilibrium Versus Transient Dispersion," Journal of Rheology, 37, 597 (1993).
26. Machado, J.M., and Lee, C.S., "Compatibilization of Immiscible Blends with a Mutually Miscible Third Polymer," Polymer Engineering and Science, 34, 59 (1994).
27. Di Lorenzo, M.L. and Frigione, M., "Compatibilization Criteria and Procedures for Binary Blends: a Review," Journal of Polymer Engineering, 17, 429 (1997).
28. Koning, C., Van Duin, M., Pagnoulle, C., and Jerome, R., "Strategies for Compatibilization of Polymer Blends," Progress in Polymer Science, 23, 707 (1998).

29. Van Puyvelde, P., Velankar, S., and Moldenaers, P., “Rheology and Morphology of Compatibilized Polymer Blends,” Current Opinion in Colloid & Interface Science, 6, 457 (2001).
30. Milliken, W. J., Stone, H. A., and Leal, L. G., “The Effect of Surfactant on The Transient Motion of Newtonian Drops,” Physics of Fluids A: Fluid Dynamics, 5, 69 (1993).
31. Stone, H.A., Stroock, A.D., and Ajdari, A., “Engineering Flows in Small Devices: Microfluidics Toward a Lab-on-a-Chip,” Annual Review of Fluid Mechanics, 36, 381 (2004).
32. Barea, J.S, Lee, J., and Kang, D.-K., “Recent Advances in Droplet-based Microfluidic Technologies for Biochemistry and Molecular Biology,” Micromachines, 10, 412 (2019).
33. Shui, L., Eijkel, J.C.T, and Van den Berg, A., “Multiphase Flow in Microfluidic Systems – Control and Applications of Droplets and Interfaces,” Advances in Colloid and Interface Science, 133, 35 (2007).
34. Van Puyvelde, P., Velankar, S., Mewis, J., and Moldenaers, P., “Effect of Marangoni Stresses on The Deformation and Coalescence in Compatibilized Immiscible Polymer Blends,” Polymer Engineering and Science, 42, 1956 (2002).
35. Delaby, I., Ernst, B., Froelich, D., and Muller, R., “Droplet Deformation in Immiscible Polymer Blends During Transient Uniaxial Elongational Flow,” Polymer Engineering and Sciences, 36, 1627 (1996).
36. Li, H. and Sundararaj, U., “Experimental Investigation of Viscoelastic Drop Deformation in Newtonian Matrix at High Capillary Number Under Simple Shear Flow,” Journal of Non-Newtonian Fluid Mechanics, 165, 1219 (2010).
37. Van Puyvelde, P., Vananroye, A., Cardinaels, R., and Moldenaers, P., “Review on Morphology Develpoment of Immiscible Blends in Confined Shear Flow,” Polymer, 49, 5363 (2008).

38. Cardinaels, R., Vananroye, A., Van Puyvelde, P., and Moldenaers, P., “Breakup Criteria for Confined Droplest: Effects of Compatibilization and Component Viscoelasticity,” Macromolecular Materials and Engineering, 296, 214 (2011).
39. Saito, T., Kawaguchi, T., and Satoh, I., “Dispersion Control of Immiscible Polymer Blend Using Selective Heating by Infrared Laser Irradiation,” Journal of Applied Polymer Science, 129, 3606 (2013).

2. Chapter 2: Investigation of The Thermal Radiation Requirement for Realizing the Viscosity Ratio Modification in Immiscible Fluid System

2.1.Introduction

The proposed method of selective radiation heating is based on the hypothesis that the absorption coefficient differences can be exploited for realizing a nonuniform temperature field of the immiscible droplet-matrix system. Due to the temperature-dependent nature of the viscosity, the nonuniform temperature will then realize a viscosity ratio modification of the immiscible fluid system. Therefore, the temperature dependence of the viscosity and the material's ability to absorb the applied heat radiation of the immiscible fluid system is the fundamental prerequisite condition that needs to be known before the proposed selective radiation can be implemented.

The absorption coefficient value represents the ability to attenuate an incoming light. The absorption coefficient is a material's specific properties, and its value is different from a material to another. Additionally, the absorption coefficient value also varies in a certain range of light wavelengths. For example, a material can highly attenuate an incoming light source at a low wavelength, whereas the light is highly transmitted when a high wavelength light is given, or vice versa. The absorption coefficient is obtained from the Lambert-Beer equation for a semi-transparent medium, as shown below **[1]**:

$$T = \exp(-\beta x) \tag{2-1}$$

In this equation, T is the transmissivity at the specified incident light wavelength, x is the thickness of the material along the incident light's attenuation path, and, finally, β is the absorption

coefficient. Transmissivity can also be defined as the ratio of the outgoing light to the incoming light intensity, passing through the material so that Eq. (2-1) can be expanded into:

$$T = {}^{I}/_{I_0} \tag{2-2}$$

$$I = I_0 \exp(-\beta x) \tag{2-3}$$

where I and I_0 are the light intensity leaving and entering the material, respectively. The attenuation of the incident light according to Eq. (2-3) is illustrated by Figure 2-1.

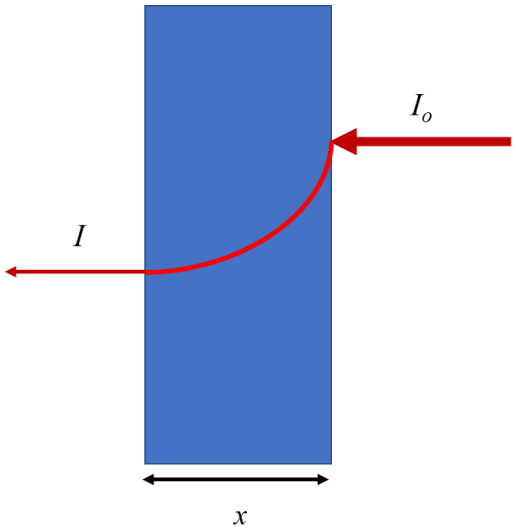

Figure 2-1. Attenuation of incident light on a semitransparent medium.

In the selective radiation heating method, the attenuated light intensity from laser irradiation is considered equal to the heat generation on the immiscible system. Further discussion about the attenuated laser irradiation and the heat absorption and generation for the immiscible fluid system will be provided later in Chapter 4.

In the aspect of the correlation between viscosity and temperature, the well-known theoretical formula for describing the temperature dependence of the viscosity was introduced by Eyring, as shown in the following form **[2,3]**:

$$\eta = \frac{N_A h}{V} \exp\left(\frac{\Delta G}{RT}\right) \tag{2-4}$$

Where η is the fluid's viscosity, N_A is the Avogadro number, h represents the Planck constant, V is the fluid molar volume, ΔG is the molar activation energy, R is the universal gas constant, and finally T is the corresponding temperature of the fluid. In this analytical correlation formula, the viscosity depends on the temperature and the activation energy. The fluid will become less viscous if it has small activation energy or is set at a higher temperature condition.

The Eyring formula assumes that the fluid is an ideal monoatomic fluid, whereas those assumptions are not applicable in the real fluid. The assumption can lead Eyring's theoretical correlation to have a certain degree of inaccuracy if applied to a real fluid. Therefore, a correction for the theoretical correlation for the viscosity and temperature is then proposed as follow **[4]**:

$$\eta = \eta_0 \exp\left(\frac{E}{k(T+T_0)}\right) \tag{2-5}$$

In this formula, E is the activation energy, which is also known as the potential barrier energy, η_o is the initial viscosity, T_0 is a temperature correction parameter, and k is a constant.

However, for most practical applications, the viscosity dependence to temperature is usually obtained by a fitting from a direct empirical measurement rather than the theoretical approach. For example, vegetable oil's viscosity measurement is crucial for implementing such oil into a diesel engine **[5]**. In this application, the suitable temperature needs to be known so that the selected vegetable oil's viscosity is made suitable with the diesel engine requirement. The experimental measurement can be represented in many empirical correlations, with some examples are shown in the following formulas **[5-7]**.

$$\ln(\eta) = A + {}^{B}/_{T} \tag{2-6}$$

$$\ln(\eta) = A + {}^{B}/_{T} + {}^{D}/_{T^2} \tag{2-7}$$

In those formulas, *A*, *B, C,* and D are specific constants from the empirical fitting. Eq. (2-6) can be applied for a more linear temperature correlation, while Eq. (2-7) is more suitable for a broader temperature range involving nonlinearity. A different form of the empirical fitting is also possible, depend on the specific experimental data and condition **[5-22]**. Due to their more simplistic and practical aspect, this chapter's following analysis will also be based on the empirical fitting approach.

2.2.Materials

The used material in this experiment was carefully selected so that any complexities arising from non-Newtonian behavior in the subsequent experimental stage can be eliminated. Polydimethylsiloxane (PDMS) silicone oils (KF-96 series, Shin-Etsu silicone) were chosen as the matrix phase. Meanwhile, polybutenes (> 90% isobutylene, Sigma-Aldrich) were then selected as the dispersed droplet phase as both fluids showed Newtonian behavior at a particular shear rate range **[23,24]**. The combination of polybutenes (or polyisobutylene) and PDMS silicone oil was quite common as a model fluid to investigate the droplet deformation behavior **[23-27].** Table 2-1 summarizes the selected samples' specifications.

Table 2-1. Selected Materials for The Immiscible Fluid System

Designation	Material Formulation [a)]
D-I	100% Polybutenes (υ = 200–235 cSt) [c)]
D-II	100% Polybutenes (υ = 4,000–4,400 cSt) [c)]
M-I	100% PDMS (υ = 5,000 cSt) [b)]
M-II	71.4% PDMS (υ = 5,000 cSt) [b)] + 28.6% PDMS (υ = 0.65 cSt) [b)]
M-III	100% PDMS (υ = 1,000 cSt) [b)]
M-IV	100% PDMS (υ = 10,000 cSt) [b)]

a) Concentrations are on a volume basis.
b) The respective manufacturer provides the kinematic viscosity (υ) values at temperature 25°C.
c) The respective manufacturer provides the kinematic viscosity (υ) values at temperature 100°C.

The viscosity value listed in the table above was used only as an initial guideline provided by the manufacturer. The actual viscosity value at the indicated temperature of 25°C and 100°C will be based on the measurement results.

2.3.Experimental Method

2.3.1. Spectrometry Experiment

The absorption coefficient of all samples was investigated using Shimadzu IRAfinity-1S FTIR and Shimadzu UV-1900i UV-VIS spectrophotometer. The measurements using two types of spectrometer were employed for covering a vast range of the light spectrum. The Fourier Transform Infrared (FTIR) spectrometer was used for measurement at short to mid-infrared (IR) wavelength (1.5 - 8 μm) while the other device was used for ultraviolet (UV), visible light, and near IR wavelength (0.4 – 1.1 μm). The image of spectrometer devices used for the measurement are provided in Figure 2-2.

The spectrometer devices, however, only measure the transmissivity of the tested materials. Therefore, the transmissivity data need to be converted into the absorption coefficient by implementing the Lambert-Beer law principle described earlier.

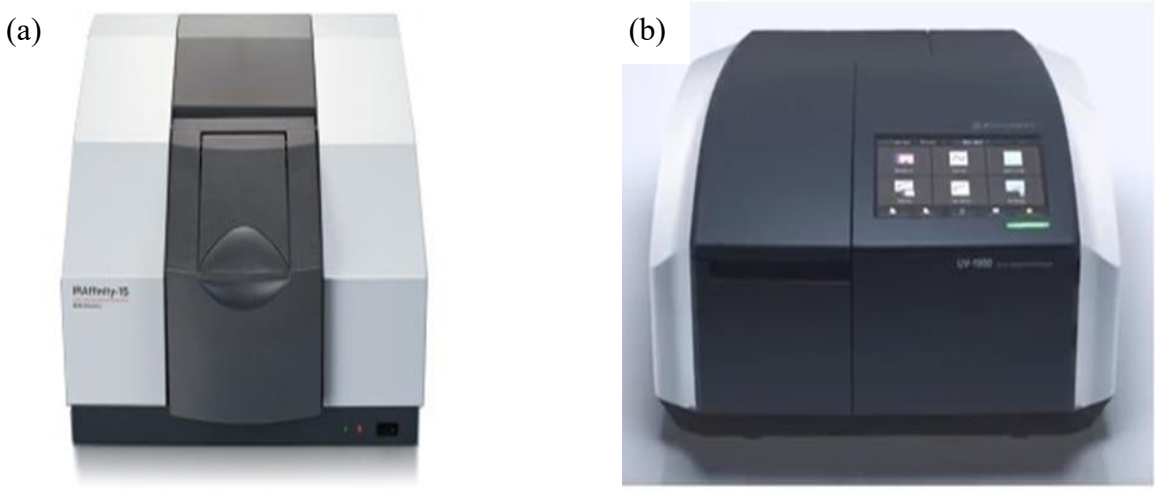

Figure 2-2. The spectrometer device for obtaining the absorption spectrum of the tested material, (a) Shimadzu IRAfinity-1S FTIR and (b) Shimadzu UV-1900i UV-VIS spectrophotometer

The typical samples for the FTIR spectrometer device were either in powdered form or a thin plate. Therefore, the liquid form of all material samples required special handling so the FTIR device can test it. Each sample fluid was put on a small rectangle container with 2 mm in width and 3 mm in length. The container was made at three different thicknesses of 1, 3, and 5 mm. The container was then sandwiched by two plates of transparent CaF_2 glasses (Edmund Optics), having 1 mm in thickness and 30 mm in diameter. The CaF_2 glass was selected as it is able to transmit the incoming light on an extensive range of wavelengths. The thin sample fluid and CaF_2 sandwich were then inserted into the spectrometer test cassette. The schematic of this thin sandwich is presented in Figure 2-3.

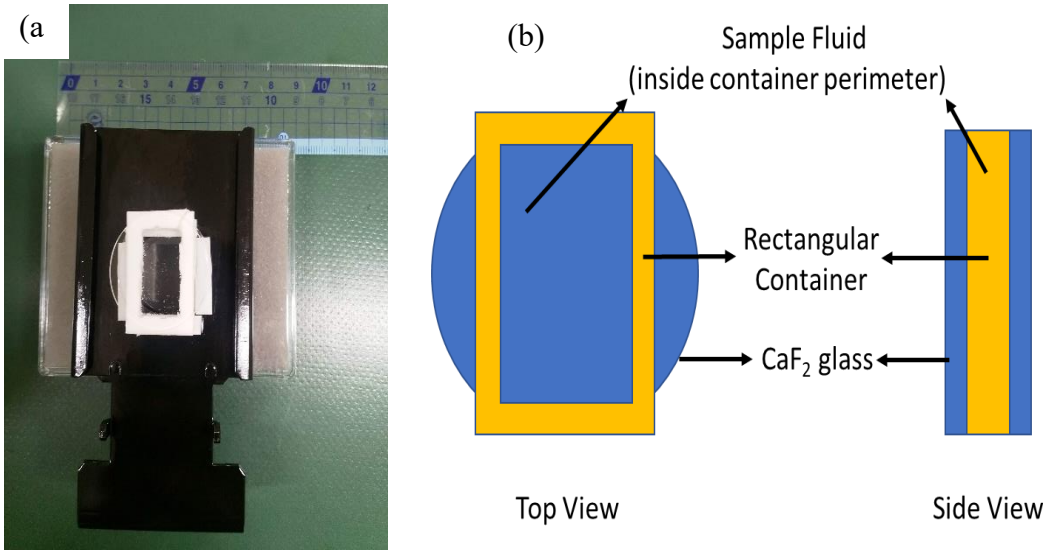

Figure 2-3. Sample preparation for FTIR spectrometer, (a) sample fluid-CaF_2 glass sandwich on the test cassette holder, and (b) schematic of the fluid-CaF_2 glass sandwich

The addition of CaF_2 glasses on the top and bottom side of the materials layer may cause a reflection effect from the glasses to the light source in the spectrometer, which is not accounted for in Eq. (2-1). When the reflectivity effect was considered, the transmissivity equation must be corrected into the following form **[1]**.

$$T = (1 - R)^2 \exp(-\beta x) \tag{2-8}$$

with R is the reflectivity at the corresponding wavelength. For an unknown value of reflectivity, samples' absorption coefficient can be acquired using transmissivity value at two different thicknesses as indicated below **[1]**.

$$T_1/T_2 = \exp\left(\beta(x_1 - x_2)\right) \tag{2-9}$$

The experimental procedure for the second spectrometer was more straightforward than the FTIR spectrometer. The measured fluid was inserted into a test cuvette specifically designed

by the manufacturer to be used in the spectrometer device. The cuvette's width was 10 mm, and the incident test light was attenuated along that length.

2.3.2. Rheometer Experiment

The following fluid properties that need to be known is the temperature dependence of the viscosity. The correlation between temperature and viscosity can be acquired by measuring the tested samples' viscosity value at different temperature conditions and make the empirical fitting from the obtained value, as mentioned earlier in section 2.1. The steady shear viscosity measurement was carried out using Anton-Paar MCR300 rheometer, as shown in Figure 2-4. This rheometer device was also equipped with a heating cell component to perform steady shear measurements at varying temperature ranges. The device was connected to a personal computer (PC) that controls all the set parameters and displays the measurement results.

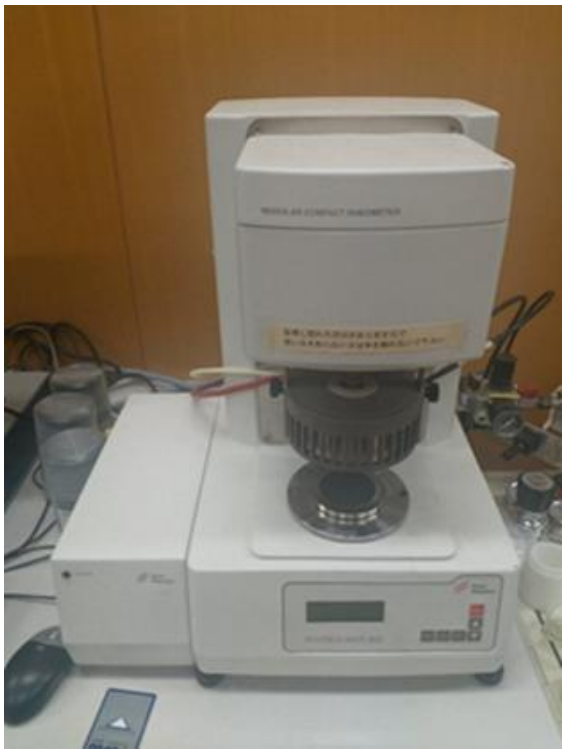

Figure 2-4. Anton-Paar MCR 300 rheometer for the steady shear viscosity measurement.

The rheometer device used for the steady shear viscosity measurement was a rotational cone and plate type rheometer. In this type of rheometer, the tested material was put between a flat base plate and a rotating cone plate, as illustrated in Figure 2-5. The conic plate's rotational movement resulted in a shear rate that works on the fluid between the base and the conic plate. The rheometer, however, does not directly measure the viscosity value at the corresponding shear rate. The directly measured quantities by the device are only the torque and the angular velocity, the shear viscosity then acquired by the computing component in the device using the following correlation **[28]**:

$$\eta(\dot{\gamma}) \cong \frac{3\beta}{2\pi R^3}\frac{M}{\Omega} \tag{2-10}$$

where β is the cone angle, R is the plate radius, Ω is the angular velocity, and M is the torque. The detailed derivation for Eq. (2-10) is available in the references **[28-30]**.

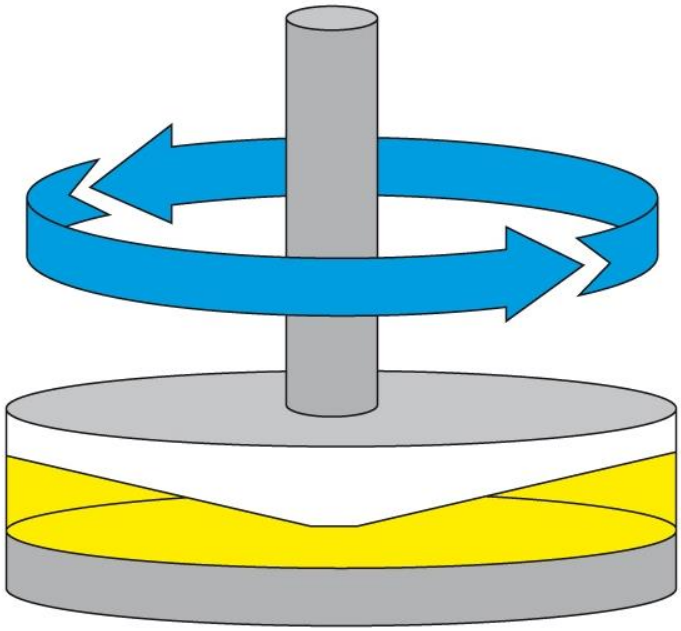

Figure 2-5. Schematic of a rotational cone and plate rheometer **[31]**.

For the shear viscosity measurement of sample fluids, the rheometer shear rate was set at 1 – 100 s^{-1} while the temperature of the test condition was set ranging from 25 to 100°C, with 15°C increments. For shear viscosity measurement higher than the ambient room temperature of 25°C, the measured fluid sample was heated until it reached the targeted test temperature and then held at that temperature range for at least 10 minutes to ensure the temperature homogeneity.

2.4.Result and Discussion

2.4.1. Spectrometry of Immiscible Fluid Materials

The FTIR spectrometer measured the transmissivity of a single sample at least eight times to ensure the acquired data precision. The obtained measurement data was then summarized and presented in Figure 2-6 and Figure 2-7 for polybutenes and PDMS.

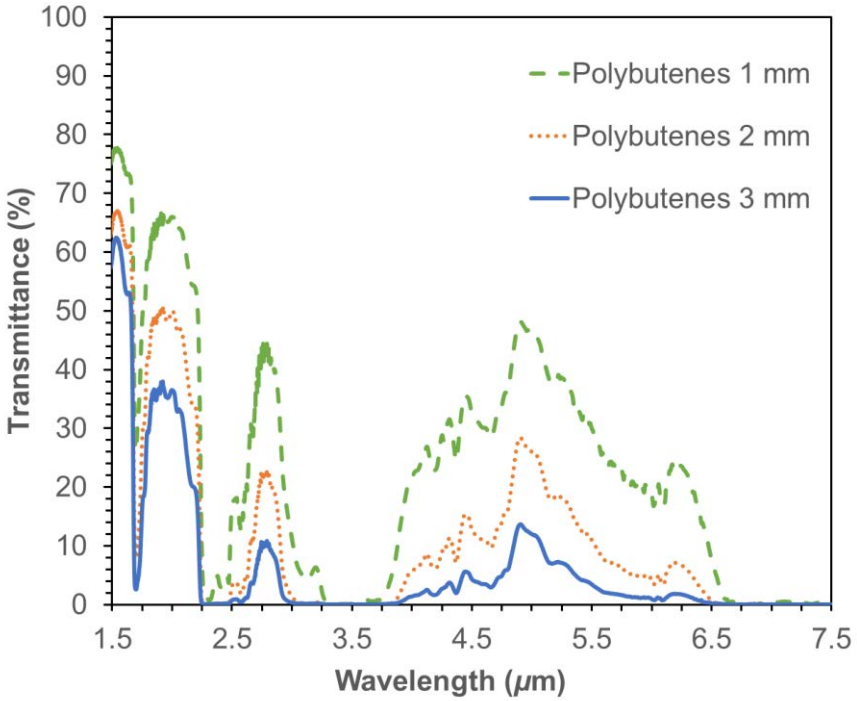

Figure 2-6. The measured transmittance spectrum of polybutenes at wavelength range 1.5 – 7.5 μm.

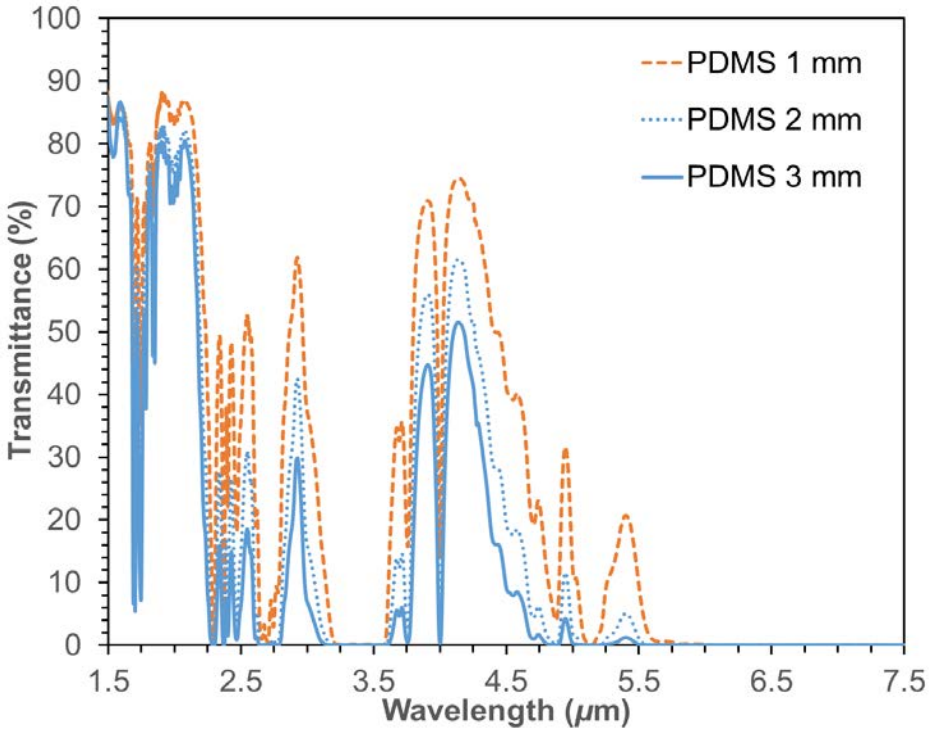

Figure 2-7. The measured transmittance spectrum of PDMS at wavelength range 1.5 – 7.5 μm.

The obtained transmittance data showed that at the lowest wavelength region about 1.5 to 2 μm, except at particular a range of 1.75 μm, both polybutenes and PDMS could easily pass the incoming light. This means that the absorption coefficient value at that region was quite low. The transmissivity level tended to decrease as the wavelength was getting longer, for polybutenes some degree of transparency can still be spotted at a specific range of 2.5 to 3 μm and 3.75 to 6.5 μm. Other than those particular regions, the incident light was almost completely attenuated, especially at the very long wavelength region of more than 6.5 μm.

The PDMS fluid showed a relatively similar pattern of transmissivity, although the fluctuation in the high transmittance and high attenuation was found more often compared to the polybutenes, for example, at the region of 2.25 to 2.5 μm or a specific wavelength of 4 μm. It was also found that in the light transmitting-semitransparent region of both fluid samples, polybutenes

tended to show a slightly lower transmittance level. This means that in general, polybutenes have a higher absorption coefficient compared to the PDMS.

The actual absorption coefficient value of each fluid sample can be calculated by converting the acquired transmittance data using the Lambert-Beer law. Therefore, a light wavelength range, where the disparity in the absorption coefficient between the droplet and matrix fluid is significant enough, can be selected for the proposed selective radiation method. For example, at the specific wavelength of 4.25 μm, polybutenes have the absorption coefficient value of 1350 m^{-1}, while for PDMS, the absorption coefficient is merely at 290 m^{-1}. That absorption coefficient value was an average value obtained by implementing Eq. (2-9) for different sample thicknesses (x_1 and x_2).

An accurate absorption coefficient value was quite difficult to determine at high attenuation levels, such as in longer wavelength regions (> 6.5 μm). The sample thickness was too high for measurement at this particular range so that the measured transmittance value was too low to be converted into an accurate absorption coefficient value. The measurement needs to be performed at a much thinner sample layer to obtain more accurate absorption coefficient data at those specific regions.

The second spectrophotometer then continuously measured the transmittance spectrum of polybutenes and PDMS at lower wavelength ranges of 0.4 – 1.1 μm. The result for this measurement is then shown in Figure 2-8. Both droplet (polybutenes) and matrix (PDMS) fluids were highly transparent at the tested region of UV to near IR (NIR) wavelength. The transmittance of the polybutenes fluid was slightly lower than the PDMS at the currently tested wavelengths.

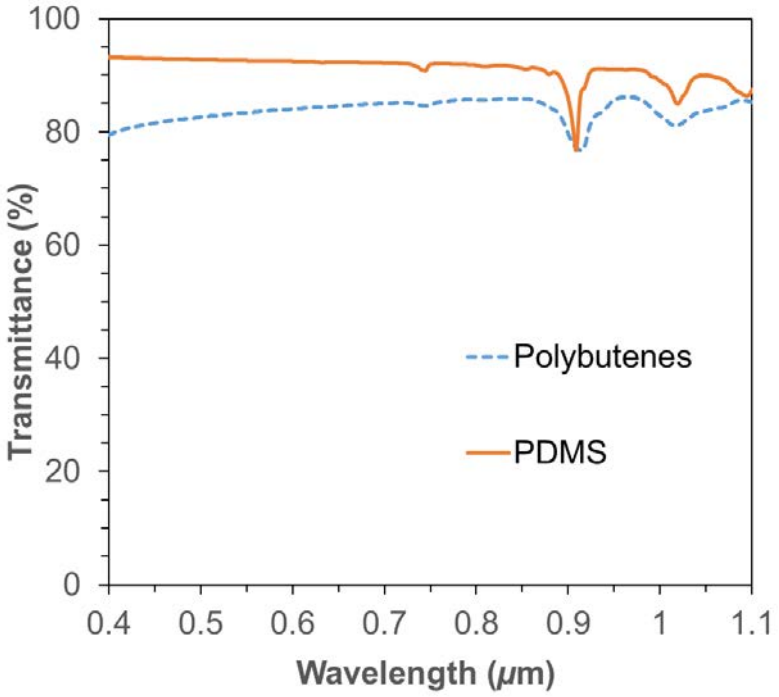

Figure 2-8. The measured transmittance spectrum of polybutenes and PDMS at wavelength range 0.4 – 1.1 μm.

The transmissivity data was then converted into the absorption coefficient value and shown in Figure 2-9. It was then clearly shown that the polybutenes always have a higher absorption coefficient value than PDMS at all tested wavelengths, except at a specific wavelength of 0.92 μm. This suggests that selective radiation heating can still be applied in these visible-NIR wavelength regions, although an enormous level of light intensity is needed to give significant rises in the fluids' temperature due to the poor absorption coefficient value. Alternatively, an additive substance can be given into the droplet fluid, such as carbon black, to enhance their absorption coefficient value.

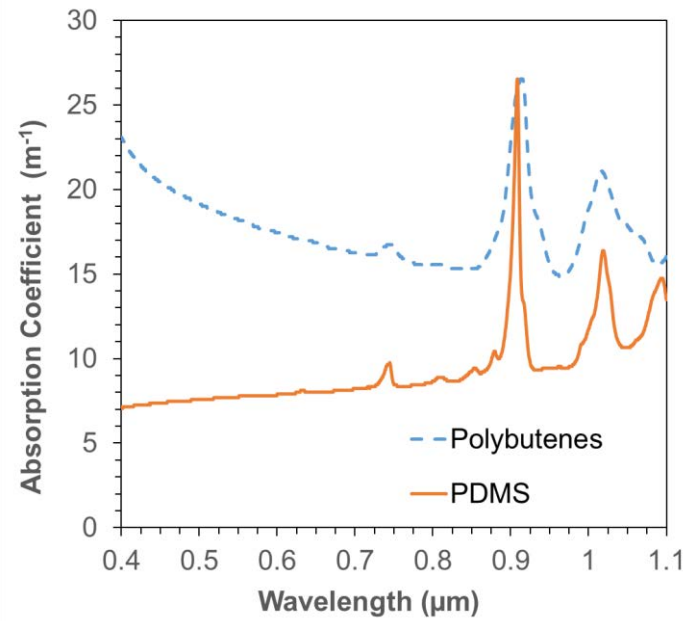

Figure 2-9. The absorption coefficient of polybutenes and PDMS at wavelength range 0.4 – 1.1 μm.

2.4.2. Shear Viscosity of Immiscible Fluid Materials

The steady shear viscosity measurements for all samples are shown in Figure 2-10 and Figure 2-11 for PDMS and polybutenes fluid, respectively. The steady shear viscosities of both PDMS silicone oils and polybutenes exhibited the Newtonian behavior at all shear rates and temperature ranges. However, for the fluid samples of *M-II* (PDMS) and *D-I* (polybutenes), there was more noticeable data fluctuation at higher temperatures (> 70°C) and lower shear rate range (< 10 s^{-1}).

We confirmed that data fluctuation was due to the rheometer device's technical condition rather than the limited accuracy of the specific samples, rather than from the tested materials' physical behavior. The confirmation was supported by the fact that the tested materials showed minimum data fluctuation at all previous sample measurements. The device manufacturer technician also corroborated the technical condition of the rheometer device.

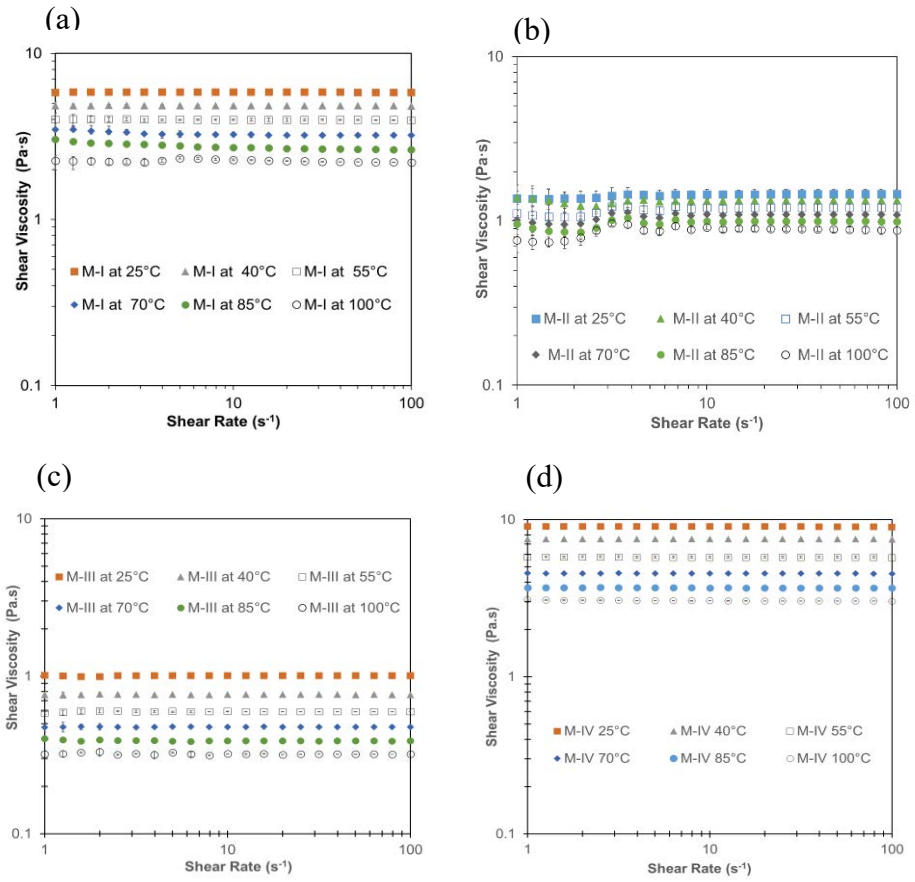

Figure 2-10. The measurement result of steady shear viscosity at temperature range 25-100°C for (a) *M-I* PDMS fluid, (b) *M-II* PDMS fluid, (c) *M-III* PDSMS fluid, and (d) *M-IV* PDMS fluid.

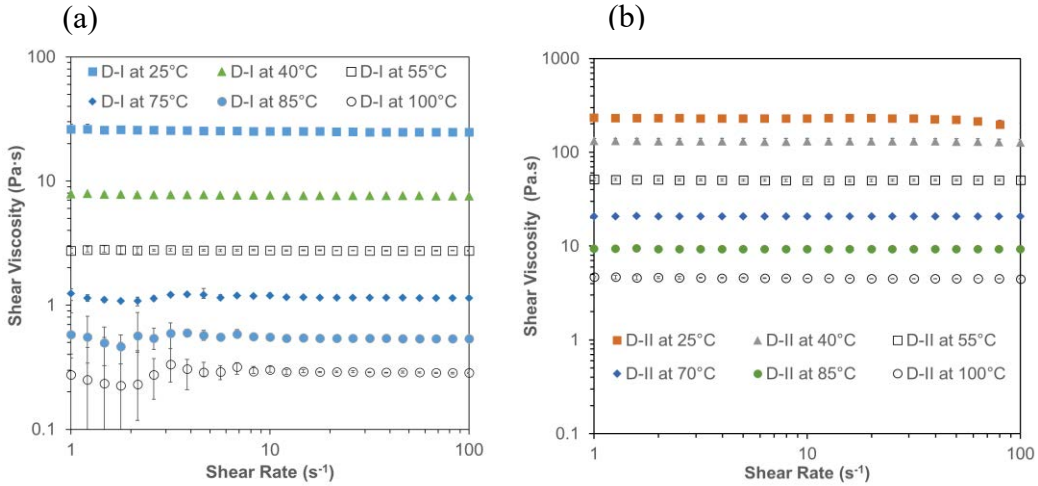

Figure 2-11. Steady shear viscosity measurement at temperature range 25-100°C for (a) *D-I* polybutenes fluid, and (b) *D-II* polybutenes fluid.

The actual shear viscosity value at the ambient temperature of 25°C has also become available from the rheometer measurement. From this information, the initial viscosity ratio for different fluid combinations can be known. The information of the viscosity ratio at the ambient temperature of 25°C is then tabulated in the following Table 2-2.

Table 2-2. Initial viscosity ratio at the ambient temperature of 25°C for the selected combination of immiscible fluid.

Immiscible Fluid Blend	Viscosity Ratio, p
D-I/M-I	4.32
D-I/M-II	17.69
D-I/M-III	25.10
D-I/M-IV	2.81
D-II/M-I	40.28
D-II/M-II	160.56
D-II/M-III	227.78
D-II/M-IV	25.50

The shear viscosity measurement confirmed the temperature dependency and their degree of dependence to the viscosity. The viscosity decreased along with the increase in the temperature, as suggested in the theoretical analysis in Eq. (2-4) and Eq. (2-5). The results also showed that the viscosity reduction due to temperature effect was much less dominant for PDMS than for polybutenes. The polybutenes displayed a much higher temperature dependency on viscosity, especially in sample *D-II* where initial viscosity was as high as 220 Pa·s at the temperature of 25°C and significantly decreased to only 4.7 Pa·s at the temperature of 100°C.

This temperature dependency will subsequently affect the initial viscosity ratio listed in Table 2-2 above. The changes in the viscosity ratio should be made carefully so that it can accommodate the control of droplet dispersion on the immiscible fluid system.

2.4.3. Prediction of Viscosity Changes in Different Temperatures

The preceding subsections provided the necessary background information for implementing the selective radiation heating method to control the droplet phase through viscosity modification. By selecting a suitable irradiation source, according to the criterion and discussion in subsection 2.4.1, the absorbed thermal irradiation will be realized into a non-homogenous temperature field in the immiscible system. The formation of a non-homogenous temperature field has then influenced the viscosity changes following the shear viscosity data available in subsection 2.3.2. By implementing the empirical fitting process listed in the references **[5-22]**, the measured shear viscosity data was then plotted in terms of the natural logarithmic of the viscosity against the inverse temperature value presented in Figure 2-12.

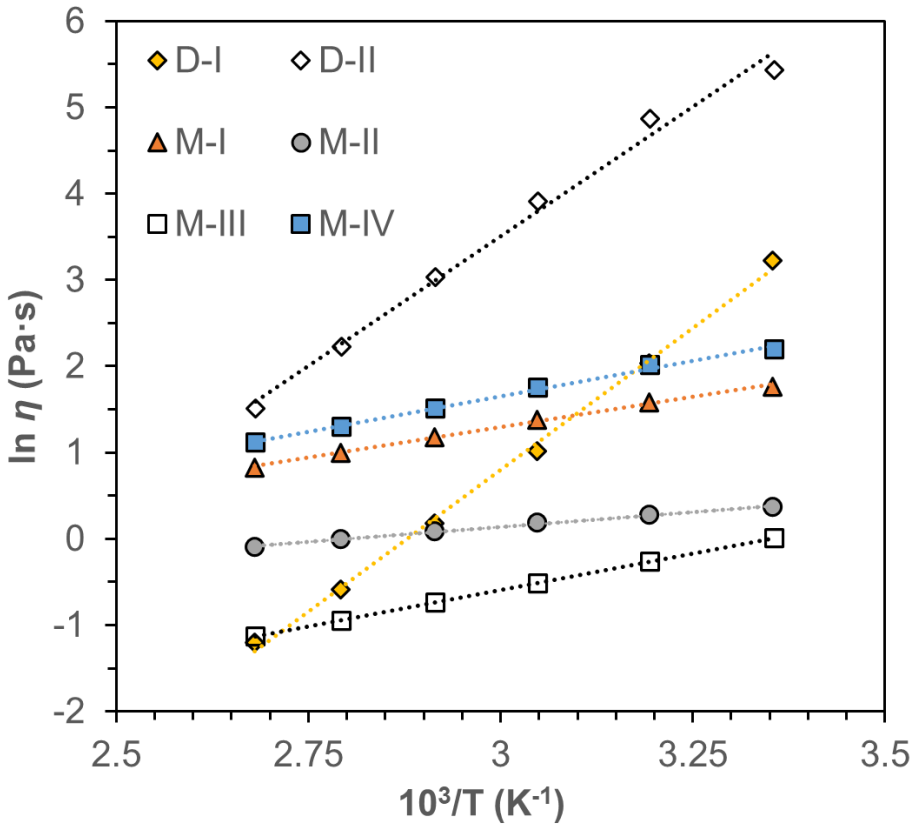

Figure 2-12. The steady shear viscosity-temperature correlation of the tested materials at 10 s^{-1}

The gradient line of each material represents the temperature dependency of their viscosity. The acquired viscosity data was then fitted into a general correlating fitting function expressed in Eq. (2-11). The constants parameter for Eq. (2-11) is then specified in Table 2-3.

$$\ln(\eta) = A_1\left({}^{A_2}/_{T}\right) - A_3 \tag{2-11}$$

Table 2-3. The value of constant for the viscosity-temperature fitting function of Eq. (2-11).

Designation		Value of Constant		
		A₁	***A₂***	***A₃***
Droplet	***D-I***	6.5766	1000	18.929
	D-II	6.0058	1000	14.507
Matrix	***M-I***	1.4046	1000	2.9219
	M-II	0.6848	1000	1.9128
	M-III	1.6914	1000	5.6704
	M-IV	1.6524	1000	3.3053

The viscosity ratio adjustment is achieved if the discrepancy between the absorption coefficient is realized into a pair of inhomogeneous temperatures when the immiscible fluid system was under the influence of direct thermal radiation heating. The prediction of the modified viscosity ratio is performed by an analysis employing the empirical fitting of Eq. (2-11) and the accompanying Table 2-3. For example, the shifting to the viscosity ratio about unity can be reached when the temperature of droplet phase *D-I* is made to reach the temperature range of 40°C (3.19 K^{-1}) while the matrix fluid *M-I* is relatively kept at an initial temperature of 25°C (3.35 K^{-1}). In

this example, the viscosity ratio is modified from an initial value of 4.32 to about 1. The viscosity ratio is shifted into a range that allowing the droplet to deform and breakup, which initially cannot be attained due to the limiting viscosity ratio regardless of the applied shear rate.

2.5. Conclusion

From the current investigation, it was shown that the viscosity ratio tuning by means of exploiting the temperature dependence nature of the viscosity is a feasible feat. Two prerequisite conditions for the selective radiation heating method, which are the disparity on the absorption coefficient value and significant temperature dependency of the droplet phase, can be proved and fulfilled in this chapter.

In a case of the available option of the radiation source wavelength is limited, and the contrast of the absorption coefficient is insignificant at the available heat source wavelength, the non-isothermal condition of the immiscible fluid system can still be achieved either by immensely increase the radiation source intensity or introducing a heat-absorbing additive (e.g., carbon black). The empirical fitting of the viscosity-temperature dependence can provide an analytical tool to estimate the viscosity ratio modification.

2.6.References:

1. Pankove, J.I., “Optical Process in Semiconductor,” Prentice-Hall, Englewood Cliffs (NJ), (1971).
2. Bird, R. B., Stewart, W. E., and Lightfoot, E. N., “Transport Phenomena. 2nd ed,” John Wiley and Sons, Inc, New York (2002).
3. Glasstone, S., Laidler, K. J., and Eyring. H., “Theory of Rate Process,” McGraw-Hill, New York, (1941).

4. Fogel'son, R.L., and Likhachev, E.R. "Temperature Dependence of Viscosity," Technical Physics. 46, 1056 (2001).
5. Esteban, B., Riba, J-R., Baquero, G., Rius, A., and Puig, R., "Temperature Dependence of Density and Viscosity of Vegetable Oils," Biomass and Bioenergy, 42, 164 (2012).
6. Gutmann, F. and Simmons, L.M., "The Temperature Dependence of the Viscosity of Liquids," Journal of Applied Physics, 23, 977 (1952).
7. Haj-Kacem, R.B., Ouerfelli, N., Herráez, J.V., Guettari, M., Hamda, H., and Dallel, M., "Contribution to Modeling the Viscosity Arrhenius-Type Equation for Some Solvents by Statistical Correlations Analysis," Fluid Phase Equilibria, 383, 11 (2014).
8. Andrade, E.N. DA C, "The Viscosity of Liquids," Nature., 125, 309 (1930).
9. Andrade, E.N. DA C, "A Theory of the Viscosity of Liquids.–Part I," The London, Edinburgh, and Dublin Philosophical Magazine, 17, 497 (1934).
10. Andrade, E.N., "A Theory of the Viscosity of Liquids.–Part II," The London, Edinburgh, and Dublin Philosophical Magazine, 17, 698 (1934).
11. Duhne, C.R., "Viscosity-Temperature Correlations for Liquids," Chemical Engineering, 86, 83 (1979).
12. Viswanath, D.S., and Natarajan, G., "Databook on Viscosity of Liquids," Hemisphere, New York (1989).
13. Girifalco, L.A., "Temperature Dependence of Viscosity and Its Relation to Vapor Pressure for Associated Liquids," Journal of Chemical Physics, 23, 2446 (1955).
14. Noureddini, H., Teoh, B.C., and Clements, L.D., "Viscosities of Vegetable Oils and Fatty Acids," Journal of American Oil Chemist' Society, 69, 1189 (1992).

15. Noureddini, H., and Zhu, D., "Kinetics of Transesterification of Soybean Oil," Journal of American Oil Chemist' Society, 74, 1463 (1997).
16. Lang, W., Sokhansanj, S., and Sosulski, F.W., "Modelling the Temperature Dependence of Kinematic Viscosity for Refined Canola Oil," Journal of American Oil Chemist' Society, 69, 1054 (1992).
17. Dutt, N.V.K., "A simple Method of Estimating the Viscosity of Petroleum Crude Oil and Fractions," The Chemical Engineering Journal, 45, 83 (1990).
18. Perry, R.H., "Perry's Chemical Engineers' Handbook (6th Ed.)," McGraw–Hill, New York, 278 (1984).
19. Wochnowsky, H., and Müssig, B., "On the Viscosity-Temperature Behavior of Organic Liquids," Chemistry, 111, 123 (1983).
20. Kotas, J., and Valešová, M., "Thermodynamic Activation Functions of Viscous Flow on Non-Polar Liquids," Rheologica Acta, 25, 326 (1986).
21. Gupta, A., Sharma, S.K., and Toor, A.P., "An Empirical Correlation in Predicting the Viscosity of Refined Vegetable Oils," Indian Journal of Chemical Technology, 14, 642 (2007).
22. Stanciu, I., "A New Viscosity-Temperature Relationship for Vegetable Oil," Journal of Petroleum Technology and Alternative Fuels, 3, 19 (2012).
23. Sibillo, V., Pasquariello, G., Simeone, M., Cristini, V., Guido, S., "Drop Deformation in Microconfined Shear Flow," Physical Review Letter., 97, 054502 (2006).
24. Han, C. D., and King, R. G., "Measurement of the Rheological Properties of Concentrated Emulsions," Journal of Rheology, 24, 213 (1980).

25. Cardinaels, R., Vananroye, A., Van Puyvelde, P., and Moldenaers, P., "Breakup Criteria for Confined Droplets: Effects of Compatibilization and Component Viscoelasticity," Macromolecular Materials and Engineering, 296, 214 (2011).
26. Mighri, F. and Huneault, M.A., "Dispersion Visualization of Model fluids in a Transparent Couette Flow Cell," Journal of Rheology, 45, 783 (2001).
27. Verhulst, K., Moldenaers P., and Minale, M., "Drop Shape Dynamics of a Newtonian Drop in a Non-Newtonian matrix During Transient and Steady Shear Flow," Journal of Rheology, 51, 261 (2007).
28. Münstedt, H., and Schwarzl, F. R., "Deformation and Flow of Polymeric Materials," Springer, Berlin Heidelberg (2014).
29. Macosko, C. W., "Rheology: Principles, Measurements and Applications," VCH Publishers, New York (1994).
30. Dealy, J.M, and Wang, J., "Melt Rheology and Its Applications in the Plastics Industry. 2nd ed," Springer, Dordrecht (2013).
31. https://wiki.anton-paar.com/en/basics-of-rheology/#rotational-tests (accessed March 2021).

3. Chapter 3: Droplet Deformation of an Immiscible Fluid System by Infrared Laser Heating

3.1. Introduction

The simple shear flow condition can be realized when a viscous fluid is contained between a moving parallel surface. The motion from the moving surface is resulting in shear stress. This shear stress then subsequently causes flow. This specific flow condition is commonly known as the Couette flow. When an immiscible droplet-matrix system is subjected to this simple shear from the Couette flow, the droplet phase will experience some form of deformation due to the presence of the shear stress as shown in Figure 3-1. Taylor is the defined the degree of deformation of the Newtonian droplet as the deformation parameter, *Def,* which can also be linearly correlated with the capillary number (Ca). **[1]**

$$Def \equiv \frac{a-b}{a+b} = \mathrm{Ca}\frac{19p+16}{16p+16} \tag{3-1}$$

Where a and b represent the major and minor axis of the droplet and p is the viscosity ratio of the immiscible droplet system.

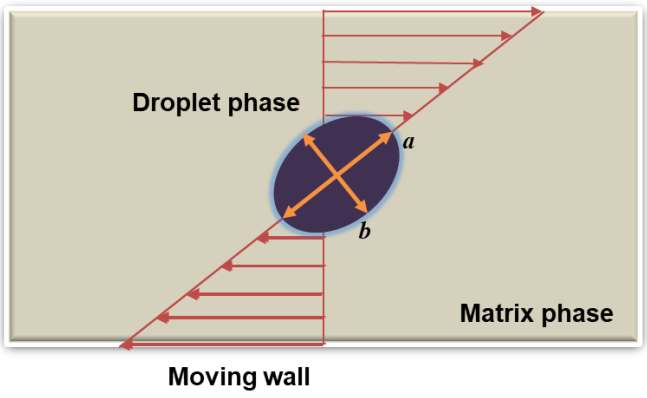

Figure 3-1. Schematic of a simple shear flow on a droplet fluid suspended by a matrix fluid.

It is known that the deformation of the droplet will eventually reach a breakup point when the applied shear rate is resulting in the Ca that exceeds the critical capillary number (Ca_c) requirement **[2,3]**. At the region of the viscosity ratio (p) almost zero, where the dispersed droplet phase comes in the form of an extremely fine bubble, the Ca_c value is quite excessive ($\gg 100$). The Ca_c value will steadily decrease along with the rise in the value of p. At the region of $p \approx 1$, the Ca_c will reach the minimum value ($Ca_c \cong 0.5$). From this minimum region, Ca_c is then rapidly increasing and becomes almost infinite at $p > 4$. Therefore, no droplet breakup can occur for the immiscible droplet-matrix system with a viscosity ratio of more than the limiting value of four, regardless of the resulting Ca. In this condition, the droplet will instead reach a steady-state deformation into a more ellipsoidal form **[4]**. For the region of viscosity ratio less than four, the steady-state droplet deformation will also realize when the Ca value is below the Ca_c.

In this chapter, the selective radiation technique is then proposed to overcome the droplet deformation restriction due to the limiting factor of the viscosity ratio.

3.2.Counter-Rotating Couette Cylinder

The simple shear Couette flow for the experiment was emulated in a specifically designed counter-rotating cylinder, as shown in Figure 3-2. This Couette cylinder apparatus consists of two concentric main cylinders that can be rotated independently. The outer cylinder is made from a transparent polycarbonate (PC) with a radius of 75 mm, while the inner cylinder was made of solid aluminum with a radius of 71 mm, so that ratio between cylinders was 0.95. The gap or annulus between the cylinder was 4 mm, and the observed immiscible fluid was contained in this space. Each rotating cylinder was connected to a DC motor (BLM230HP-GFV, Oriental Motor) using a belt gear system. The DC motor's speed can be adjusted manually using a control knob so that the

combined rotation speed resulted in the required shear rate. A thin thermocouple wire with a diameter of 0.25 mm was inserted in the cylinder's gap to ensure the immiscible system's initial temperature.

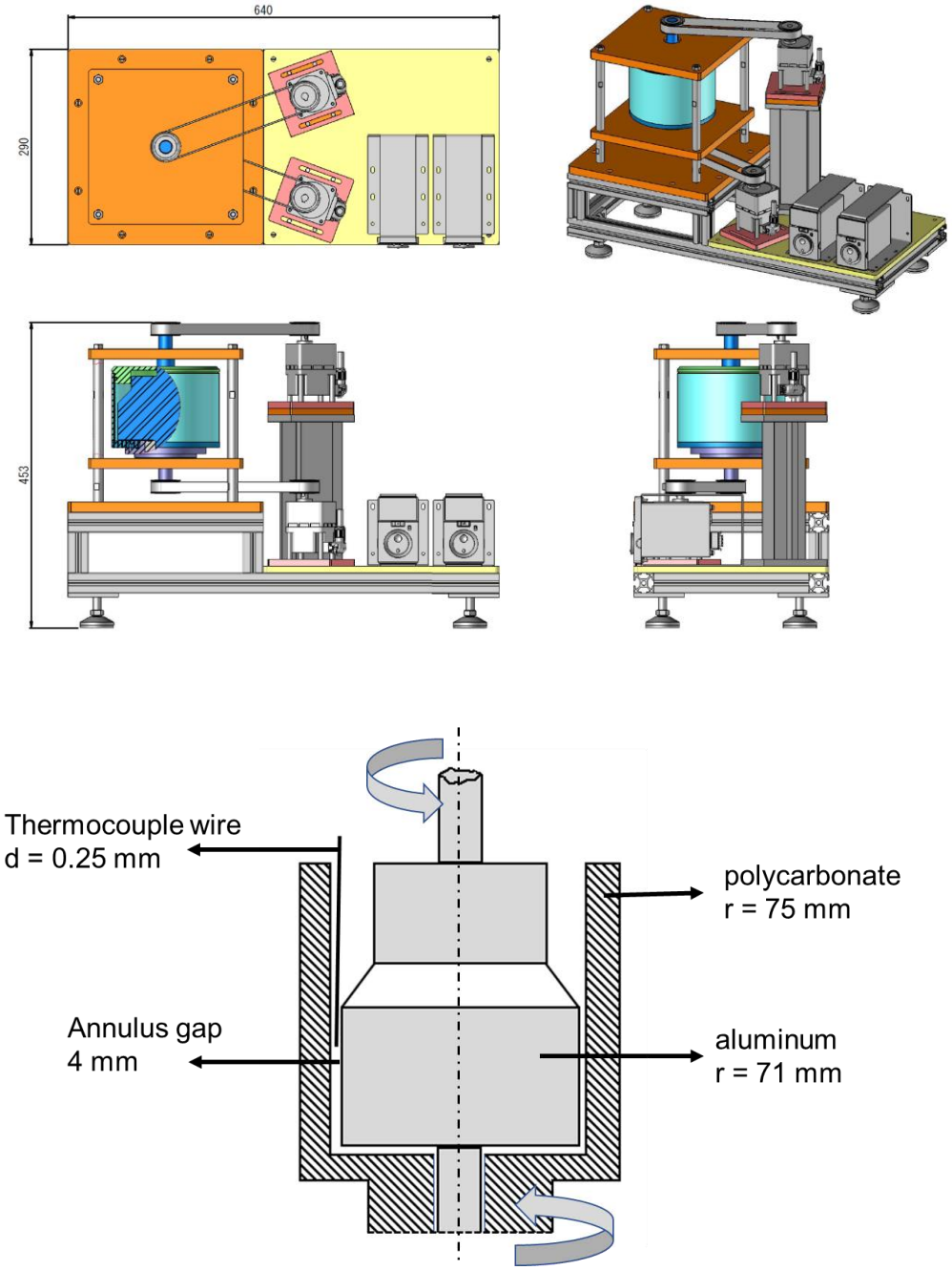

Figure 3-2. Schematic of the counter-rotating Couette cylinder.

A high-speed camera (acA1300-200um, Basler) was placed in front of the Couette cylinder. The high-speed camera was equipped with a macro zoom lens (MLM3X-MP, Computar). The combination of the high-speed camera and the zoom lenses can capture the deformed microdroplet's continuous images during the shear flow implementation. The camera was connected to a computer that displays the captured droplet images and records them. The experiment employed a fiber laser (fiber cw 100, Jen Las) as the radiation source for the selective radiation heating process. The fiber laser oscillation wavelength was at 1.07 µm with a maximum emitted power of 100 W (intensity 436.64 W/cm^2). An infrared (IR) optical barrier (IR cut-off filter, Edmund Optics) was set in front of the macro zoom lenses to protect the lenses from laser irradiation. Finally, illumination sources (LA-HDF105A, Luminar Ace) were also in place to provide adequate lighting for the high-speed camera. Figure 3-3 shows the complete experimental setup of the Couette cylinder apparatus. After the images were successfully recorded to the computer, the droplets' recorded image was then analyzed using an image processing tool software (ImageJ).

Figure 3-3. The complete experimental setup of the Couette cylinder apparatus.

The expected flow condition in the Couette cylinder for the experiment is a simple shear flow. The simple shear flow condition can only be obtained if the fluid flow inside the Couette cylinder is maintained in a steady laminar flow condition. The fluid inside the Couette cylinder is moving only in a circular motion for laminar flow so that only the tangential component (v_θ) of the velocity should exist, as shown in Figure 3-4. The absence of radial (v_r) and axial (v_z) components of the velocity will prevent any occurrence of wavy or vortex flow.

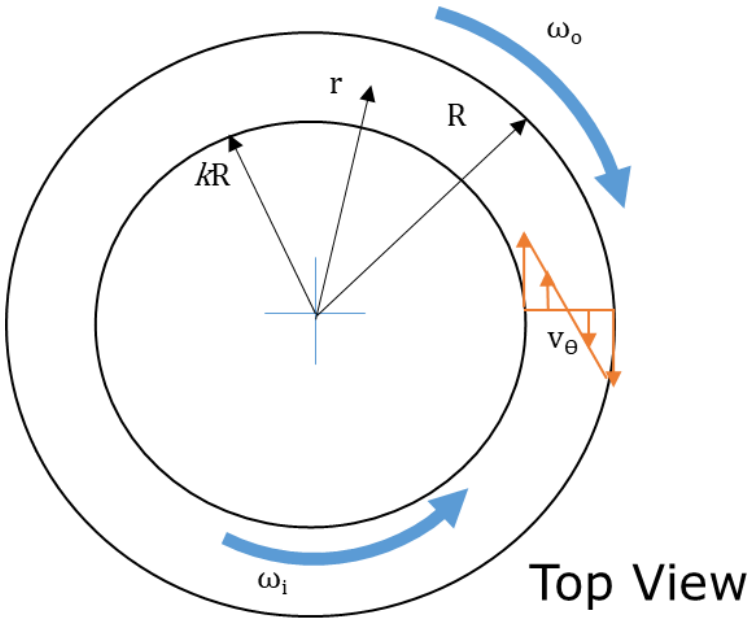

Figure 3-4. The angular and tangential velocity for laminar flow inside the Couette cylinder.

The tangential velocity (v_θ) and the droplet deforming shear rate ($\dot{\gamma}$) can be obtained by solving the continuity equation and the equation of motion inside the Couette cylinder. The continuity equation for cylindrical coordinate inside the Couette cylinder is expressed as:

$$\frac{1}{r}\frac{\partial}{\partial r}(r\,v_r) + \frac{1}{r}\frac{\partial v_\theta}{\partial \theta} + \frac{\partial v_z}{\partial z} = 0 \qquad (3\text{-}2)$$

for incompressible fluid assumption:

$$\nabla\vec{v} = 0 \tag{3-3}$$

The radial (v_r) and axial (v_z) components do not exist in the laminar flow, and tangential velocity is not the function of the rotation angle θ. Hence the continuity equation can be reduced into the following form:

$$\frac{\partial v_\theta}{\partial \theta} = 0 \tag{3-4}$$

With neglecting end effects from depth in the z-direction, tangential velocity v_θ is only a function of the radius r.

$$v_\theta = v_\theta(r) \tag{3-5}$$

No pressure gradient is in the θ component so that the equation of motion inside the Couette cylinder can be simplified into:

$$\text{In r component: } -\rho\, {v_\theta^2}/{r} = -{\partial p}/{\partial r} \tag{3-6}$$

$$\text{In } \theta \text{ component: } \frac{d}{dr}\left(\frac{1}{r}\frac{d}{dr}(rv_\theta)\right) = 0 \tag{3-7}$$

$$\text{In z component: } -{\partial p}/{\partial z} - \rho g = 0 \tag{3-8}$$

For obtaining the tangential velocity profile, v_θ, θ component of the equation of motion is then need to be integrated:

$$\int \frac{d}{dr}\left(\frac{1}{r}\frac{d}{dr}(rv_\theta)\right) = \int 0 \tag{3-9}$$

$$\frac{1}{\mathrm{r}}\frac{d}{d\mathrm{r}}(\mathrm{r}\mathrm{v}_\theta) = \mathrm{C}_1 \tag{3-10}$$

$$\mathrm{r}\mathrm{v}_\theta = \frac{\mathrm{C}_1\,\mathrm{r}^2}{2} + \mathrm{C}_2 \tag{3-11}$$

$$\mathrm{v}_\theta = \frac{\mathrm{C}_1\mathrm{r}}{2} + \frac{\mathrm{C}_2}{\mathrm{r}} \tag{3-12}$$

The exact value of the unknown constants C_1 and C_2 can be calculated by inserting the value of v_θ at the known boundary conditions. The boundary conditions are at the surfaces of each cylindrical surface and assumed as the non-slip surface. In the calculation of the boundary condition, R is the largest radius (radius of the outer cylinder), and k is the radius ratio between the two-rotating cylinder:

Boundary Condition 1 at r = kR (radius of the inner cylinder)

$$\mathrm{v}_\theta = \omega_i k\mathrm{R} = \frac{\mathrm{C}_1 k\mathrm{R}}{2} + \frac{\mathrm{C}_2}{k\mathrm{R}} \tag{3-12}$$

Boundary Condition 2 at r = R (radius of the outer cylinder)

$$\mathrm{v}_\theta = \omega_o\mathrm{R} = \frac{\mathrm{C}_1\mathrm{R}}{2} + \frac{\mathrm{C}_2}{\mathrm{R}} \tag{3-13}$$

The integration constants are then given by:

$$(\omega_i - \omega_o)k\mathrm{R} = \mathrm{C}_2\left(\frac{1}{k\mathrm{R}} - \frac{k}{\mathrm{R}}\right) \tag{3-14}$$

and

$$\left(\omega_i k\mathrm{R} - \omega_o\frac{\mathrm{R}}{k}\right) = \frac{\mathrm{C}_1}{2}\left(k\mathrm{R} - \frac{k\mathrm{R}}{k}\right) \tag{3-15}$$

Where ω_o is the angular velocity of the outer cylinder and is ω_i the angular velocity of the inner cylinder, it should be noted that ω_o and ω_i value will have an opposite sign due to their countering direction of rotation.

By substituting the integration constant C_1 and C_2, the tangential velocity profile is finally obtained as follows:

$$v_\theta = \frac{\omega_o - \omega_i k^2}{1-k^2} r + \frac{(\omega_i - \omega_o)}{1-k^2} \frac{k^2 R^2}{r} = \frac{kR}{1-k^2} \left[(\omega_o - \omega_i k^2) \frac{r}{kR} + (\omega_i - \omega_o) \frac{kR}{r} \right] \quad (3\text{-}16)$$

$$v_\theta(r) = \frac{\omega_o kR}{1-k^2} \left(\frac{r}{kR} - \frac{kR}{r} \right) + \frac{\omega_i k^2 R}{1-k^2} \left(\frac{R}{r} - \frac{r}{R} \right) \quad (3\text{-}17)$$

The obtained Eq. (3-17) can describe the velocity profile at any distance inside the Couette cylinder annulus, as shown in Figure 3-5. The velocity is at maximum in the edge of the annulus distance, which corresponds to the inner and outer cylinder's radius dimension on the Couette apparatus. There is a small difference (5.3%) on the velocity value at the annulus's end side. This difference is emerged due to the cylindrical geometry of the Couette apparatus. The difference in the maximum velocity can be reduced by increasing the dimension of the Couette cylinder. However, the increment in the apparatus dimension will affect the required experimental space and the manufacturing cost. Therefore, the Couette apparatus's dimension is considered the optimum condition for the current work in terms of accuracy, size, and production cost.

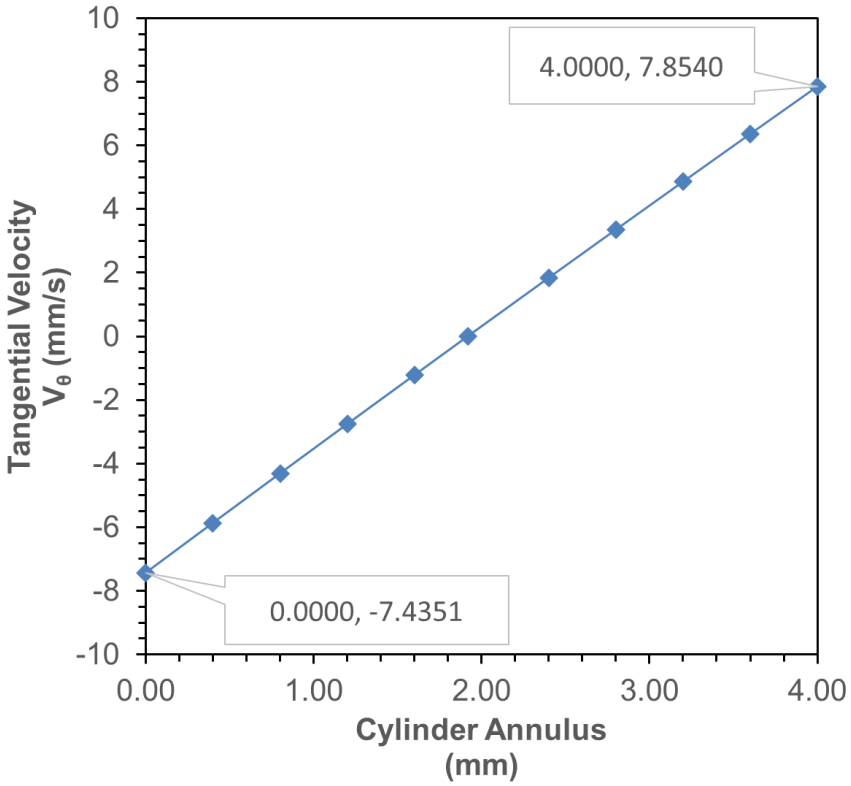

Figure 3-5. Tangential velocity (v_θ) distribution on the Couette cylinder annulus for ω_o and ω_i set at 1 RPM.

From the tangential velocity profile, the momentum flux or shear stress is defined as:

$$\tau_{r\theta} = -\mu r \frac{d}{dr}\left(\frac{v_\theta}{r}\right) \tag{3-18}$$

With μ is the fluid viscosity. The shear rate is then determined as:

$$\dot{\gamma} = \frac{\tau_{r\theta}}{\mu} = -r \frac{d}{dr}\left(\frac{v_\theta}{r}\right) = 2\frac{(\omega_i - \omega_o)}{1-k^2}\frac{k^2 R^2}{r^2} \tag{3-19}$$

The equation can determine the shear at any location r, of the cylinder annulus. In the counter-rotating Couette cylinder, the mean shear rate is expressed in the following form **[5,6]**.

$$\dot{\gamma} = 2\,(\omega_o - \omega_i)\,\frac{kR^2}{(R^2 - kR^2)} \tag{3-20}$$

Figure 3-6 provided the example of the calculated shear rate distribution (from Eq. 3-19) and mean shear rate (from Eq. 3-20). The Couette apparatus's cylindrical geometry also causes some deviation in the shear rate's value along with the annulus distance. The shear rate at the middle of the annulus distance is comparable with the mean shear rate. The maximum deviation is found at the edge of the annulus, with a shear rate difference is found at 5.63% relative to the mean shear rate. The observed droplet should be either in the middle-distance of the annulus or near to this middle distance so that the shear rate value taken in the experiment is the mean shear rate or the shear rate in the middle of the annulus distance.

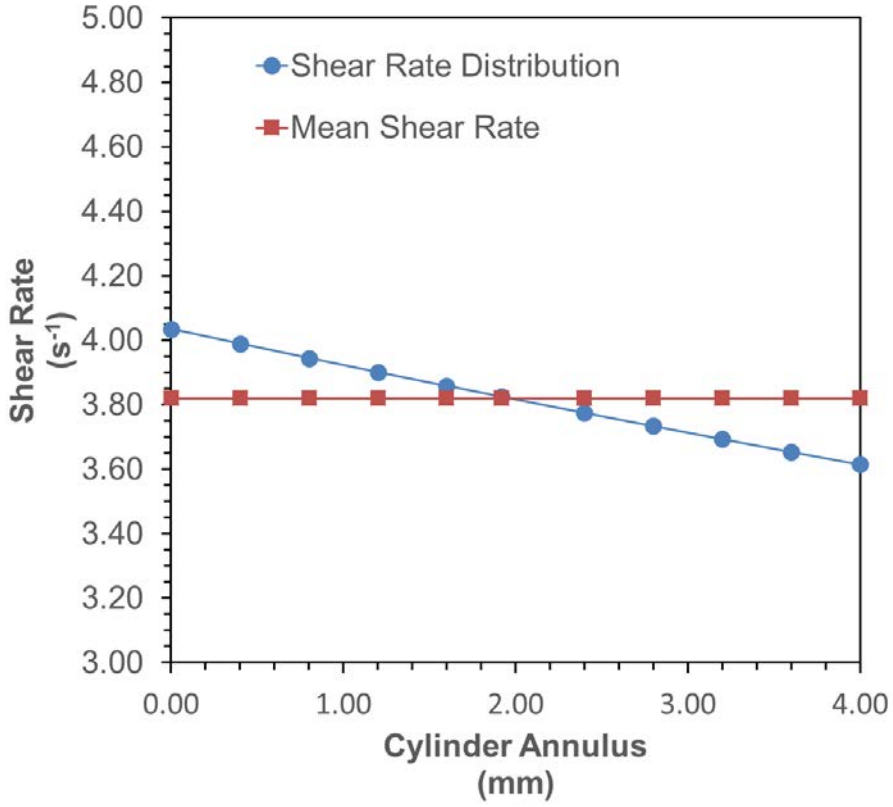

Figure 3-6. Shear rate distribution and mean shear rate on the Couette cylinder annulus for ω_o and ω_i at 1 RPM

3.3. Experimental Method and Materials

3.3.1. Materials of The Immiscible Fluid System and Droplet Preparation

The experiment employed a model immiscible fluid system consisting of Polybutenes (Sigma-Aldrich) and PDMS (Shin-Etsu silicone) as the droplet and the matrix phase. The initial viscosity at ambient temperature and the absorption coefficient value for each fluid was determined according to the measurement described and carried out in the preceding chapter. The viscosity ratio (p) value is then obtained as 4.32 and 17.69. In the specific range of the employed IR laser wavelength, the droplet's absorption coefficient (β) was slightly higher than the matrix fluid, although the actual value was still meager. Therefore, a special colorant dye (Epolight 1178, Epolin) was added to the droplet phase. The addition of the colorant dye will have a twofold purpose. First, the colorant dye can give a chromatic contrast between the droplet and the matrix fluid as both were originally clear and transparent fluids so that the droplet can be more easily identified in the experiment. Second, the addition of colorant dye will amplify the droplet phase's ability to absorb the radiation energy emitted at the corresponding laser wavelength. Table 3-1 then summarizes the specifications for the selected model fluid.

The density difference between the Polybutenes and PDMS (0.085 g/ml) was not apparent and negligible in the system of *D/M-1*. However, the lower viscosity PDMS (the kinematic viscosity, $\upsilon = 0.65$ cSt) exhibits a much lower density value ($\rho = 0.760$ g/ml) so that the effect of density difference is more noticeable for this specific combination of fluid, i.e., the slightly lighter droplet phase, *D* moves upward significantly faster than in the *M-1* fluid. A mix of PDMS fluid was then made. The purpose of this new mix of PMDS was to provide matrix fluid that has a

similar density with the Polybutenes droplet but at a much lower viscosity. The combination then resulted in the matrix fluid *M-2*.

Table 3-1. Selected materials of the immiscible model fluid

System	Droplet [a] Fluid Component	ID	ρ (g/ml)	β (m^{-1})	Matrix [a] Fluid Component	ID	ρ (g/ml)	β (m^{-1})	p (-)
D/M-1	100% Polybutenes	*D*	0.890	17.07[c] 9057.38[d]	100% PDMS (υ = 5,000 cSt) [b]	*M-1*	0.975	11.54	4.32
D/M-1	100% Polybutenes	*D*	0.890	17.07[c] 9057.38[d]	71.4% PDMS (υ = 5,000 cSt) [b] + 28.6% PDMS (υ = 0.65 cSt) [b]	*M-2*	0.915	11.54	17.69

a) Concentrations are on a volume basis.
b) The respective manufacturer provides the kinematic viscosity (υ) values at 25°C.
c) Without the IR absorbing colorant dye
d) With the IR absorbing colorant dye

The interfacial tension between the selected immiscible model fluid component was known at 2.4 mN/m, and this value was obtained from several experimental procedures based on Taylor's theory **[7, 8]**. The immiscible system's preparation was started by pre-mixing about 1 gram of the Polybutenes fluid with 5 grams of the PDMS fluid until a droplet emulsion was formed. The pre-mixed emulsion was then poured into the Couette apparatus that had been half-filled by the PDMS fluid. An additional PDMS fluid matrix is then poured into the Couette cylinder apparatus until the cylinders were filled entirely (Figure 3-7).

Figure 3-7. The emulsion formed after the pre-mixed process (left) and the droplet inside the Couette cylinder after the pouring process (right).

3.3.2. Experimental Method and Procedure

In the experiment, the main technical challenge for capturing the droplet image on the experimental apparatus is to keep the droplet inside the camera field of view during the shearing process, as shown in Figure 3-8. The droplets need to be positioned at a stationary plane resulting from the counter-rotating movement of either cylinder. Otherwise, the droplet will tend to drift away from the field of view and follow the direction of the cylinder's rotation. For dealing with this problem, several solutions can be implemented. The first is by continuously adjusting each cylinder's speed for attaining a stationary plane in the matrix fluid **[5,6]**. However, this scheme is quite challenging to achieve in the case of manual speed adjustment **[9]**.

Another solution is by increasing the area covered by the camera's field of view by adjusting the lens's magnification scale. This method will give the droplets some extended time before it passes from the observation window. The larger observation window is compensated by smaller image resolution in this method, resulting in a reduced accuracy **[9]**. Hence, a delicate

trade-off between accuracy and the ability to capture the droplet image must be in place. In our experiment, the latter method was taken due to the reason mentioned in the former approach. Additionally, a high-speed camera with a reasonable frame rate can accommodate the droplet's passing from the camera field of view. Therefore, even when the set cylinder rotation was relatively high (e.g., >15 RPM) and makes the droplet passes the camera field of view at a rapid pace, a sufficient number of images can still be acquired. In the experiment, the camera framerate was set at 80 frames per second (FPS).

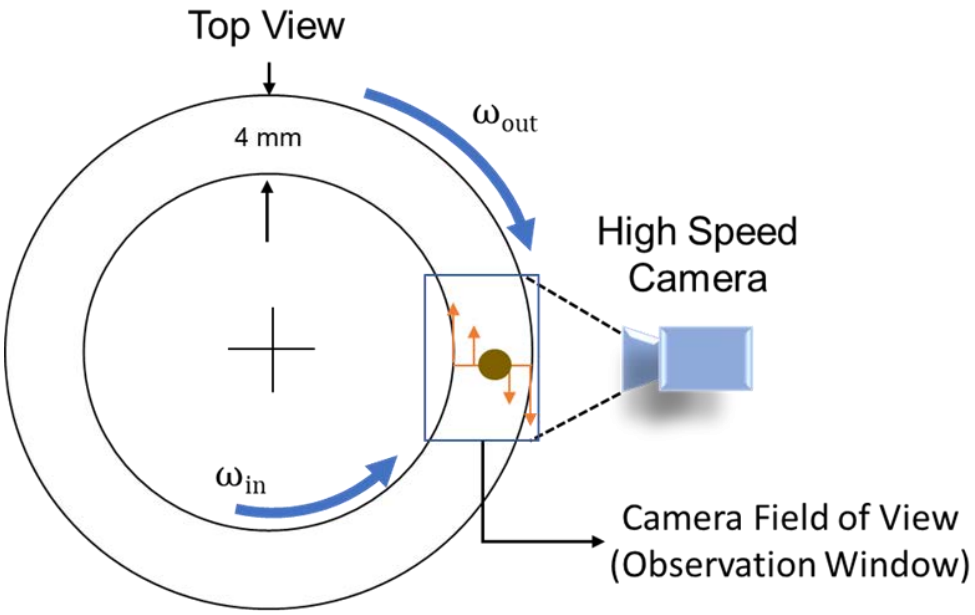

Figure 3-8. Schematic of the observation from the camera for capturing droplet deformation.

3.3.2.1. Steady State Droplet Deformation at Ambient Room Temperature

The immiscible fluid system measured temperature for this experiment was found at 25-26°C. The shear viscosity changes for both droplet and matrix due to this small temperature variation were negligible, so that the temperature of 25°C was taken as a reference point of the fluid properties. Before the experiment was conducted, a metal calibration ball with 1.5 mm in

diameter was inserted into the Couette apparatus. The images of the metal calibration ball were then used as a scale of reference for the experiment. The procedure for capturing droplet image at ambient room temperature condition was as follow: (1) after the pre-mixed droplet was poured, the Couette cell was started at a designated speed (shearing rate) until the droplet reached the steady-state deformation, (2) Once a suitable size droplet was entering the observation window, the image of that deformed droplet was immediately recorded, (3) The applied shear rate then stop right after image of the deformed droplet was successfully captured, and the droplet was let relaxed until it returned to its spherical shape, during this droplet relaxation period the camera continuously recorded the image of the relaxed droplet. The completely retracted droplet was taken as the initial spherical droplet form.

The size of the droplet diameter was suggested to be less than 20% of the annulus distance to eliminate the wall effect on the droplet **[10]**. The gap or annulus distance of the Couette apparatus was 4 mm, so that only droplet with a diameter less than 800 μm will be considered.

3.3.2.2.Droplet Deformation Under Selective Radiation Heating

For the experiment under selective radiation heating, the first couple of steps were similar to the experiment at the isothermal condition of ambient room temperature. However, after the steady-state deformed droplets' image was recorded, the shearing was not stopped, but instead, the laser source was turned on at the predetermined intensity level. The image of the sheared droplets was continuously recorded during this laser heating sequence for obtaining the droplet deformation under radiation heating.

The condition for the laser intensity was set at two different conditions. At the first experimental condition, the droplet was irradiated at a certain level of laser intensity with the same

irradiation period to investigate the effect of the laser intensity parameter on droplet deformation. In the second experiment mode, the droplet was irradiated with an IR laser with an intensity level similar to the former experimental condition. However, the irradiation period was set at a different rate so that the pairing between the laser intensity level and irradiation period resulted in similar total radiation energy. Table 3-2 and Table 3-3 provide a detailed description for each of the experimental modes.

Table 3-2. The experimental condition for the laser intensity parameter.

No	Initial Viscosity Ratio at 25°C	Shear Rate (s^{-1})	Laser Intensity (W/cm^2)	Irradiation Time (s)	Irradiation Energy (J/cm^2)
1	4.32	1.9	10.9	2	21.8
2	4.32	1.9	21.8	2	43.6
3	4.32	1.9	43.6	2	87.3
4	4.32	1.9	87.3	2	174.6
5	17.69	1.9	10.9	2	21.8
6	17.69	3.8	10.9	2	21.8

Table 3-3. The experimental condition for the total energy parameter.

No	Initial Viscosity Ratio at 25°C	Shear Rate (s^{-1})	Laser Intensity (W/cm^2)	Irradiation Time (s)	Irradiation Energy (J/cm^2)
1	4.32	1.9	10.9	8	87.3
2	4.32	1.9	21.8	4	87.3
3	4.32	1.9	43.6	2	87.3
4	4.32	1.9	87.3	1	87.3
5	17.69	1.9	10.9	8	87.3
6	17.69	3.8	10.9	8	87.3

3.3.2.3.Modified Deformation Parameter

The captured image from the high-speed camera was in the plane of the vorticity and velocity direction (side view of Couette cell) as indicated in Figure 3-9 so that only the length of the major axis a^* and radial axis c and can be measured directly from experimental observation. The major axes of a and b of the ellipsoidal droplet can be related with a^* and c, with two conditions: 1) the droplet affine angle of rotation, θ, is known and 2) the volume conservation of the ellipsoid droplet is preserved, as described in the following equations **[11]**.

$$a^* = 2\sqrt{a\cos^2(\theta) + b^2\sin^2(\theta)} \tag{3-21}$$

and

$$r_o^3 = a\,b\,c \tag{3-22}$$

r_o is the radius of the undeformed droplet.

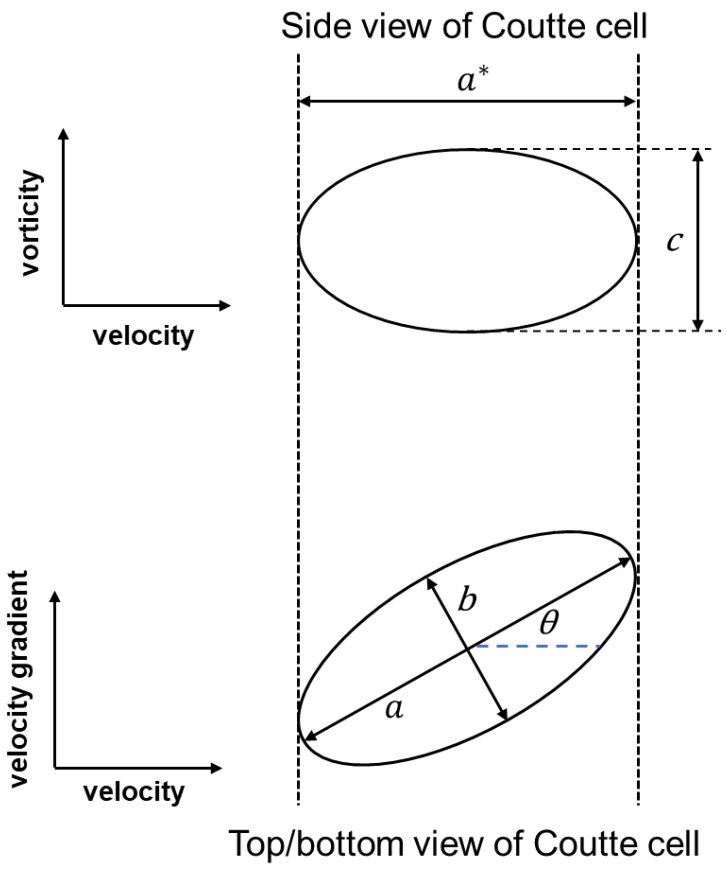

Figure 3-9. Schematic of deformed droplet observed from the side and top view of Couette cylinder apparatus, a and b are the major axes in the velocity - velocity gradient plane with affine angle θ; The droplet axis a^* is the projection of the major axis a to the velocity - vorticity plane and c is the principal axis in the radial direction.

However, the information on the affine angle was also lacked in our experimental observation. A modified deformation parameter, *Def**, was then introduced for describing the droplet deformation **[12, 13]**. In this approach, a quantitative measure of droplet deformation can be obtained using the experimental data of a^* and c.

$$Def^* \equiv \frac{a^* - c}{a^* + c} \tag{3-23}$$

3.4.Droplet Deformation in Ambient Room Temperature

This part will discuss the observation of the droplet deformation at the isothermal condition of ambient room temperature of 25°C. The viscosity ratios for these experiments were set above four. In this experiment, the applied shear rate was increased gradually, and the droplet images were captured according to the procedure mentioned in the previous section. The observed droplet diameter ranges at 350-720 μm, and examples of the droplet images are given in Figure 3-10 and Figure 3-11.

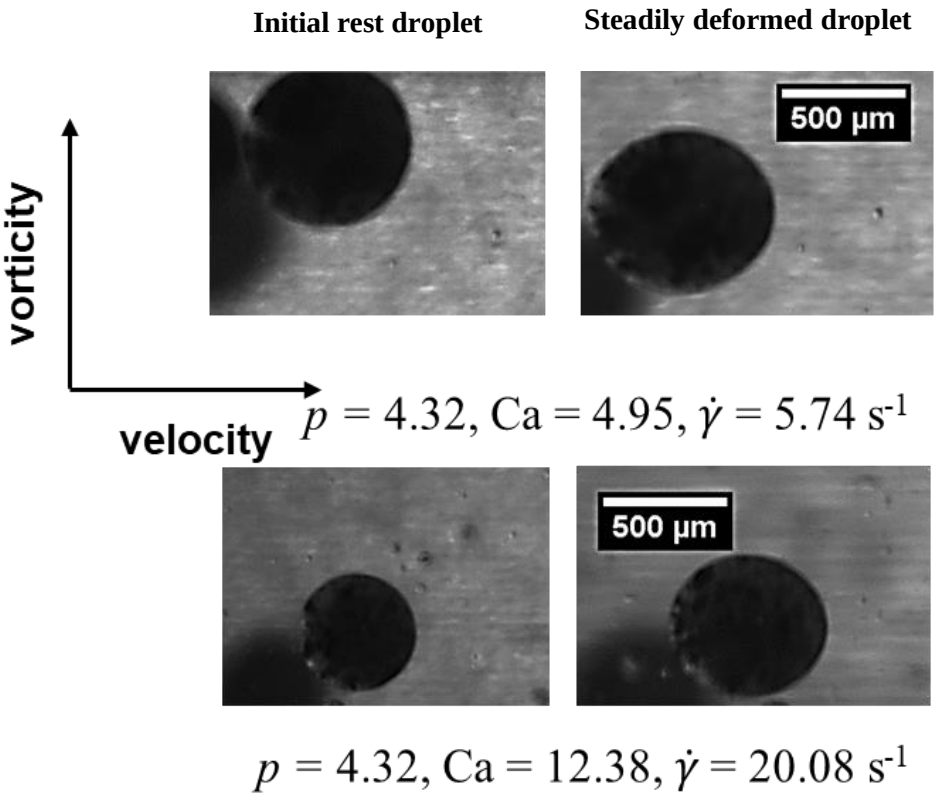

Figure 3-10. Visualization of droplet deformation at ambient room condition at no shear rate (left) and steady state deformation (right) for the immiscible system of *D/M-1*.

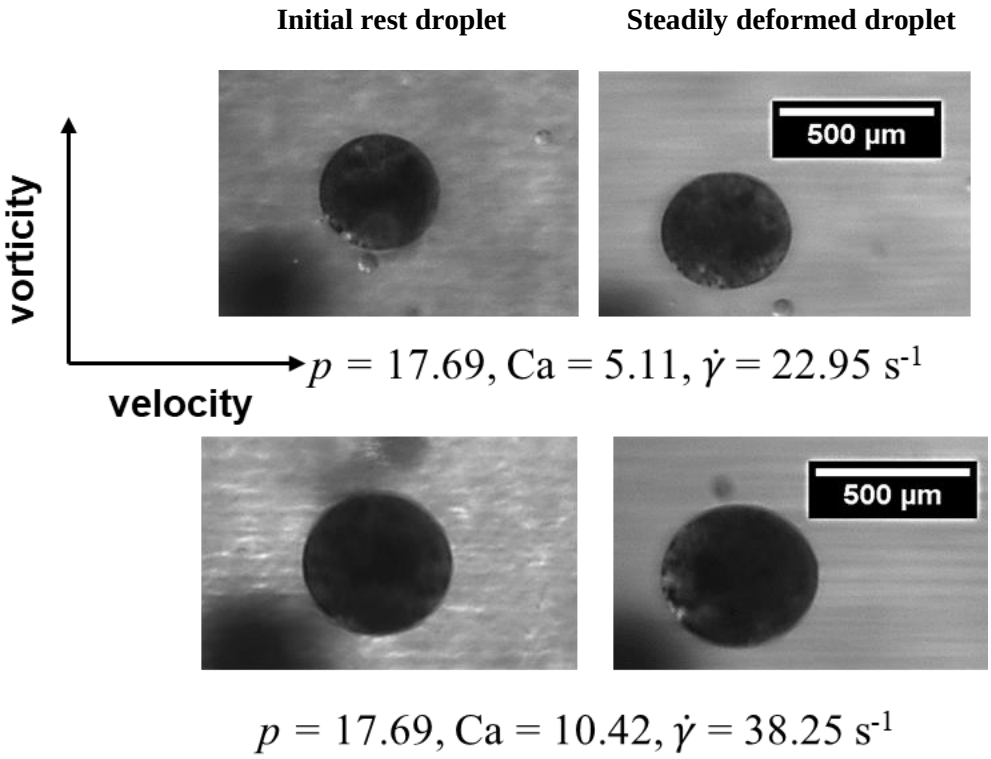

Figure 3-11. Visualization of droplet deformation at ambient room condition at no shear rate (left) and steady state deformation (right) for the immiscible system of *D/M-2*.

At steady-state deformation condition, the images of the observed droplets show that the droplets experience minimal deformation, even at a higher shear rate of 20.08 s^{-1} (Ca = 12.38) for the fluid system of *D/M-1* (Figure 3-10) and 38.25 s^{-1} (Ca = 10.42) for the case of *D/M-2* (Figure 3-11), due to the high degree of their viscosity ratios of 4.32 and 17.69, respectively. The qualitative observation from the droplet's visual images appeared to be consistent with the Newtonian fluid system's deformation condition, that deformation is restricted by their viscosity ratios and can be escalated by the level of shear rate **[2,14]**.

To discuss the droplet's deformation at a different value of Ca, parameter *Def** as described in Eq. (3-23) is then implemented. The results are plotted in Figure 3-12. The *Def** results for

viscosity ratio 4.32, for immiscible fluid system *D/M-1*, is found to be averaged at 0.12 with a minimum value of 0.08 at Ca value of 1.61 and a maximum value of 0.14 at corresponding Ca of 41.46. For the immiscible system of *D/M-2*, having viscosity ratios of 17.69, the range value of *Def** is lower than the former case with an average of 0.08. The minimum value was found at 0.07 for Ca 0.43 and a maximum value of 0.09 for Ca value of 11.92.

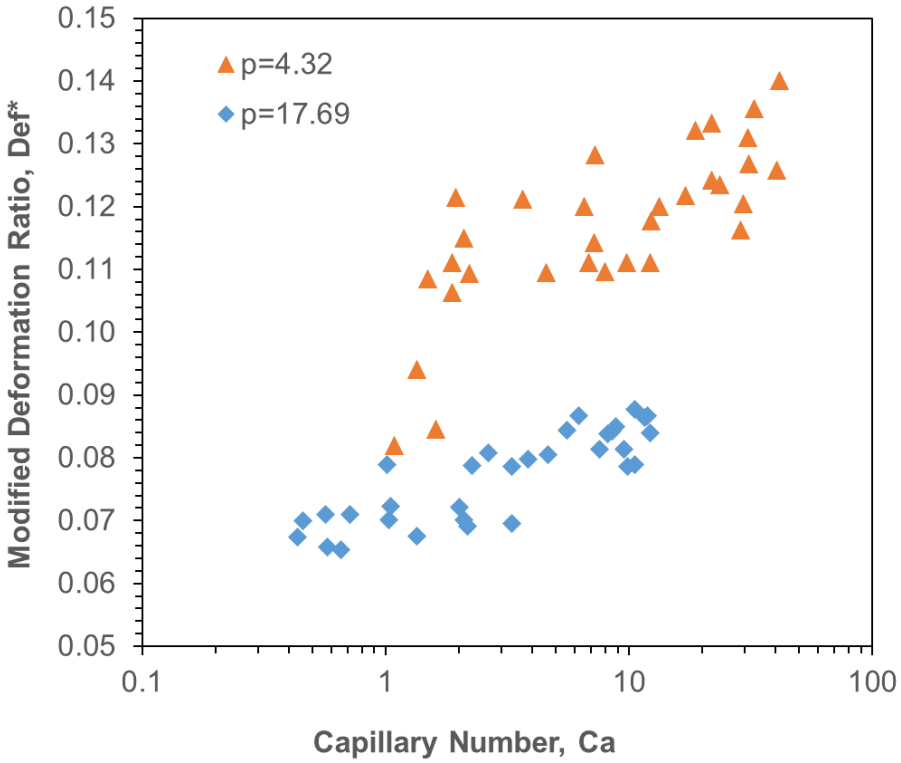

Figure 3-12. Deformation of droplets at ambient temperature is represented as the modified deformation parameter, *Def**.

At the experiment, the interfacial tension between the droplet and matrix phase acts as a counterforce for the hydrodynamic viscous force from the applied shear rate. When the shear rate was strengthened, a larger hydrodynamic viscous force resulted, whereas the interfacial tension was unchanged. This is the condition that drives more droplet deformation if the applied shear was amplified. On the other hand, the higher degree of viscosity ratio reinforces the droplet, acting

more like a solid body. The effect from the higher viscosity factor of the droplet becomes more dominant as the viscosity ratio was magnified, which made the droplet more difficult to deform. The smaller value of *Def** for the case of *D/M-2* verify that the droplet deformation was more suppressed at a higher viscosity ratio.

For both experimental cases, it is observed that small Ca tend to give a more limited deformation or *Def**. More apparent deformation, represented by a higher value of *Def**, is gradually observed along with the increase in Ca. This condition is consistent with the reference that deformation can be escalated by increasing the Ca **[2,14]**. Nevertheless, the escalation of deformation for either case is still very limited due to the high level of viscosity ratio. This is indicated by the value of *Def** that cannot exceed the value of 0.14. Moreover, the deformation is fixed once the droplets reach the steady condition; hence no droplet breakup was possible in this scenario.

The limiting value of viscosity ratio, where no breakup is allowed, is typically found at four. The value was obtained experimentally and valid for the case of a simple shear rate **[2]**. The limiting value of four is also shown in our experimental observation. If the viscosity ratio is lower than four, the degree of droplet deformation was supposedly to take place continuously in proportion to their shear rate until the given shear rate resulted in Ca that exceeds its critical value. In that condition, droplet breakup is expected to happen eventually. A more detailed discussion about the droplet breakup mechanism in the immiscible fluid system is provided by Janssen and Meijer **[15]**.

Due to the viscosity ratio's limiting factor, the droplet breakup condition cannot be attained in the current experimental investigations, even at a high value of Ca. It is suggested that at this region of no droplet breakup, the addition of a surfactant may not give a significant impact, as the surfactant effect is reported to diminish sharply along with the increase in the viscosity ratio **[16]**. The selective radiation method will then be implemented in these cases with a limiting viscosity ratio to shift their viscosity ratio to below the limiting value of four.

3.5. Droplet deformation under selective radiation heating

The initial experimental condition was identical with previous observation at ambient room temperature that the droplet deformation was severely restricted by the high order of viscosity ratios and fixed once it reached the steady-state condition. The laser irradiation was then given to the droplet to investigate its evolution under such conditions. The observation was first carried out in the case of droplets without the aid from special absorbing dye to check the feasibility of the selective radiation method at a low absorption coefficient. The later experiments investigated the droplet deformation under radiation heating as described earlier in section 3.3.2.2.

3.5.1. Droplet deformation on non-dyed droplet

The selected viscosity ratio was set at both fluid systems *D/M-1* and *D/M-2*, having initial viscosity of 4.32 and 17.69, respectively. The laser intensity was then set from 10.92 to 218.32 W/cm^2 at a shear rate of 3.8 s^{-1}. The results for this test experiment are then given in Figure 3-13 and Figure 3-14.

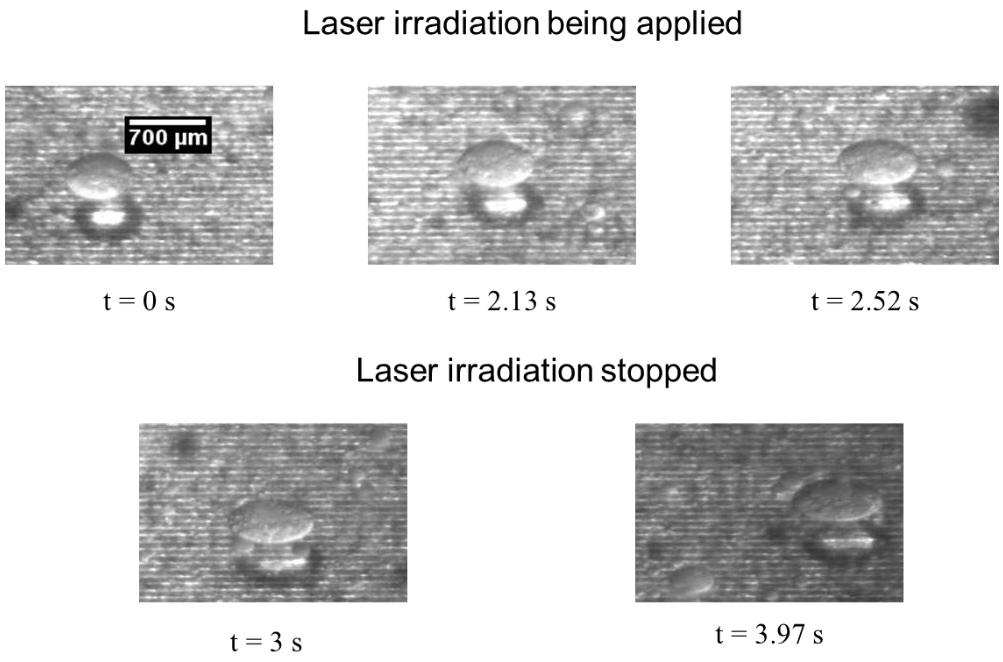

Figure 3-13. Example of a non-dyed Polybutenes droplet under laser irradiation for initial viscosity ratio of 4.32 at Ca = 1.81 and laser intensity 218.32 W/cm^2; the laser irradiation period was at time 0 to 2.52 s.

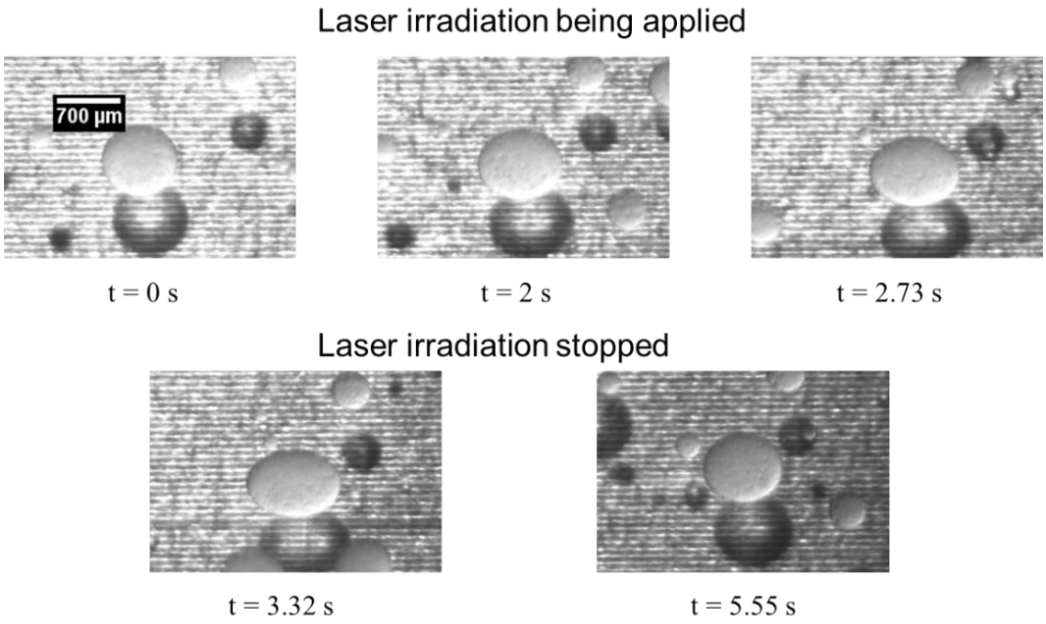

Figure 3-14. Example of a non-dyed Polybutenes droplet under laser irradiation for initial viscosity ratio of 17.69 at Ca = 0.85 and laser intensity 218.32 W/cm^2; the laser irradiation period was at time 0 to 2.73 s.

It was found that even in the case of a very low absorption coefficient (droplet phase β = 17.07 m^{-1} and matrix phase β = 11.54 m^{-1}), the enhancement of droplet deformation was possible, although the improvement was quite modest. The droplet was visibly more elongated during the implementation of direct radiation heating. The droplet then contracted back to its initial shape once the heat source was cut. This suggests that the addition of absorption coefficient enhancer substance was not mandatory, as long as the provided irradiation source is within the attenuated region of the droplet phase, as explained in the previous chapter.

The addition of special IR absorbing dye on the following experiment was due to the fact that the only available laser source for the experiment was in the low IR region of 1.07 μm so that better discussion of the selective radiation method can be made available.

3.5.2. Droplet deformation on dyed droplet

3.5.2.1.Laser Intensity Parameter

Figure 3-15 shows the visualization examples of the droplet behaviors when radiation heating is applied for the immiscible system *D/M-1*. The laser irradiation at a different level of intensity was uniformly applied for 2 seconds before finally turned off. In the first fluid system of *D/M-1*, having an initial viscosity ratio of 4.32, the droplet was visibly experiencing a significant deformation enhancement and even reached breakup at a shear rate of 1.91 s^{-1}, the lowest shear rate made by the Couette apparatus. The applied shear rate corresponds to the Ca value of 1.75 – 2.23, this variation in Ca was determined by the specific size of the irradiated droplets that ranged at 470 - 740 μm.

This condition contrasted with the cases at ambient room temperature. At a similar range of Ca, the droplet deformation was limited at the *Def** value of about 0.11 (Figure 3-12). Without the laser irradiation intervention, such a significant deformation that leads to the breakup was not possible even at the high range of Ca (Ca > 20). At the isothermal ambient room temperature condition, the deformation was severely restricted by the viscosity ratio regardless of the applied shear rate or the resulting Ca.

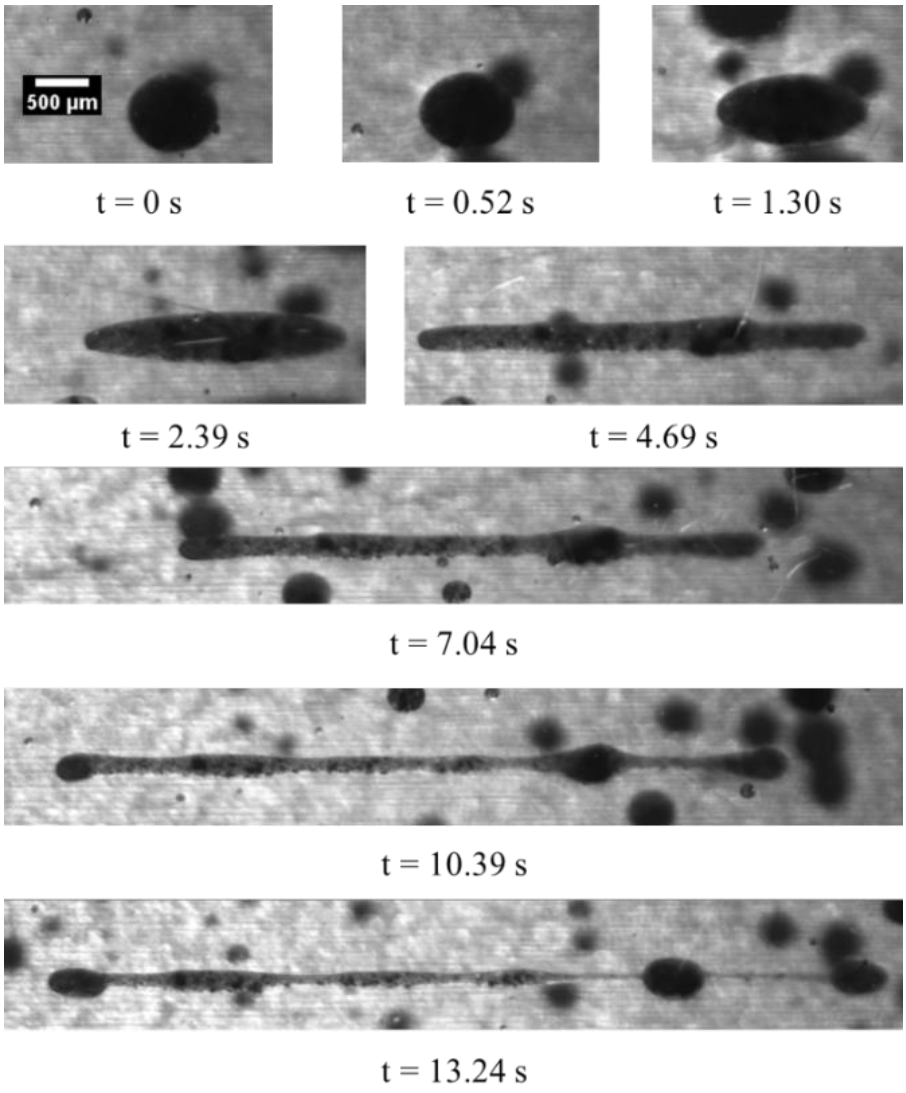

Figure 3-15. Droplet deformation of an immiscible system by selective radiation at Ca = 1.75 for D/M-1 with initial p = 4.32 at room temperature; the laser irradiation period was at time 0 to 2 s.

Measurement of the droplet elongation using the *Def** parameter was implemented for the irradiated droplet and presented in Figure 3-16 and Figure 3-17 for the immiscible fluid system of *D/M-1* and *D/M-2*, respectively. Although the laser's irradiation lasted only for the first couple of seconds, the droplets continuously experienced deformation and reached breakup even after the laser was turned off. The laser irradiation was sufficient to modify the constraining factor from the viscosity ratio. It was implied that the fluid viscosity was indeed shifted, which subsequently led to forming a critical capillary number requirement that corresponds with the new viscosity ratio. This newly emerged Ca_c can be overcome easily by the smallest shear rate produced by the Couette cylinder apparatus.

However, at the highest laser intensity of 87.33 W/cm2, a minor bursting of bubbles was observed from the Polybutenes droplet. For a moment, these formations of bubbles slightly disrupt the droplet's deformation, but the droplet can immediately return to its typical elongated form so that clear images of the deformed droplet can still be acquired. The bubbles are most likely come from a very fine air droplet trapped during the pre-mixing of the droplet and matrix phase before insertion into the Couette apparatus. When the given laser intensity was high enough, the air bubbles were rapidly expanding and bursting out from the droplet due to the sudden rising in the temperature. At laser intensity lower than 87.33 W/cm^2, the formation of air bubbles was not significantly perturbating the observation for the immiscible system of *D/M-1*. However, the bubbles bursting was quite dominant in the immiscible system of *D/M-2* and will be explained promptly in the discussion part of the *D/M-2* experiment.

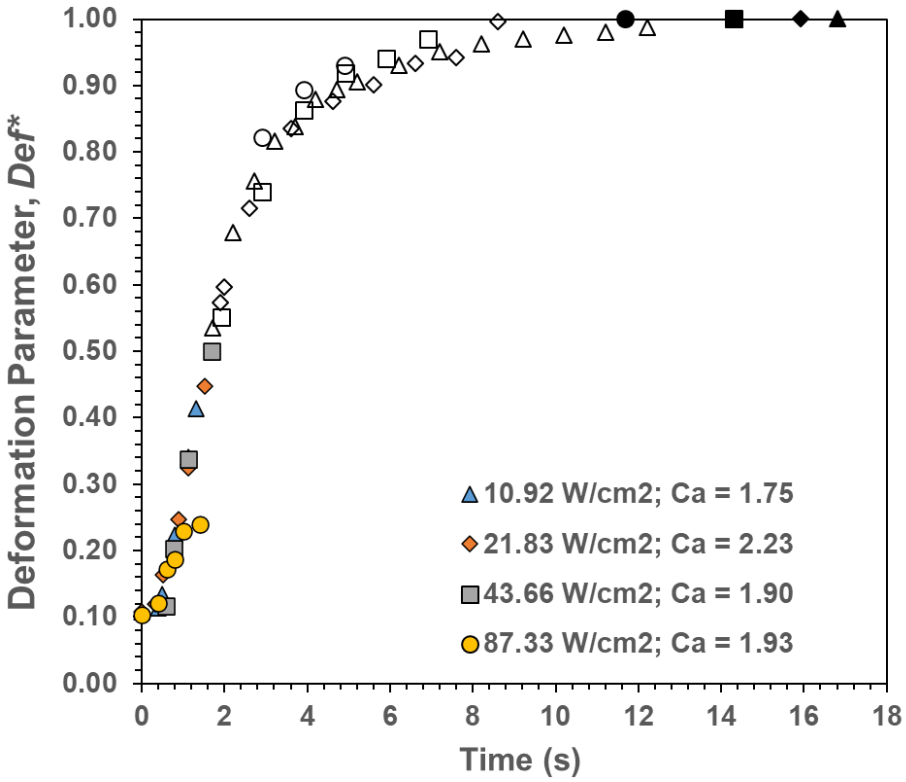

Figure 3-16. Modified deformation parameter, *Def** under selective radiation for case D/M-1 with initial p = 4.32 at room temperature; filled marker represents deformation during the irradiated period, blank marker represents deformation after laser irradiation is turned off, and dark marker signed the breakup point.

For the cases of *D/M-2* with an initial viscosity ratio of 17.69, the employed matrix phase's viscosity, *M-2*, was much lower than the matrix phase of the previous experimental condition, *M-1*, so that for the same shear rate, the *D/M-2* fluid system will have a significantly smaller Ca compared with the *D/M-1* fluid system. The smaller Ca substantially affected the ability of the immiscible system to allow the droplet deformation. At the Couette cylinder's lowest shear rate of 1.9 s^{-1}, no enhancement in droplet deformation was observed even when the laser irradiation was applied.

The droplet deformation happened when the shear rate was doubled into 3.8 s^{-1}, as showed in Figure 3-17. Nonetheless, not all irradiated droplets were able to continuously deform after the heat source was stopped. In some droplets, the deformation enhancement only lasted during the irradiation period. Once the irradiation source was cut, those droplets slowly retracted back to their steadily deformed shape. After the absence of the heat source, the retraction was suggested to be happened due to the rapid temperature dissipation after the irradiation was stopped. At this specific condition, the modification of the viscosity ratio from selective radiation was diminished along with temperature diffusion to the ambient temperature, and as a result, the viscosity ratio reverted to its initial state. If the applied Ca was sufficient to outpace the reversing effect, the droplet could reach an extended elongation and reach breakup.

A droplet with a smaller diameter size was more likely to be retracted to its initial shape, as the absorbed thermal energy dissipates faster in the smaller droplet compare to the larger one. Moreover, a smaller droplet will give a smaller Ca for the same given shear rate. The smaller droplet with diameter 530 μm (Ca = 0.60) experienced the retraction, while the larger droplet (diameter = 720 μm and Ca = 0.82) was continuously deformed and break. The combination of rapid temperature dissipation and smaller Ca suggests that the selective radiation method was less effective in the smaller droplet size. This condition differed from the conventional method of surfactant implementation, where the added surfactant can only start to work once the dispersed phase is on a much smaller scale **[17]**. Prolonging the laser irradiation for a few more hundreds of milliseconds was found to prevent the retraction for a certain droplet (> 550 μm).

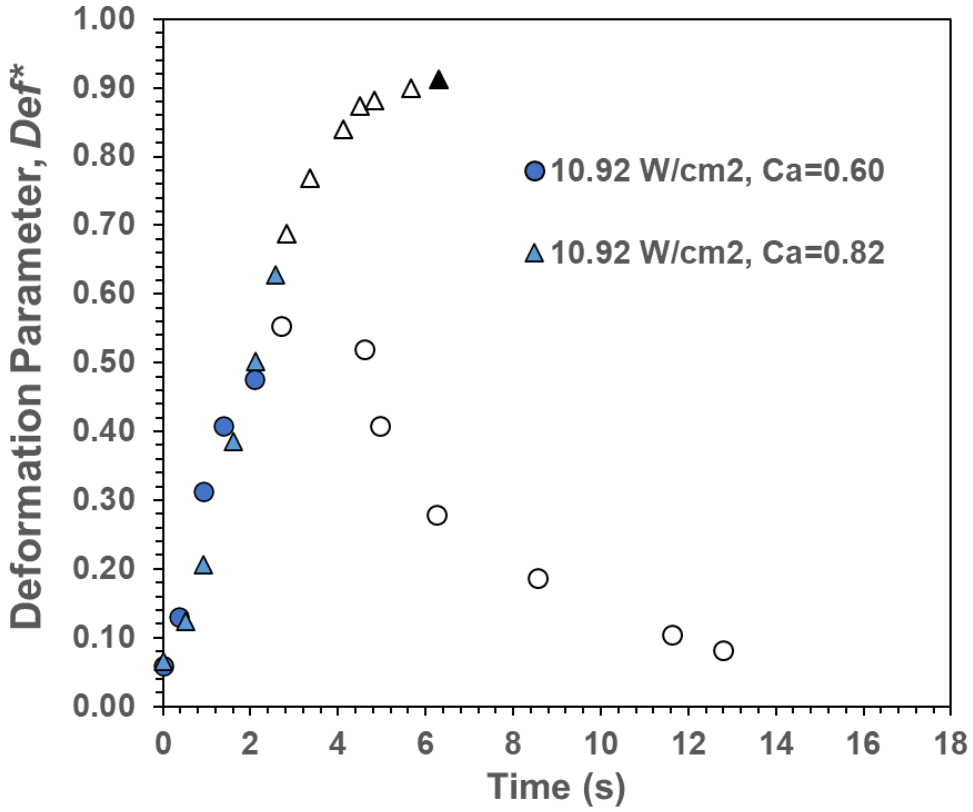

Figure 3-17. Modified deformation parameter, *Def** under selective radiation for case *D/M-2* with initial p = 17.69 at room temperature; filled marker is deformation during the irradiated period, blank marker represents deformation after laser irradiation is turned off dark marker signed the breakup point.

For the immiscible fluid of *D/M-2*, however, the formation of air bubbles was much more prevalent than in the *D/M-1* fluid. The bubbles were immediately formed and always occurred at a laser intensity of 21.83 W/cm^2 and higher. The bubbles bursting was more intense and violent in higher-level laser intensity, as provided in Figure 3-18. In this case of a higher viscosity ratio, the formation of the more prevalent bubbles seemingly comes from the finer and much higher number of air droplets trapped in the pre-mix step. The *M-2* fluid has a much lower viscosity so that air bubbles are more prone to be formed during the pre-mixing phase. Many of these finer and more

abundant air bubbles can be trapped inside the droplet phase and are very sensitive to the sudden temperature changes inside the droplet. Therefore, even at a moderate level of laser intensity, air bubbles can immediately burst out from droplets in a foam like shape and become more intense with the increase in laser intensity. Due to this condition, presentable images for *Def** calculation cannot be acquired for cases with a laser intensity of 21.83 W/cm^2 and higher. Nevertheless, the droplet elongation and breakup trace can still be seen in the droplet image at t = 3.80 s in Figure 3-18 below.

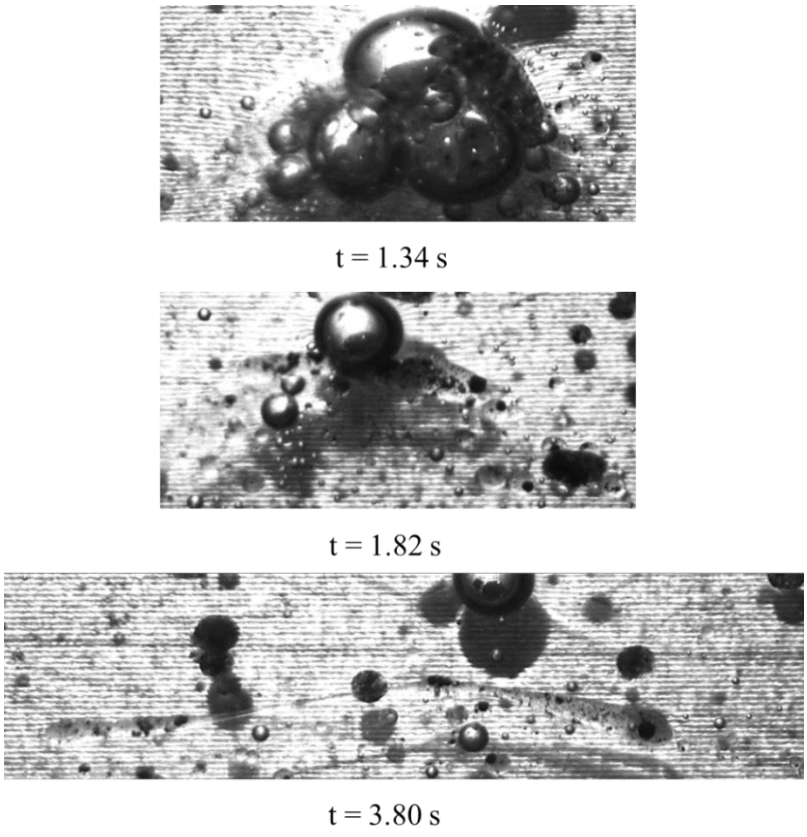

Figure 3-18. The burst of air bubble for a droplet in an immiscible system of *D/M-2* with initial parameter p = 17.69 at room temperature; the laser irradiation intensity was 87.33 W/cm^2. The laser irradiation period was at time 0 to 2 s.

3.5.2.2. Total Energy Parameter

The laser irradiation experiment continued for the second mode. In this case, the droplet phase also immediately experiences a significant deformation and eventually reached a breakup, with example results shown in Figure 3-19. The deformation and breakup occurred at a flow shear rate of 1.9 s^{-1}, the lowest shear rate that the Couette cylinder can produce. In the current work, the droplet was also continuously elongated after the laser source was turned off.

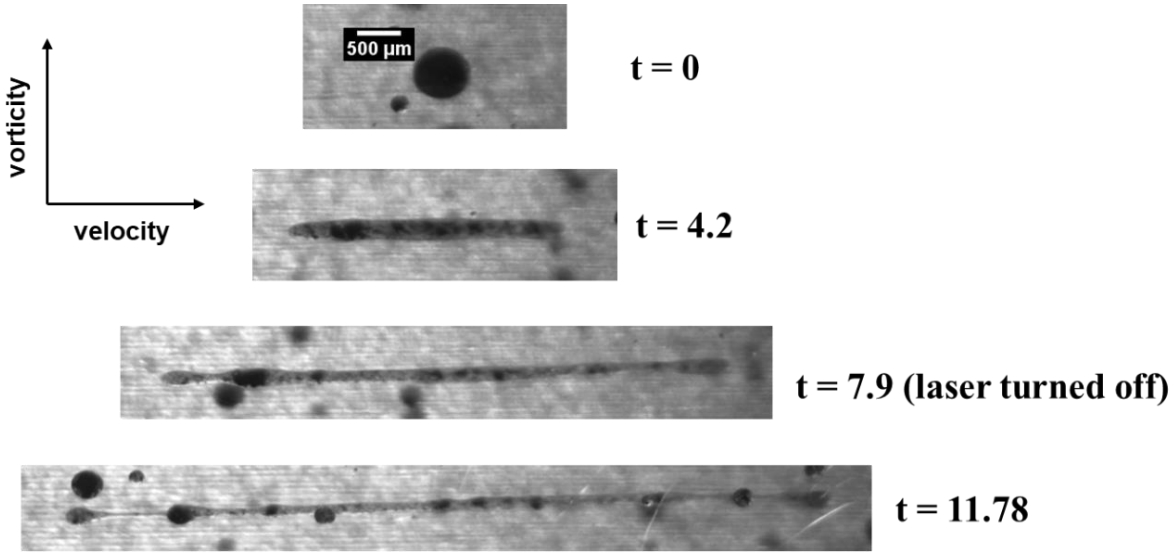

Figure 3-19. Droplet deformation at Ca = 1.23 with initial p = 4.32 at ambient room temperature of 25° C. Laser irradiation period was from 0 to 8 s.

The experimental observation then proceeds for a different level of laser intensity and irradiation. Figure 3-20 summarized the droplet deformation in terms of *Def** for the specified experimental conditions. For the initial case of the viscosity ratio of 4.32 (*D/M-1*), the observed droplets (droplet size 540-610 μm) were continuously elongated and reached breakup even for different laser intensities and irradiation periods. It was observed that the breakup point occurred earlier for droplets with the highest (87.33 W/cm^2) and second highest (43.66 W/cm^2) laser

intensity. Even though the irradiation period was the shortest at the mentioned intensity level, it lasted only for 1 and 2 seconds, respectively. At this moderately high viscosity ratio, it seemed that all the applied laser irradiation was adequate to alter the initial viscosity ratio. It was also implied that the laser intensity level was much more prevalent than the heating period, indicated by the early breakup reached in the higher-level laser intensity. Furthermore, the laser irradiation effect takes place immediately, once the temperature disparity between droplet and matrix was sufficient to accommodate viscosity ratio modification and supported with an adequate level of shear rate, the deformation enhancement and breakup was reached regardless of the irradiation period.

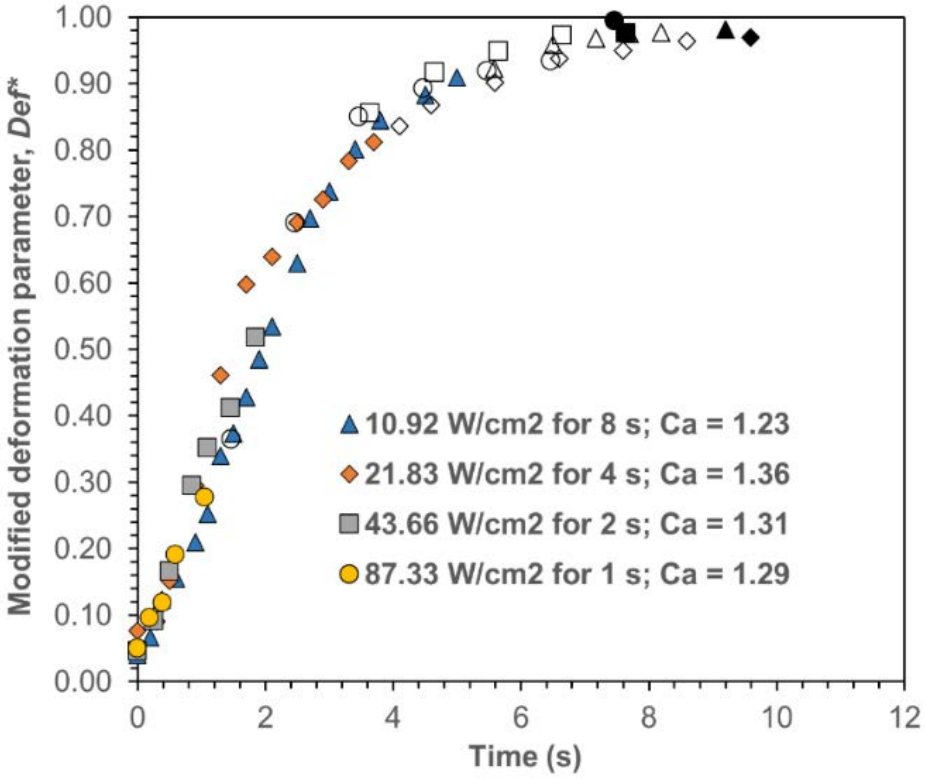

Figure 3-20. The modified deformation parameter, *Def** for the case of initial $p = 4.32$ at ambient room temperature. The filled marker signed the irradiated period, the blank marker signed the period after laser irradiation is turned off, and the dark marker signed the breakup point.

For the cases of *D/M-2* (17.67), At Couette cylinder's lowest shear rate of 1.9 s^{-1}, no enhancement in droplet deformation (droplet size 580-790 μm) was visually observed even when the laser irradiation was applied as plotted in Figure 3-21, this condition is identical to the previous mode of the experiment. Even though, at a laser intensity of 10.92 $W/cm^{2,}$ the irradiation period extends into 8 s. Only when the shear rate was increased to 3.8 s^{-1}, noticeable changes appeared in the droplet deformation. At the laser intensity of 10.92 W/cm^2 and 8 s irradiation period, the droplet was deformed significantly during the laser irradiation, but it slowly retracted to its initial form in the absence of laser irradiation. On the subsequent observation, at the same laser implementation, the continuous droplet deformation was observed instead. This behavior was similar to the experiment at p = 4.32, some droplets can reach breakup point even when the laser radiation was cut, but others reversed back to their steadily deformed shape once the heat source was turned off. This implied that even in the case of a very high viscosity ratio, the laser was able to shift the initial viscosity ratio in both cases of moderately high (4.32) and very high initial viscosity ratio (17.69). However, the smaller Ca result in the latter case may still be insufficient for some droplets to realize the breakup condition.

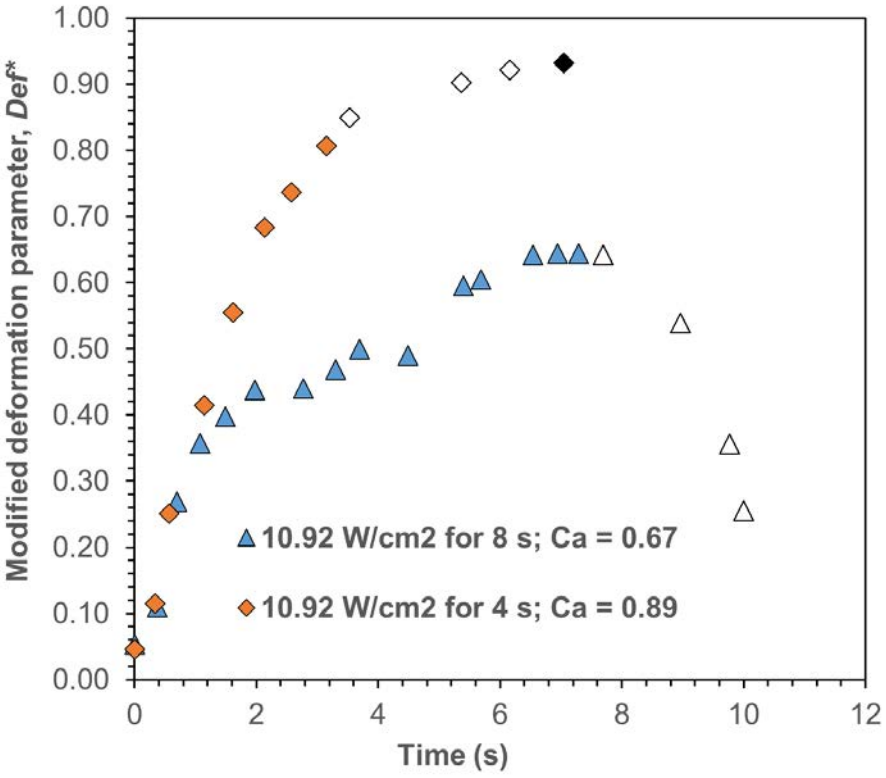

Figure 3-21. The modified deformation parameter, *Def** for the case of initial $p = 17.69$ at ambient room temperature. The filled marker signed the irradiated period, the blank marker signed the period after laser irradiation is turned off, and the dark marker signed the breakup point.

3.5. Conclusion

The investigation of the droplet deformation under the selective radiation heating method was carried out to confirm the proposed method's feasibility to alter the droplet dispersion via a thermo-physical approach. The mean range of the droplet deformation parameter, *Def**, is limited to 0.11 and 0.06 at ambient temperature conditions for an initial viscosity ratio of 4.32 and 17.69. Visualization of the droplet under selective radiation has been performed and confirms the deformation improvement during the irradiation process. The experimental investigation has shown that the selective radiation method can enhance the droplet deformation and even allows droplet breakup. At a moderate level of viscosity ratio of 4.32, the selective radiation can be

applied effectively, and no droplet retraction was observed. However, at a higher range of viscosity ratio of 17.69, both droplet elongation-breakup and droplet retraction were observed. The prolonged elongation of the irradiated droplet and their breakup is inextricably linked to the shifting of viscosity ratio and the emerging of critical capillary numbers. In the current state of experimental investigation, however, accurate temperature data cannot be provided yet. The current approach of using thermocouple wire cannot capture the droplet and matrix phase temperature separately and accurately. So, independent work for describing the temperature distribution is suggested to be carried out for better understanding and developing the selective radiation heating method.

Further study is needed to be carried out to advance the current result. The subsequent work needs to describe the temperature distribution information resulting from selective radiation heating. The temperature distribution data is essential for the viscosity and critical capillary number prediction to understand this phenomenon better.

3.6. References

1. Taylor, G.I., "The Formation of Emulsions in Definable Fields Flow," Proceedings of The Royal Society of London. Series A, Containing Papers of Mathematical and Physical Character, 146, 501, (1934).
2. Grace, H. P., "Dispersion Phenomena in High Viscosity Immiscible Fluid Systems and Application of Static Mixers as Dispersion Devices in Such Systems," Chemical Engineering Communications, 14, 225, (1982).
3. De Bruijn, R. A., "Deformation and Breakup of Drops in Simple Shear Flows," PhD Thesis, Technicshe Universtiteit Eindhoven, Netherlands, (1989).

4. Rumscheidt, F. D., and Mason, S. G., “Particle Motions in Sheared Suspensions XI. Internal Circulation in Fluid Droplets (Experimental),” Journal of Colloid Science, 16, 201, (1961).
5. Mighri, F. and Huneault, M.A., “Dispersion Visualization of Model Fluids in a Transparent Couette Flow Cell,” Journal of Rheology, 45, 783 (2001).
6. Verhulst, K., Moldenaers P., and Minale, M., “Drop Shape Dynamics of a Newtonian Drop in a Non-Newtonian Matrix During Transient and Steady Shear Flow,” Journal of Rheology, 51, 216 (2007).
7. Sibillo, V., Pasquariello, G., Simeone, M., Cristini, V., Guido, S., “Drop Deformation in Microconfined Shear Flow,” Physical Review Letter, 97, 054502 (2006).
8. Torza, S., Cox, G., Mason, S. G., “Particle motions in Sheared Suspensions XXVII Transient and Steady Deformation and Burst of Liquid Drops,” Journal of Colloid Interface Science, 38, 395, (1972).
9. Megias-Alguacil, D., Feigl, K., Dressler, M., Fischer, P., and Windhab, E.J., “Droplet Deformation Under Simple Shear Investigated by Experiment, Numerical Simulation and Modelling,” Journal of Non-Newtonian Fluid Mechanics, 126, 153, (2005).
10. Mighri, F., Carreau, P. J., and Ajji, A., “Influence of Elastic Properties on Drop Deformation and Breakup in Shear Flow,” Journal of Rheology, 42, 1477, (1998).
11. Almusallam, A. W., Larson, R. G., and Solomon, M. J., “A Constitutive Model for the Prediction of Ellipsoidal Droplet Shapes and Stresses in Immiscible Blends,” Journal of Rheology, 44, 1055 (2000).
12. Cherdhirankorn, T., Lerdwijitjarud, W., Sirivat, A., and Larson, R.G, “Dynamics of Vorticity Stretching and Breakup of Isolated Viscoelastic Droplets in an Immiscible Viscoelastic Matrix,” Rheologica Acta, 43, 246 (2004).

13. Tanpaiboonkul, P., Lerdwijitjarud, W., Sirivat, A., and Larson, R.G., "Transient and Steady-State Deformations and Breakup of Dispersed-Phase Droplets of Immiscible Polymer Blends in Steady Shear Flow," Polymer, 48, 3822 (2007).
14. Taylor, G.I., "The Viscosity of a Fluid Containing Small Drops of Another Fluid," Proceedings of The Royal Society of London. Series A, Containing Papers of Mathematical and Physical Character, 138, 41, (1932).
15. Janssen, J. M. H. and Meijer, H. E. H., "Droplet Breakup Mechanisms: Stepwise Equilibrium Versus Transient Dispersion," Journal of Rheology, 37, 597 (1993).
16. Milliken, W. J., Stone, H. A., and Leal, L. G., "The Effect of Surfactant on the Transient Motion of Newtonian Drops," Physics of Fluids A, 5, 69 (1993).
17. Utracki, L.A., "Polymer Blends Handbook," Kluwer Academic: Dordecht, (2003).

4. Chapter 4: Droplet Breakup of a High Viscosity Ratio System in a Non-Isothermal Field Under Laser Irradiation

4.1. Introduction

The deformation and breakup of an immiscible droplet under simple shear flow is known to be governed by two dimensionless parameters, the viscosity ratio (p) and the capillary number (Ca). If the Ca is small, the droplet and matrix phase's interfacial stress is more dominant, resulting in a steady ellipsoidal droplet **[1-7]**. When Ca exceeds a certain critical point (Ca_c), the droplet will become unstable and eventually break. The experimental investigation from Grace showed the dependency of Ca_c to the parameter p **[8]**. It was found that no droplet breakup is possible at the region of $p > 4$, regardless of the applied Ca. Meanwhile, the droplet is easily deformed and breaks from a simple shear flow at the region of $p \approx 1$.

At the ideal region of $p \approx 1$, the droplet breakup mechanism is exhibited by the continuous elongation of an ellipsoidal droplet along the flow direction. As the elongation was continued, the droplet's midsection is shrinking, and eventually, the two ends of the droplet break apart, leaving a modest size satellite droplet in between. The described breakup condition typically occurs at $p \approx 1$, so this breakup mechanism is also known as the ideal breakup at the equilibrium of both viscosities **[9-13].** The droplet's minimum size for reaching the required Ca_c to realize a breakup condition can be derived from the correlation plot of Ca_c and p. By knowing the material properties, the applied shear, and the additional assumption that the droplet breaks into two equal parts without leaving a satellite droplet, the final droplet size is defined as following **[9]**:

$$R_{\text{drop}} = \frac{\text{Ca}_\text{c}}{\eta_m \dot{\gamma}/_\sigma} 2^{-\frac{1}{3}} \tag{4-1}$$

Where R_{drop} is the estimated maximum size of the droplet after the breakup, η_m is the matrix phase viscosity, $\dot{\gamma}$ is the applied shear rate, and σ is the interfacial tension between the immiscible fluid component.

However, a droplet breakup in an actual mixing process can follow a transient breakup mechanism rather than a stepwise multiple equilibrium breakup. In the transient mode, the droplet is continuously elongated into and forms a thin thread. The long thread then breaks into multiple droplets at once, rather than split into two likes in the ideal condition mentioned earlier. The illustration for both breakup mechanisms is illustrated in Figure 4-1.

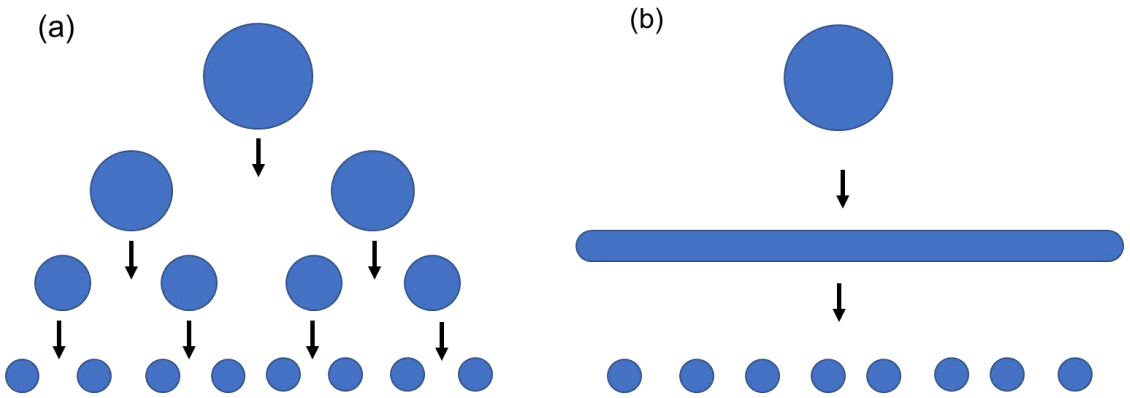

Figure 4-1. Schematic of the droplet breakup mechanism for (a) a multiple stepwise equilibrium breakup at Ca_c and (b) transient breakup mechanism of long thread during flow. The image is adapted from an illustration in **[9]**.

The experimental investigation showed that the transient breakup mode was developed in the form of a long thin tread when $Ca/Ca_c > 2$ for a simple shear condition **[9,12,13]**. At this breakup condition, the applied shear is found to suppress the growth of instability on the interface region, thus facilitates the forming of an elongated thread rather than a direct breakup. The thread needs to be considerably thin before it can be splintered into multiple droplets **[14-16]**. A long thin thread's disintegration is also exhibited for the case involving geometry confinement, especially in an immiscible system with parameter p higher than the equilibrium ($p \approx 1$) **[17-20]**.

In the case of $p > 1$, the Ca_c requirement for the droplet breakup in a confined space is shown to be lower than the droplet in bulk condition, and the degree of confinement is proportional with the decrease in the Ca_c requirement. For $p < 1$, the confinement resulting in the opposite effect, i.e., the Ca_c is instead found to be increased rather than decrease, makes the droplet more difficult to break **[18,19]**.

The experimental work and discussion in the previous chapter 3 have confirmed the steady deformation with no breakup condition of the immiscible droplet system at region $p > 4$. The limiting condition from the viscosity ratio was then able to be outmaneuvered by the proposed selective radiation method. The influence of direct heat radiation from an infrared laser was suggested to successfully shift the viscosity ratio into a region lower than the limiting value of four. This modification of the viscosity ratio directly resulted from the non-isothermal field in the immiscible droplet system, which was then exploited by the viscosity's temperature dependence nature.

However, the droplet temperature distribution report under the selective radiation process was still absent from the previous chapter's discussion. The acquisition of the non-isothermal field of the laser-irradiated immiscible droplet was quite challenging to provide experimentally. Therefore, a numerical simulation of unsteady heat transfer is then implemented in this chapter to estimate the temperature distribution. The estimated temperature distribution will be used to approximate the level of viscosity ratio modification and their correlating Ca_c requirement. The droplet breakup mechanism analysis will also be included in this part in relation to the tuning of the viscosity ratio from the laser radiation heating method. Finally, a brief section discussion for applying the selective radiation method is added later in this chapter.

4.2. Numerical Simulation Scheme

In the discussion of the previous chapter, it was found that the effect of viscosity changes from laser irradiation happened immediately in the early stage of the shearing, and the impact from irradiation still lasted even when the heat source was absent. Therefore, considering this immediate effect, several simplification assumptions were then applied for the numerical scheme. The flow was not considered in the simulation. Additionally, the irradiated laser's scattering was also not included, nor the internal radiation from temperature distribution. The physical properties of the droplet and matrix phase were taken as constant. The governing equation then can be defined as follows:

$$\rho_{\mathrm{sub}} c_{\mathrm{sub}} \frac{\partial T_{\mathrm{sub}}}{\partial t} = \frac{\partial}{\partial x}\left(k_{\mathrm{sub}} \frac{\partial T_{\mathrm{sub}}}{\partial x}\right) + \frac{\partial}{\partial y}\left(k_{\mathrm{sub}} \frac{\partial T_{\mathrm{sub}}}{\partial y}\right) + \frac{\partial}{\partial z}\left(k_{\mathrm{sub}} \frac{\partial T_{\mathrm{sub}}}{\partial z}\right) + E_{\mathrm{sub}} \qquad (4\text{-}2)$$

(sub: droplet or matrix phase fluid)

The heat radiation was introduced and move in the *x*-axis direction so that the heat source term can be described as:

$$E_{\mathrm{sub}} = \left|\frac{\partial I}{\partial x}\right| = \beta_{\mathrm{sub}} I_o \exp(-\beta_{\mathrm{sub}} x) \qquad (4\text{-}3)$$

The numerical simulation was performed using ANSYS 18.2. The numerical simulation was carried out in a three-dimensional computational domain, as shown in Figure 4-2. The length of the computational domain, defined as L, was set at 4000 μm. The length L, in the horizontal axis-x, is equal to the width of the Couette cylinder. The length of the domain in the direction of axis-y and axis-z set at 5.4L corresponds to the irradiation beam's size. The droplet size, defined as d, in the numerical domain was varied from 300 to 800 μm.

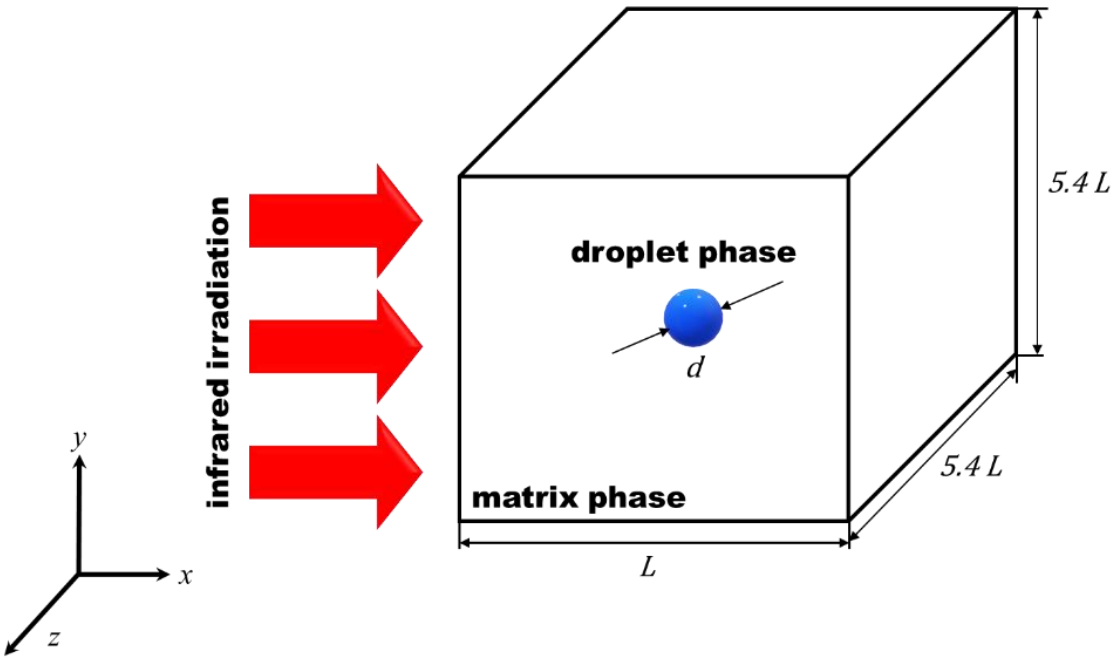

Figure 4-2. Computational domain of the numerical simulation for the estimation of temperature field.

In the ANSYS module, direct conversion from the attenuated energy source as a volumetric energy generation is not immediately available. Therefore, the governing energy equation in Eq. (4-2) and its heat source term described in Eq. (4-3) are needed to be determined first by an analytical calculation. In this calculation, the droplet was sliced into many segments having an equal thickness. Each segment, except for the most edge segment, is then further constructed into a ring-like shape domain, representing the surface of the sphere directly contacted with the heat radiation source, the image of the segmented droplet geometry is shown in Figure 4-3.

The calculation provided the thermal energy generation's magnitude at each segment for a different laser intensity level. The highest absorption region is supposedly located at the front-end segment that faces the applied irradiation source. The laser intensity will gradually decrease as it is absorbed along the droplet's irradiation path and reaches the lowest value at the most back-end

segment. The computational domain of the droplet in the simulation was also appropriately set in the segmented geometry. Therefore, each segment was assigned to the corresponding thermal energy absorbed from the analytical calculation, translating as the ANSYS module's volumetric thermal generation. A calculation with a similar principle was also performed for the matrix phase as well. Therefore, the volumetric heating magnitude corresponds to the attenuated radiation was also implemented in the matrix phase.

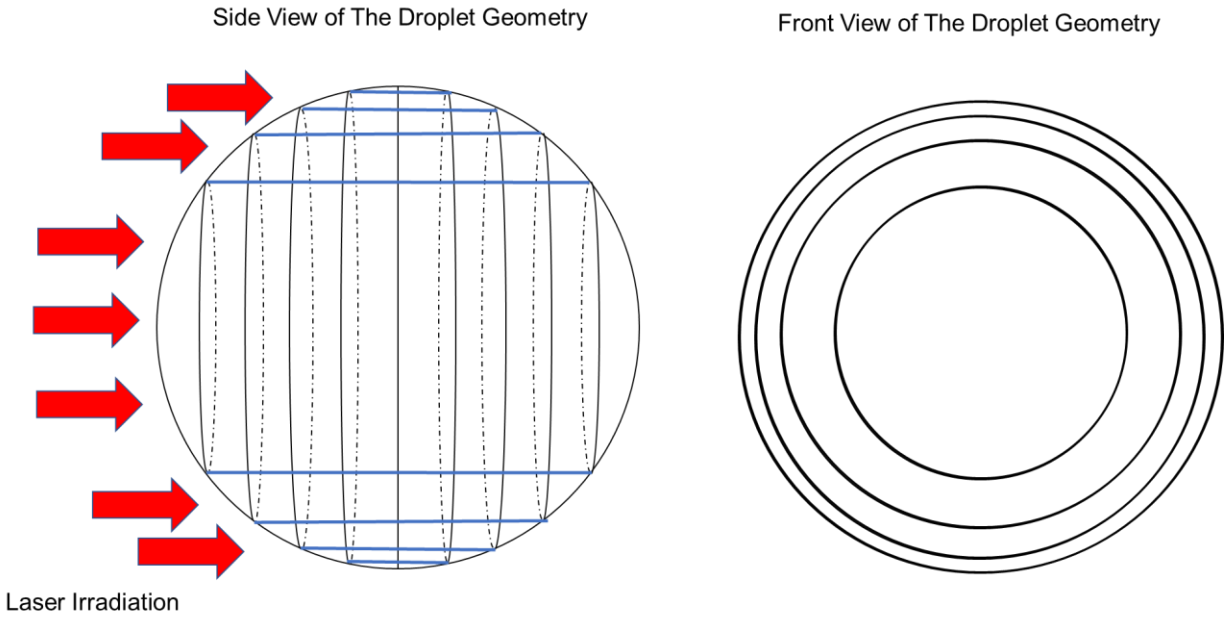

Figure 4-3. The image of the segmented droplet geometry.

The laser irradiation level and period were set following the experimental parameter explained in chapter 3. The simulation parameters were the laser intensity parameter, irradiation on different intensity levels at uniform irradiation period, and the total energy parameter, irradiation on different intensity levels but at varying irradiation periods resulting in uniform total energy.

4.3. Estimation of the non-isothermal field on the immiscible droplet

4.3.1. Laser Intensity Parameter

Figure 4-4 shows the example for the temperature field obtained from the numerical simulation at a droplet size of 500 μm. The droplet part facing the irradiation path has the highest thermal absorption. Thus, the maximum temperature contour is concentrated in that region. Due to the comparatively much lower value of the absorption coefficient, the matrix phase temperature was relatively unaffected, except in the interface region surrounding the droplet.

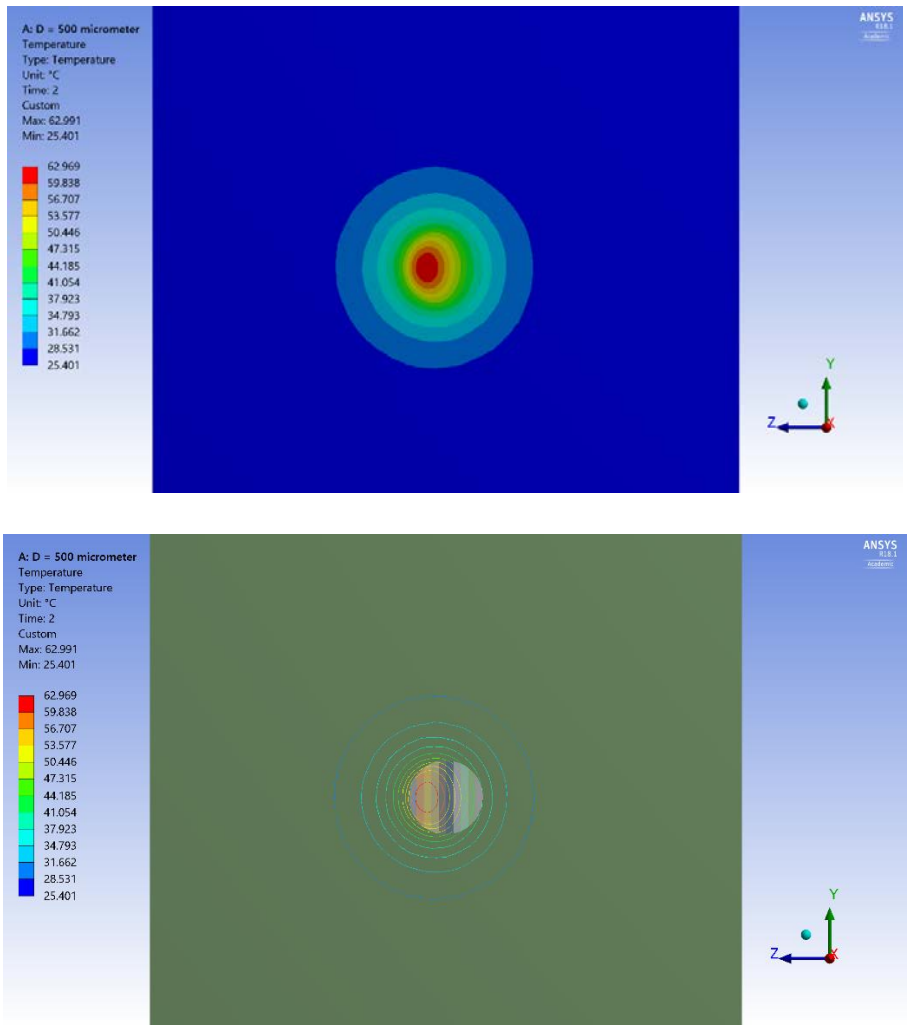

Figure 4-4. Example of the temperature change presented in contour (upper) and isoline (lower) obtained from the simulation, for the case of d = 500 μm and I_0 = 10.92 W/cm^2 at t = 2 s.

In the current uniform irradiation period's condition, it was expected that the temperature change would be determined solely from the laser intensity level. However, the droplet size has also affected the temperature distribution level, as shown in Figure 4-5 to Figure 4-7. The temperature increase happened rapidly as soon as the heat radiation was employed, with the resulting maximum temperature is in proportion to the laser intensity level. At the lowest laser intensity level of 10.9 W/cm^2, the droplet temperature was about 50°C for a droplet size of 300 μm. Meanwhile, at the droplet size of 800 μm, the similar laser intensity level resulting in a slightly higher temperature of 68°C. This temperature difference increased along with the level of the laser intensity. The highest laser intensity of 87.33 W/cm^2, the resulting temperature of the droplet reached about 220°C and 360°C, for the droplet size of 300 μm and 800 μm. It should be noted that this high temperature was not covering the whole droplet region but only at the specific point of the droplet where the maximum temperature occurred.

The maximum temperature discrepancy happened even in the same laser intensity level since a finer size droplet size has a smaller total volume and surface region that contacted with the irradiation source. That condition made the droplet absorb less thermal radiation energy, resulting in lower temperature levels. In contrast, the larger size droplet will be able to absorb much more thermal energy from its larger surface area that manifested into a greater temperature range of the droplet.

The period of temperature dissipation back to ambient level after the radiation was stopped was also proportional to the level of laser intensity and droplet size. The temperature dropped almost instantly to the ambient temperature level for the lowest laser intensity of 10.92 W/cm^2 when the heat radiation source was cut. Meanwhile, in the higher irradiation intensity, the

temperature dissipation is realized in two phases. The temperature dissipated to about half the maximum temperature value immediately after the irradiation was cut. The temperature dissipation then happened more gradually, and finally, after a few seconds, the temperature reached back to the initial ambient temperature. In the intermediate laser intensity level (21.83 and 43.66 W/cm^2), the second phase of temperature dissipation occurred at about 3 to 4 seconds. Meanwhile, a more extended period (> 7 seconds) was found for the highest laser intensity of 87.33 W/cm^2 in the droplet size of 800 µm.

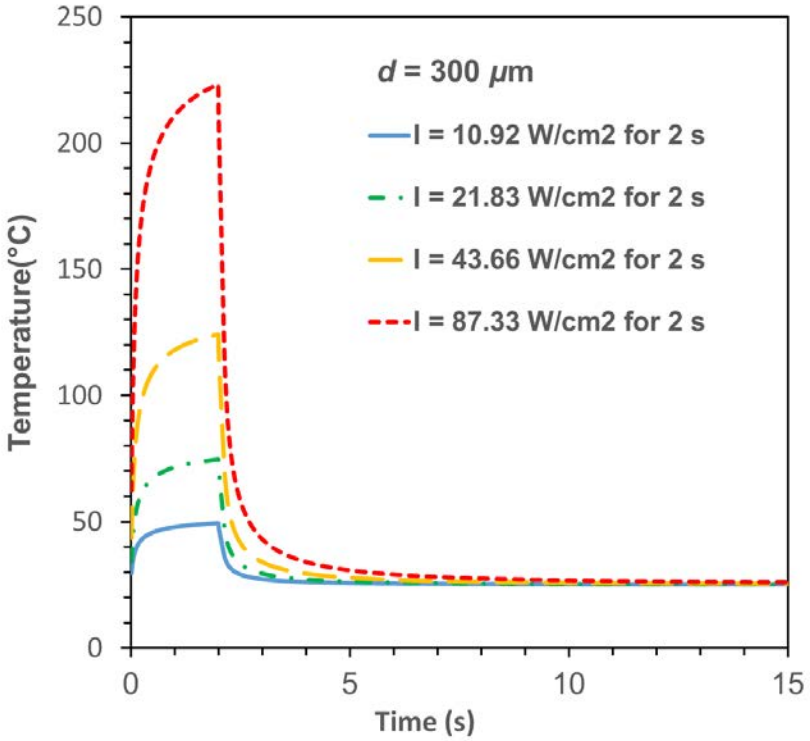

Figure 4-5. The maximum temperature change of the droplet phase for the laser intensity parameter at droplet diameter, d = 300 µm

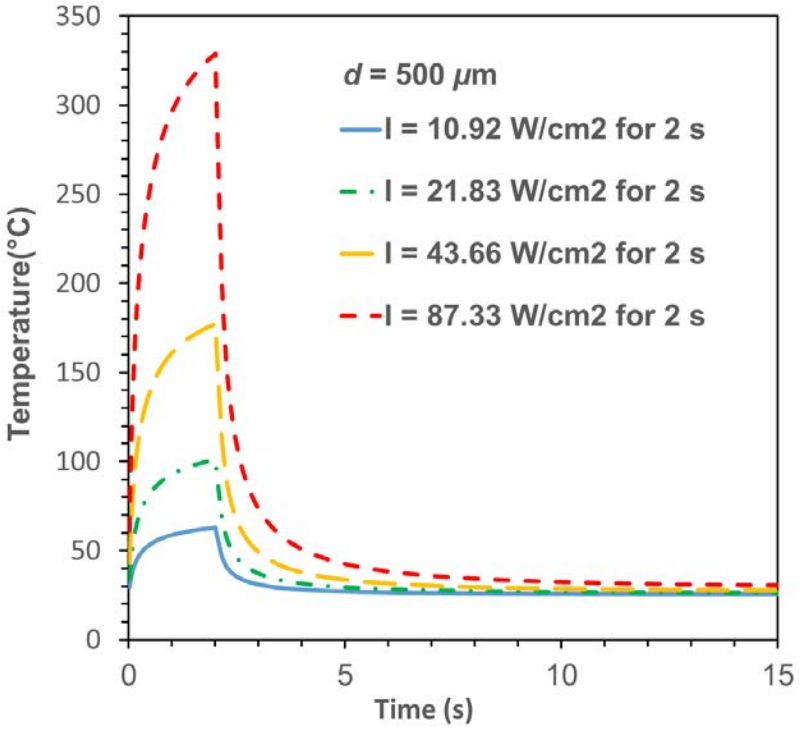

Figure 4-6. The maximum temperature change of the droplet phase for the laser intensity parameter at droplet diameter, d = 500 μm.

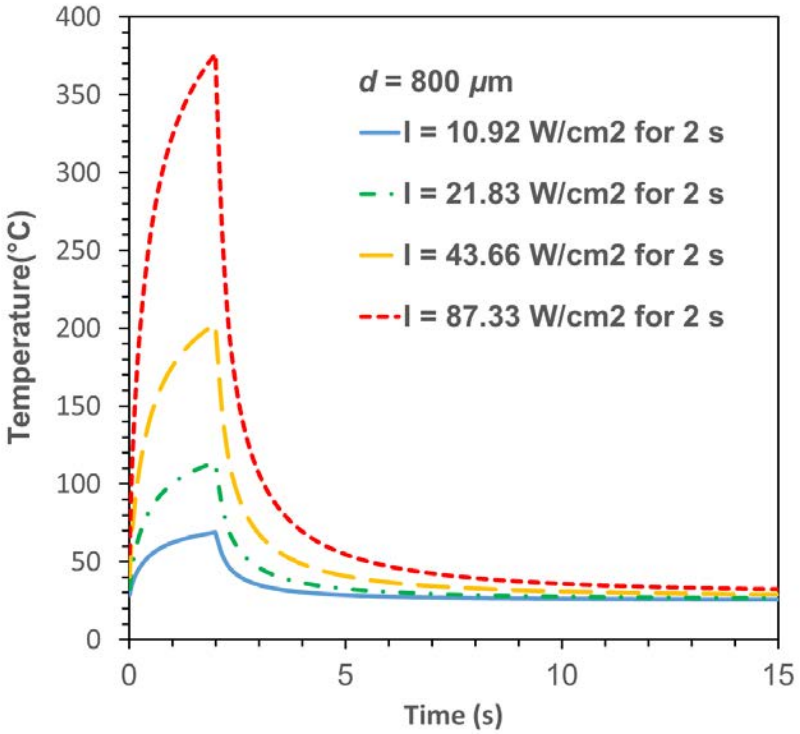

Figure 4-7. The maximum temperature change of the droplet phase for the laser intensity parameter at droplet diameter, d = 800 μm.

After the maximum temperature distribution was obtained, the droplet's temperature profile was then provided in Figure 4-8 to Figure 4-10. The displayed temperature was the temperature of the droplet at its centerline. As mentioned earlier, the highest attenuation region located at the front-end segment faces the applied thermal irradiation so that the temperature was higher than the temperature on the latter part of the droplet in that region. Additionally, the inclination toward the irradiation source was even more apparent as the droplet size was increased. In larger-sized droplets, most of the heat irradiation was already attenuated in the droplet's front-end part that faced the irradiation path. Thus, the irradiation intensity was significantly reduced in the latter part due to dominant attenuation or absorption in the frontal part of the droplet, resulting in a lower temperature range of the back-end part and tilting of the higher temperature region more apparent.

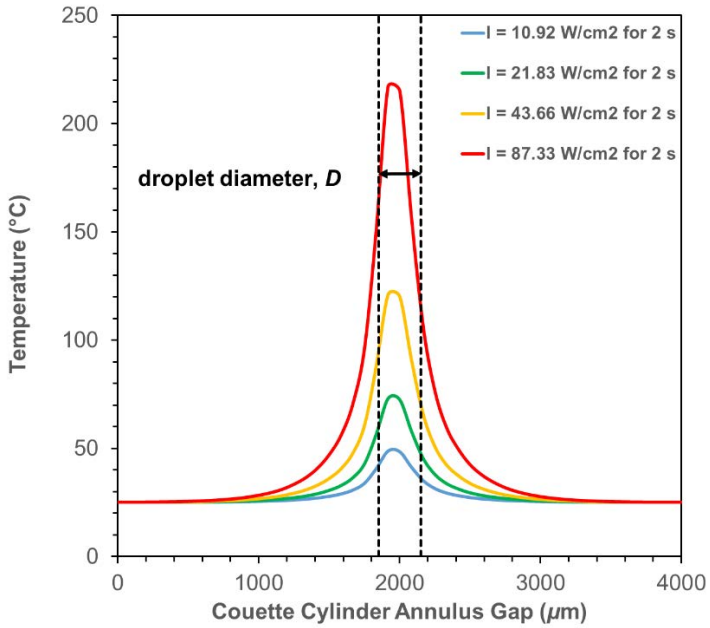

Figure 4-8. Temperature change along centerline of the immiscible system for the laser intensity parameter at the droplet diameter, d = 300 μm.

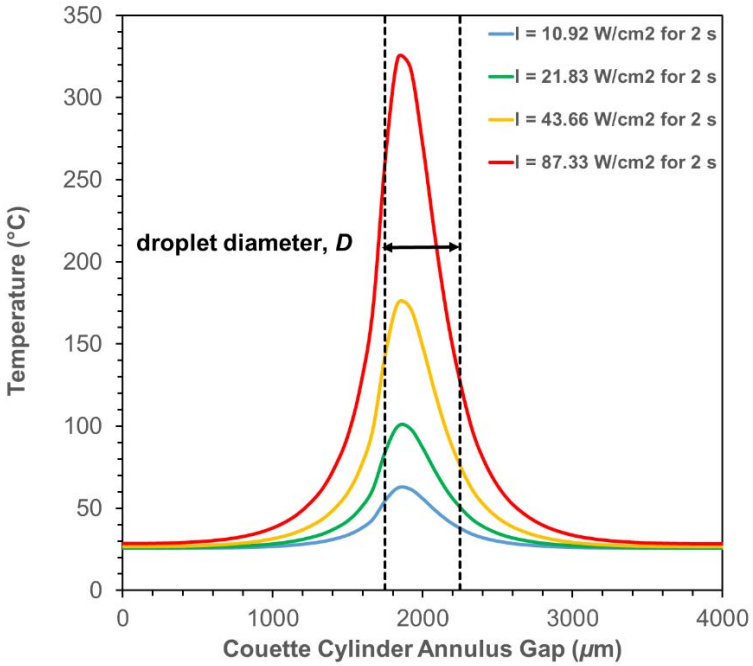

Figure 4-9. Temperature change along centerline of the immiscible system for the laser intensity parameter at the droplet diameter, d = 500 μm.

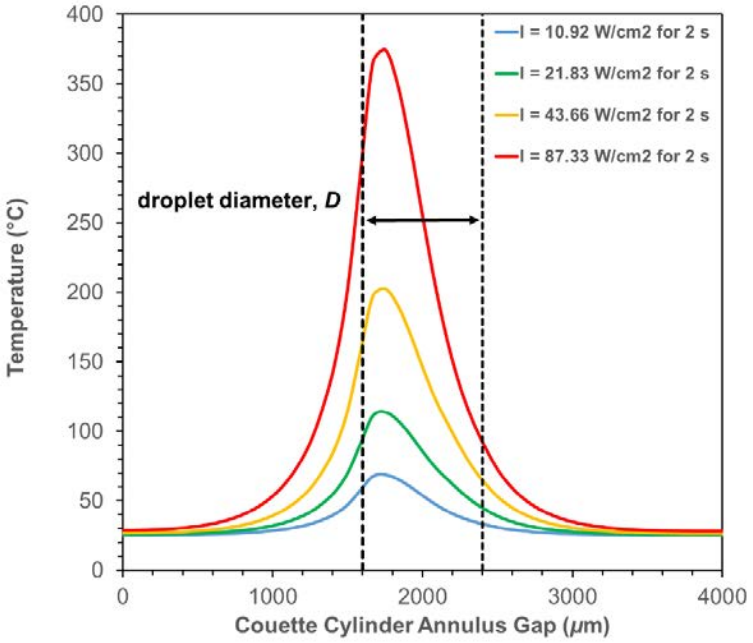

Figure 4-10. Temperature change along centerline of the immiscible system for the laser intensity parameter at the droplet diameter, d = 800 μm.

4.3.2. Total Energy Parameter

The simulation work using ANSYS continued for the second irradiation condition, the total energy parameter. The maximum temperature distribution for different droplet diameters is provided in Figure 4-11 to Figure 4-13. Since the irradiation period was set longer at the two lowest laser intensity levels (8 and 4 seconds for laser intensity of 10.9 W/cm^2 and 21.83 W/cm^2), the droplets' maximum temperature was above the temperature range in the laser intensity parameter. The temperature ranged from 52°C to about 77°C, for a droplet dimension of 300 to 800 μm, respectively. The maximum temperature range was found at the subsequent intensity of 21.83 W/cm^2 at 77°C-124°C for a droplet dimension of 300-800 μm. The realized maximum temperature of the droplet for these levels of laser intensity seemingly have reached the steady condition, exhibited by the relatively plateaued curve for the irradiation period of 8 and 4 seconds, except for the specific droplet size of 800 μm in the laser intensity of 21.83 W/cm^2 where the temperature curve was still showing a gradient feature.

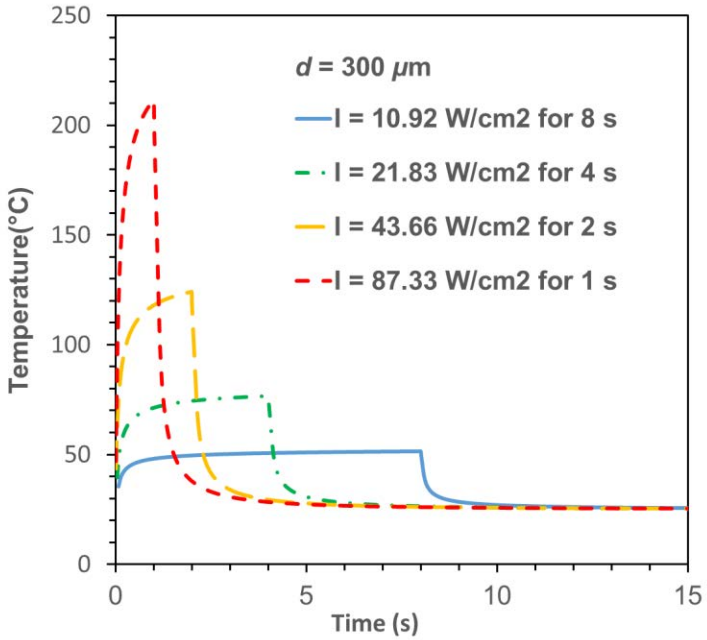

Figure 4-11. The maximum temperature change of the droplet phase for the total energy parameter at droplet diameter, d = 300 μm.

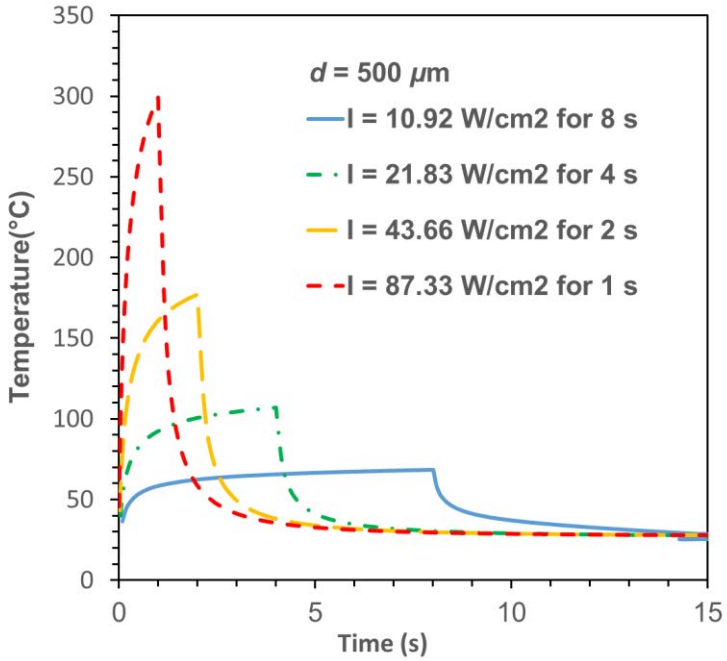

Figure 4-12. The maximum temperature change of the droplet phase for the total energy parameter at droplet diameter, d = 500 μm.

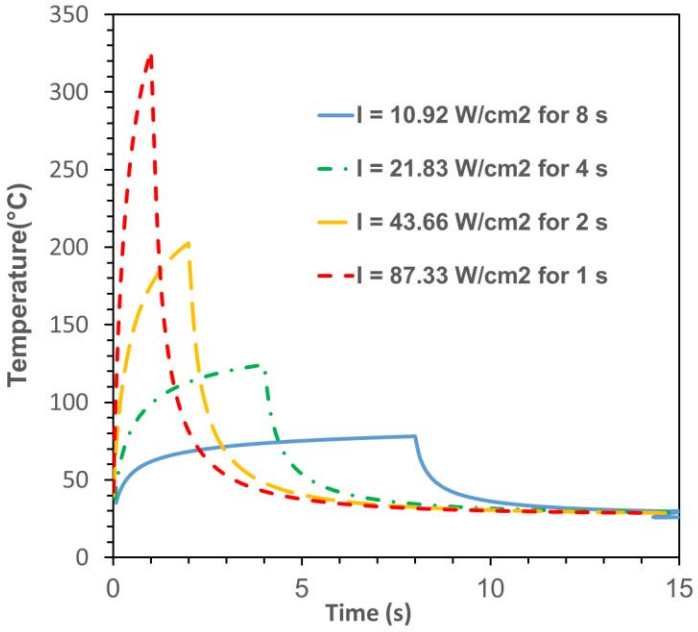

Figure 4-13. The maximum temperature change of the droplet phase for the total energy parameter at droplet diameter, d = 800 μm.

On the other hand, the obtained maximum temperature value was slightly lower than the laser intensity parameter's temperature, at the highest laser intensity of 87.33 W/cm^2. The maximum temperature at the second-highest level of laser intensity (43.66 W/cm^2) was similar to the previous results as both the laser power and irradiation period were identical. According to the droplet dimension parameter, the temperature profile characteristic was still consistent with the former heating condition in that a larger droplet dimension resulted in a greater maximum temperature. Therefore, the deviation in the maximum temperature profile compared to the previous results was solely due to the variation in the irradiation period. The temperature profiles along the centerline were obtained and then given in Figure 4-14 to Figure 4-16 for the droplet diameter of 300 to 800 μm.

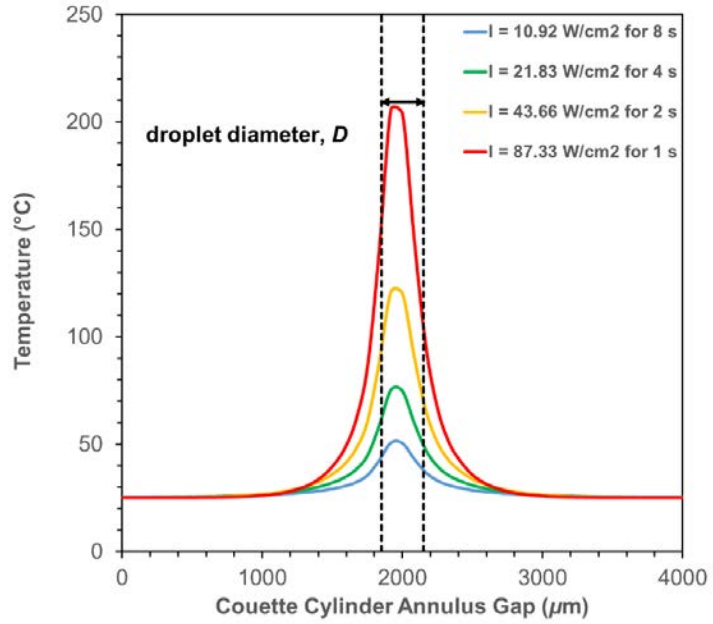

Figure 4-14. Temperature change along the centerline of the immiscible system for the total energy parameter at the droplet diameter, d = 300 μm.

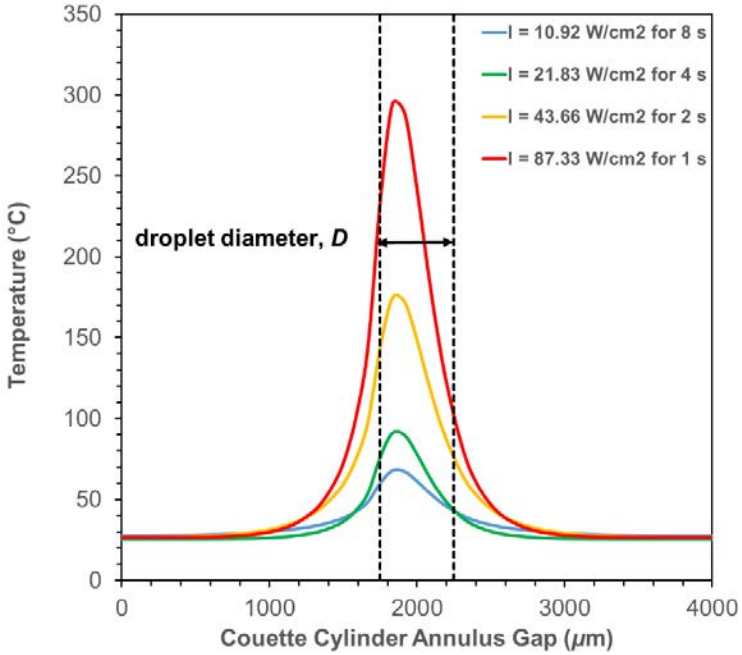

Figure 4-15. Temperature change along the centerline of the immiscible system for the total energy parameter at the droplet diameter, d = 500 μm.

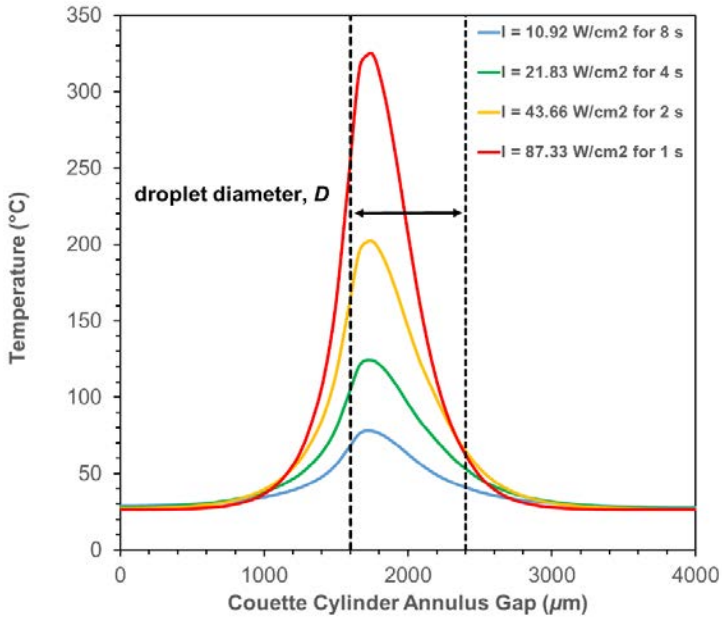

Figure 4-16. Temperature change along the centerline of the immiscible system for the total energy parameter at the droplet diameter, d = 800 μm.

4.4. Prediction of viscosity ratio modification and critical capillary number from selective radiation heating

The comparison of the droplet and the matrix phase's representative temperature plotted against the droplet diameter is available in Figure 4-17. The droplet's maximum temperature was taken to represent the droplet phase's temperature, while the average temperature in the interface was used as the temperature of the matrix. During the radiation heating implementation, the temperature surge happened in the droplet and the matrix phase. At the droplet dimension larger than 500 μm, however, the droplet's representative temperature was continuously increased while the representative matrix temperature slowly took a dip and then flattened. A higher temperature disparity between the front-end and the droplet's back-end was formed in the larger droplet size. This condition caused the average temperature in the interface to seem to be decreased and then straightened, as indicated in the plotted image.

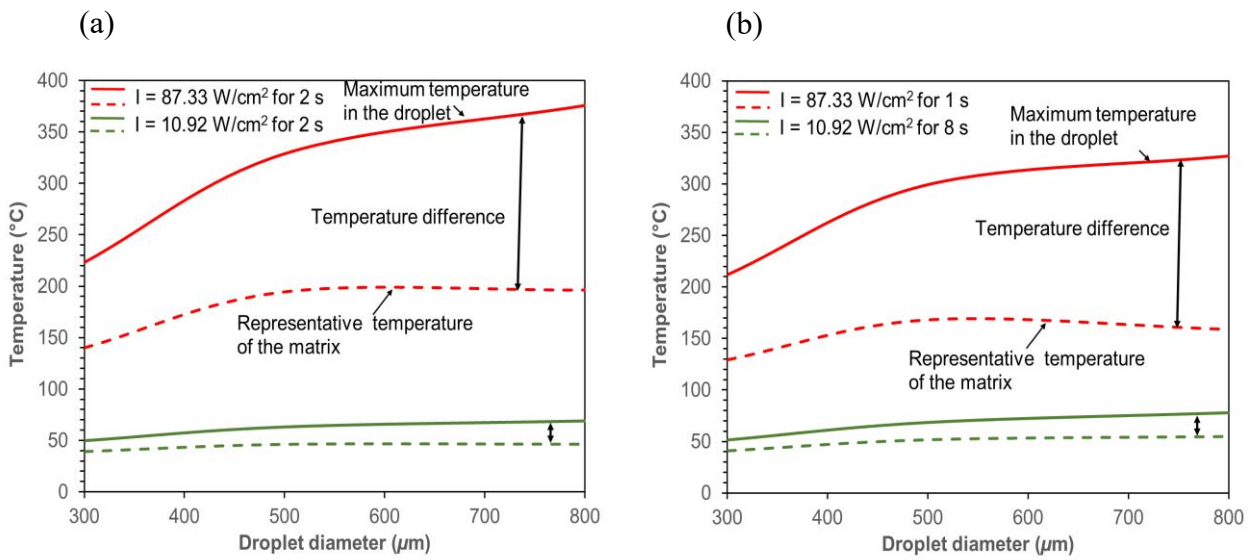

Figure 4-17. The representative temperature changes for the droplet and the matrix phase at (a) laser intensity parameter (b) total energy parameter.

The estimated temperature distribution from the numerical simulation provided important information to evaluate the immiscible fluid's viscosity changes. This newly obtained temperature data needs to be combined with the empirical fitting of the viscosity-temperature curve provided in chapter 2 (Eq. (2-11) and the accompanying Table 2-3) to produce the predicted viscosity ratio immiscible droplet system at the new temperature.

Once the modified viscosity ratio value is acquired, the viscosity's latest value and ratio are plugged into the critical capillary number equation's fitting equation. The most well-known viscosity ratio-critical capillary number function is the five parameters fitting, introduced by De Bruijn **[21]**.

$$\log \mathrm{Ca_c} = -0.506 - 0.0994 \log p + 0.124 (\log p)^2 + \frac{-0.115}{\log p - \log p_{\max}} \qquad (4\text{-}2)$$

In the equation, variable p_{max} is the maximum viscosity ratio, taken at 4.08. The plot of $\mathrm{Ca_c}$ against parameter p bases on the fitting formula of Eq. (4-2) provided in Figure 4-18.

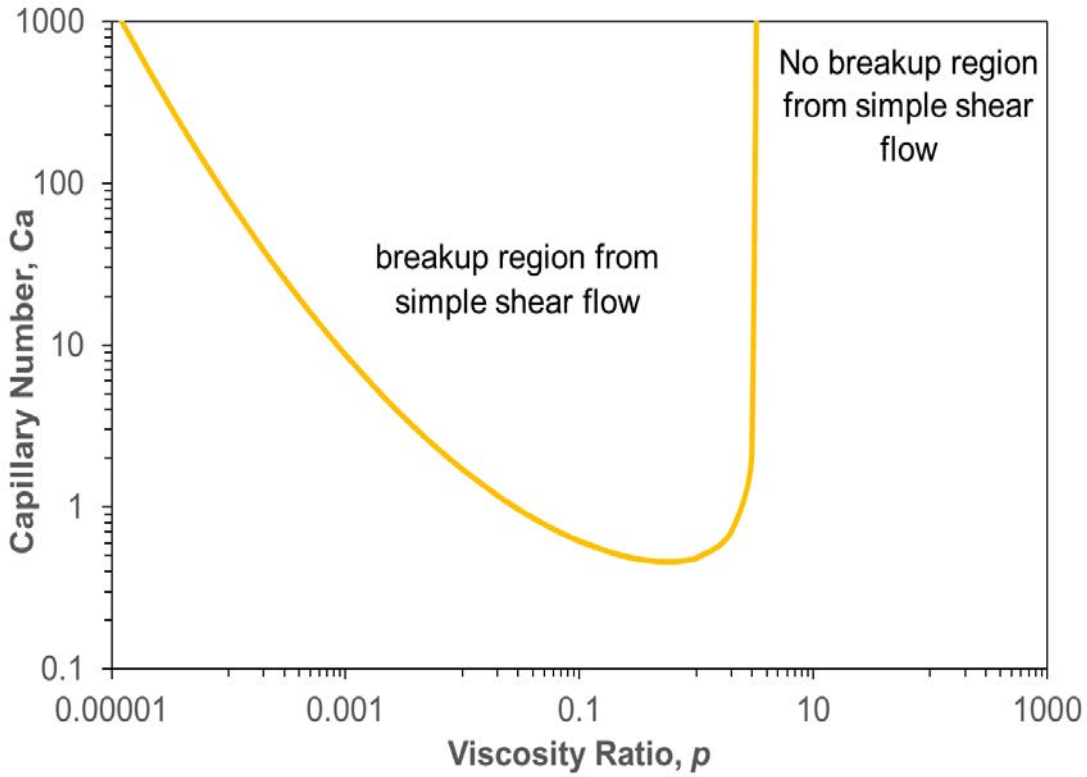

Figure 4-18. Critical capillary number curve based on the fitting approach by De Bruijn **[21]**.

The considered immiscible systems to be fitted into the viscosity ratio and critical capillary plot function are then the immiscible systems described in the experimental work of chapter 3 (Table 3-1), as this numerical work is initially intended to complement the temperature profile data that cannot be provided in the experimental work. The modified viscosity ratio and its critical capillary number are then summarized in Figure 4-19 and Figure 4-20. The colored region on the plot is representing their corresponding laser intensity.

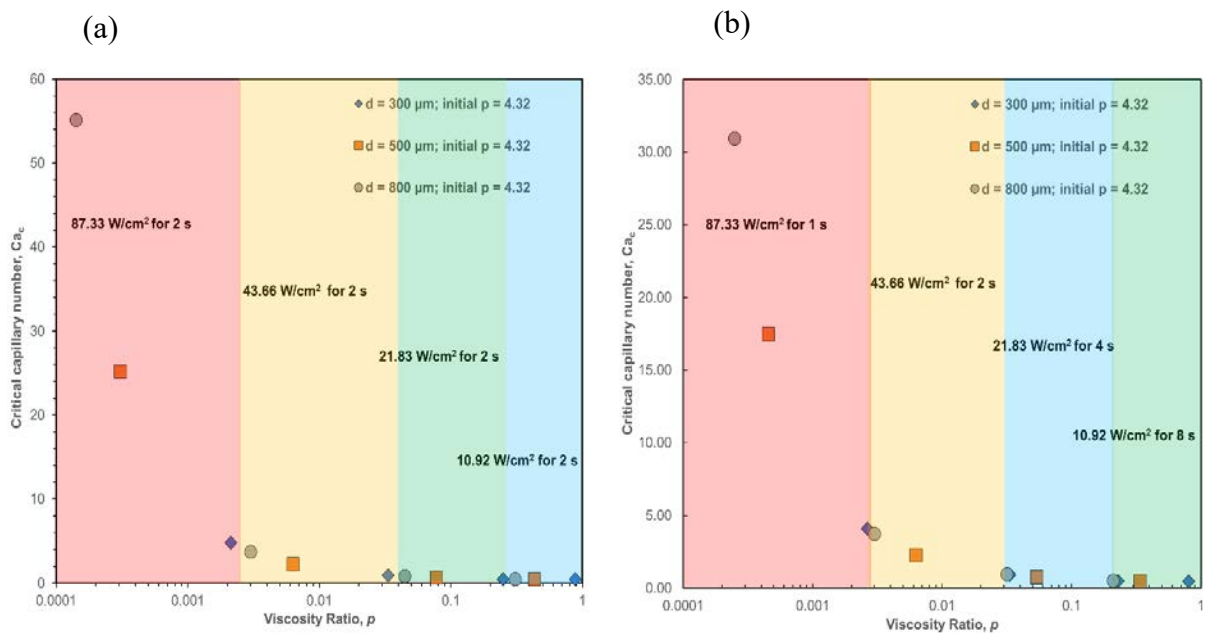

Figure 4-19. The modified viscosity ratios and their corresponding critical capillary number at initial viscosity ratio, p = 4.32 for the case: (a) laser intensity parameter and (b) total energy parameter.

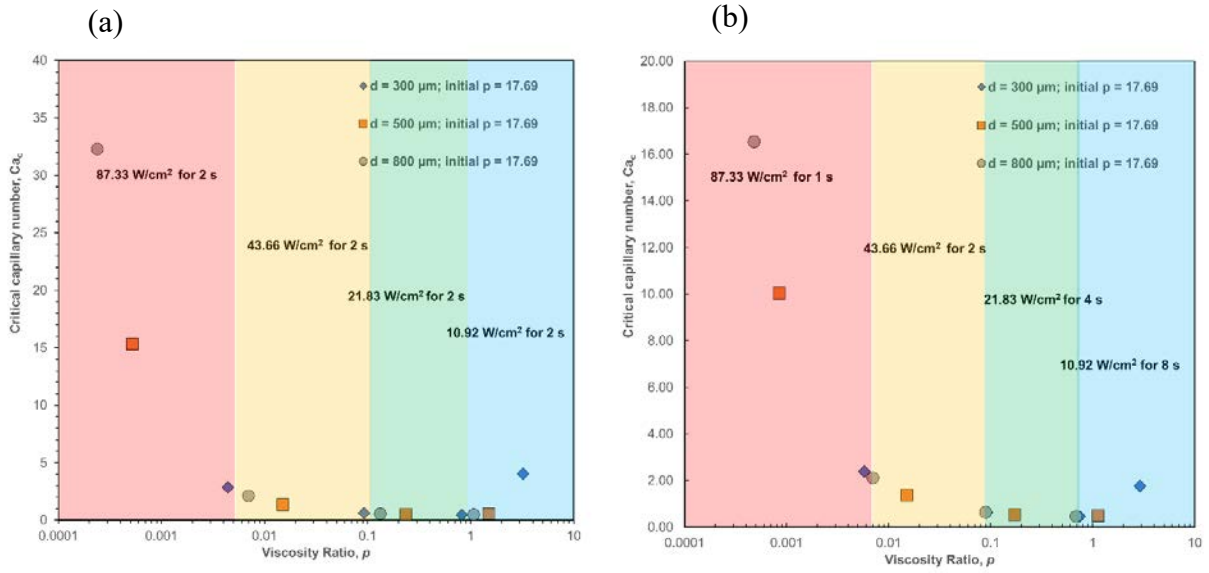

Figure 4-20. The modified viscosity ratios and their corresponding critical capillary number at initial viscosity ratio, p = 17.69 for the case: (a) laser intensity parameter and (b) total energy parameter.

In the initial viscosity ratio, $p = 4.32$, the shifting of the viscosity ratio into the equilibrium region was achieved at a low irradiation intensity of 10.92 and 21.83 W/cm^2 for all irradiation modes and droplet dimensions. The subsequent laser intensity of 43.66 and 87.33 W/cm^2 resulted in the excessive order of the viscosity ratio modification and a huge Ca_c requirement. For the second immiscible system with an initial viscosity ratio p = 17.69, the optimum irradiation intensity was observed at 21.83 W/cm^2 for all droplet sizes and irradiation mode. The lower intensity level is relatively inadequate to alter the viscosity ratio into the equilibrium zone, especially for the large-sized droplet. On the other hand, the higher laser intensity produced a viscosity ratio way beyond the ideal equilibrium region and most noticeably in the large droplet spectrum.

The attained modified viscosity ratio's prediction for the different immiscible system and irradiation mode suggests that an appropriate irradiation level will depend on the droplet diameter and the initial viscosity order, i.e., significantly large droplets need to be irradiated with lesser irradiation power. Whereas in finer droplet size, an intermediate or higher level of irradiation intensity should be applied. This fact implied that the selective radiation heating method is suitable for a wide array of possible immiscible systems with diverse droplet dimensions and viscosity ratios.

4.5. Droplet breakup from the selective radiation heating

Examples of the droplet's breakup process after implementing heat radiation are given in Figure 4-21. The droplet was stretched into a long and thin thread before finally disintegrating into multiple droplets. This breakup process followed the transient breakup mechanism as explained in the references **[9,12-16]**. The estimated Ca_c at the observed examples was about 0.46-0.67, while

the applied Ca were known at 1.75 and 1.36. The applied Ca on the immiscible droplet systems was more than twice the estimated Ca_c. Therefore, the breakup procedure conforms to the elongation behavior of the transient breakup mechanism.

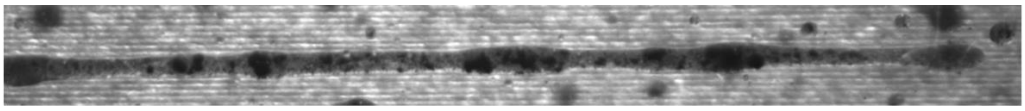

Initial p = 4.32, laser irradiation intensity 10.92 W/cm^2 for 2 seconds, Ca = 1.75

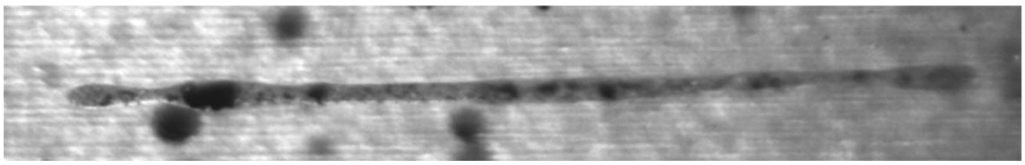

Initial p = 4.32, laser irradiation intensity 21.83 W/cm^2 for 4 seconds, Ca = 1.36

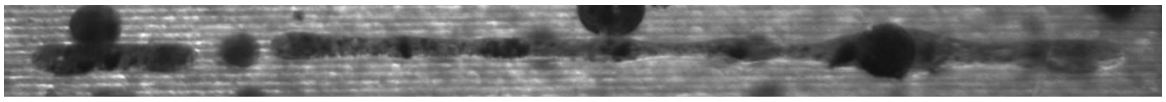

Initial p = 4.32, laser irradiation intensity 43.66 W/cm^2 for 2 seconds, Ca = 1.90

Figure 4-21. Images of the breakup droplet after the implementation of the laser radiation heating.

The estimated Ca_c for the high-level irradiation intensity ($\geq$ 43.66 W/cm^2) supposedly gave an excessive Ca_c value. However, the experimental observation in the preceding chapter showed that the droplet was still able to break up even though the applied Ca was way below the Ca_c requirement. The discrepancy between the experimental results and analytical estimation can occur due to the irradiation process's limited duration. After the irradiation source was cut, the droplet's temperature will dissipate back to the actual ambient temperature. The temperature's reversion affected the viscosity ratio and pushed the viscosity ratio back to its initial position. If the dissipation period were long enough to accommodate the applied Ca, the original droplet could still break into multiple minor droplets since the Ca still surpassed the interfacial effect and Ca_c

requirement. Otherwise, the minor droplet from the breakup process may coalesce back rather than permanently broke.

The peculiar condition where the minor droplet coalesced back is illustrated in Figure 4-22. The minor droplets from the breakup process were identified as droplets A, B, C, and D. The minor droplet A and D had detached entirely from the elongation process. Meanwhile, the minor droplets B and C were still connected. If the applied Ca were enough to counter the interfacial effect, the minor droplets B and C would be separated. However, the reversion of both temperature and viscosity ratio had reached the position where the applied Ca could no longer counter the interfacial effect and increase the Ca_c requirement. Therefore, the minor droplets B and C eventually merged back into an intermediate droplet that was smaller than its original droplet but larger than its minor droplet component.

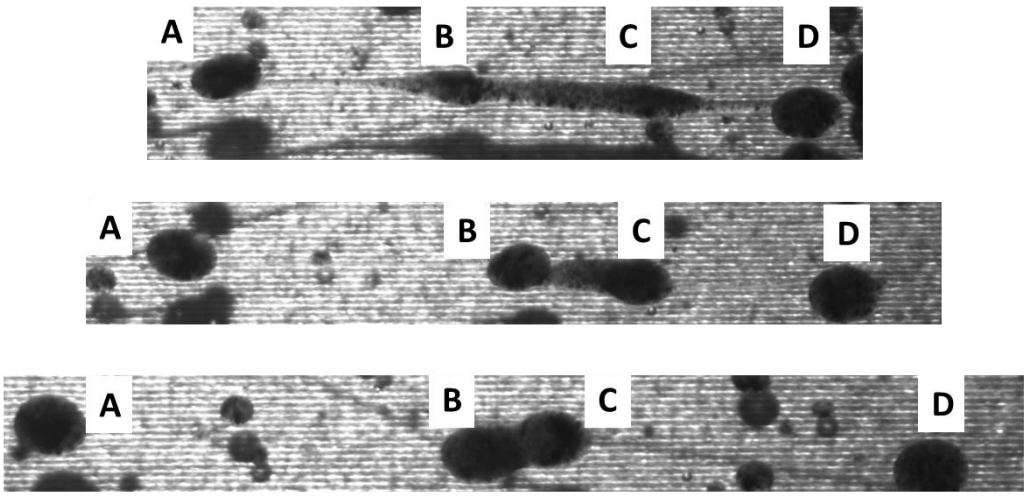

Initial p = 17.69, laser irradiation intensity 10.92 W/cm^2 for 2 seconds, Ca = 0.82

Figure 4-22. Coalescence of the initial break droplet for an immiscible system with initial parameter p = 17.69.

In the experiment, the elongated droplet's retraction behavior exclusively occurred in the case of an initial viscosity ratio of 17.69. In several observations, some droplets cannot even reach

the condition described in Figure 4-22 and retracted back to their original shape as indicated in Figure 3-17 and Figure 3-21. This condition suggested that on a particular immiscible system with a significantly high viscosity ratio, the irradiation period also holds a critical role in realizing droplet dispersion.

The obtained temperature data can be correlated with the experimental for mapping the capillary number and viscosity ratio before and after implementing the laser radiation heating, as plotted in Figure 4-23.

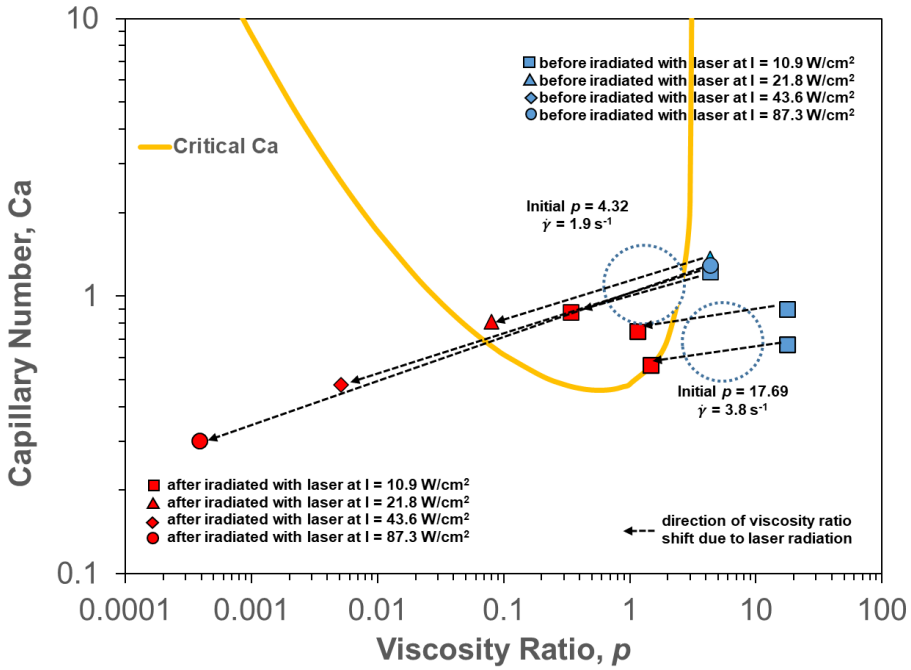

Figure 4-23 The viscosity ratio and capillary number before and after the implementation of radiation heating.

For the case with high initial viscosity of 17.69 (upper blue square on the most right side), the droplet viscosity ratio is modified into the region that exceeds its critical capillary requirement. However, in the second case for the droplet with an initial viscosity ratio of 17.69 (lower blue square at the most right side), the temperatures changes drive the droplet slightly below the critical

capillary number. Therefore, the droplet can significantly be deformed and experienced a brief breakup condition but retracted back once the laser radiation is stopped. The condition describes in the chart are in very good agreement with the experimental results.

Similarly, for cases with an initial viscosity ratio of 4.32, the condition described in the critical capillary number chart supports experimental data for the laser intensity at 10.9 and 21.8 W/cm^2. Inconsistencies with experimental results only occur at a very high laser intensity with a high estimated numerical simulation temperature. At the higher laser intensity of 43.6 and 87.3 W/cm^2, the estimated modified viscosity ratio and Ca were on the chart was way below the Ca_c line. This suggests that the laser intensity was too great, resulting in excessive order of temperature and viscosity ratio changes. Supposedly, the droplet can experience a significant deformation due to its low viscosity ratio, but the droplets cannot reach the breakup point. However, the experimental observation showed a contrary result: the breakup point could occur at those high laser intensities.

The performed numerical simulation was seemingly too simple to describe the temperature and viscosity changes in the region. In the numerical scheme, the droplet was assumed to be completely spherical during the radiation process, whereas at this high-intensity laser irradiation, the droplet immediately deformed into an elongated form. This immediate elongation of the droplet may affect the total volumetric condition of the droplet, and hence, reduce the ability of the droplet to absorb heat radiation. This implies that in the higher laser intensity range, the actual temperature changes in the droplet may be lower than the value obtained by the simple numerical simulation. This situation emphasizes the importance of suitable laser intensity for realizing viscosity modification. Although the experimental results showed that the higher laser intensity

range of 43.6 and 87.3 W/cm^2 could realize a droplet breakup, the laser intensity might be too much, resulting in excess of the wasted irradiation energy. A more complex numerical simulation system could provide a better understanding of high-intensity laser irradiation in the immiscible fluids.

4.6. The proposed application of the selective radiation heating method

The development of microfluid systems employing droplet-based structures is gaining momentum, especially in biological, pharmaceutical, and chemical analyses **[22,23]**. The micro-sized droplet is gaining attractivity in the field, as mentioned earlier due to its many advantages, such as its minimum sample requirement, enhanced mass transfer characteristic from its surface area to volume ratio, and good encapsulation efficiency from high surface tension, minimizing the possible contamination hazard **[23]**.

The generation of a microfluidic droplet is typically categorized into two methods, i.e., active and passive. In the active method, an external energy source such as electric field, magnetic field, mechanical vibration, or acoustic waves is introduced to promote instability and break the immiscible fluid system into a specific droplet **[24-27].** Meanwhile, in the passive droplet generation, the dispersed and continuous phase is arranged in a specifically designed channel in two parallel channels or cross junctions **[28-31]**. The described microdroplet generation methods can produce a high number of droplets along while maintaining its monodispersity **[32,33]**. The typical droplet generator device can only produce a pre-determined single-size droplet, whereas modern application in the chemical and biological field requires an optimum size droplet for their specific applications. The optimum size droplet can be obtained when the droplet generators can produce multiple-size droplets from a single production batch **[23]**.

The previous subsection discussion suggested that selective radiation heating can be implemented in an immiscible system with a wide array of initial droplet size spectrum and viscosity ratio. The versatility of selective radiation makes it applicable in many engineering systems. The initial proposal of the selective radiation heating method is for the polymer blending process, where the implementation of the radiation heating is suggested to improved droplet dispersion on the polymer blend **[34]**. The implementation of selective radiation heating can be expanded further to enhance the microdroplet generation's microfluid system, as mentioned above. The radiation heating can be added in conventional junction-channel type to provide droplet size diversity in a single production batch, as illustrated in Figure 4-24.

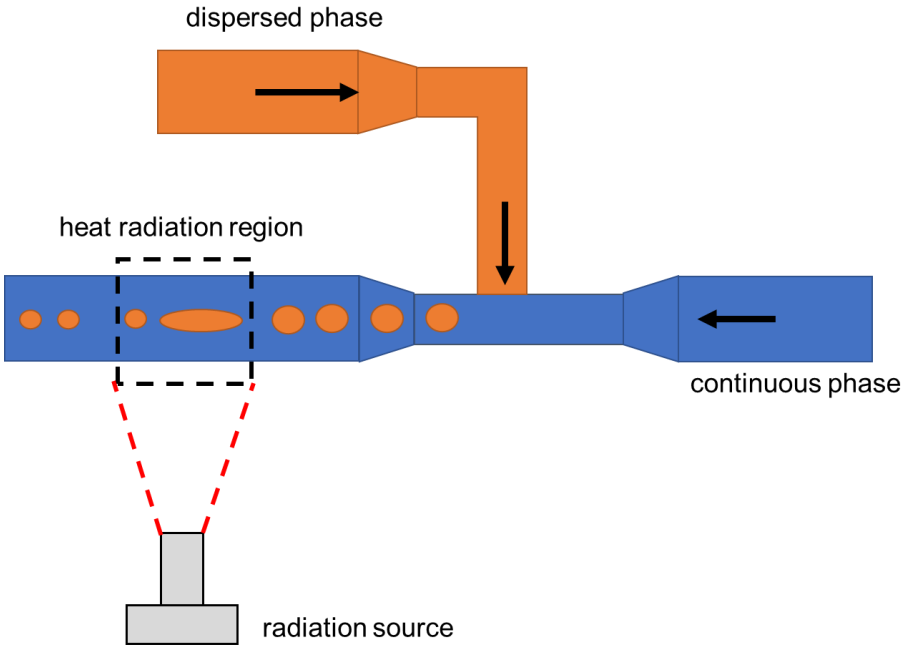

Figure 4-24. The application of selective radiation heating to droplet production for microfluid systems. The microfabricated channel is adapted from Thorsen et al., **[30]**.

The original microfabricated channel can only produce a specific monodisperse droplet, depends on the channel geometry and fluid pressure. The addition of selective radiation heating to the channel flow is suggested to improve the droplet dispersion without changing the channel

geometry or pressurized inlet condition. In this scheme, multi-sized droplets can be produced from a single production batch by adjusting the applied radiation source. However, the flow scheme on the channel is the pressure-driven Poiseuille flow rather than the force-driven Couette flow. The combined effect from channel confinement and the specific Poiseuille flow **[35]** should also be considered in conjunction with radiation heating in this proposed application.

4.7. Conclusion

In this chapter, a numerical simulation was performed to investigate the shifting of an immiscible droplet system's viscosity ratio. The temperature field estimation obtained by a numerical simulation work showed that the droplet size was highly influential in forming the immiscible fluid's non-uniform temperature field. The numerical work results suggest that selective radiation heating can be effectively applied for any immiscible system with a wide range of droplet sizes. A lesser laser intensity level is more suitable for a system with larger droplet size, whereas, for a system with a smaller droplet size, brief heating from the intermediate or higher intensity radiation source is preferable.

The breakup mechanism discussion showed that the droplet followed the transient breakup mode. The droplet was elongated into a long thread before finally disintegrated into multiple minor droplets. For a considerably high initial viscosity ratio (e.g., 17.69), coalescence between the broken droplet may happen if the applied radiation energy was insufficient to delay the viscosity ratio reversion when the radiation source was cut. Finally, selective radiation heating was proposed in the droplet production system for application in the microfluidic system.

4.8. References

1. Taylor, G.I., “The Viscosity of a Fluid Containing Small Drops of Another Fluid,” Proceedings of The Royal Society of London. Series A, Containing Papers of Mathematical and Physical Character, 138, 41 (1932).
2. Taylor, G.I., “The Formation of Emulsions in Definable Fields Flow,” Proceedings of The Royal Society of London. Series A, Containing Papers of Mathematical and Physical Character, 146, 501 (1934).
3. Taylor, G.I., “The Two Coefficients of Viscosity for an Incompressible Fluid Containing Air Bubbles,” Proceedings of The Royal Society of London. Series A, Containing Papers of Mathematical and Physical Character, 226, 34 (1954).
4. Bartok, W., and Mason, S.G., “Particle Motions in Sheared Suspensions: VIII. Singlets and Doublets of Fluid Spheres,” Journal of Colloid Science, 14, 13 (1959).
5. Rumscheidt, F.D., and Mason, S.G., “Particle Motions in Sheared Suspensions XI. Internal Circulation in Fluid Droplets (experimental),” Journal of Colloid Science, 16, 201, (1961).
6. Rumscheidt, F.D., and Mason, S.G., “Particle Motions in Sheared Suspensions XII. Deformation and Burst of Fluid Drops in Shear and Hyperbolic flow,” Journal of Colloid Science., 16, 238, (1961).
7. Trevelyan, B.J., and Mason, S.G., “Particle Motions in Sheared Suspensions. I. Rotations,” Journal of Colloid Science, 6, 354 (1951).
8. Grace, H.P., “Dispersion Phenomena in High Viscosity Immiscible Fluid Systems and Application of Static Mixers as Dispersion Devices in Such Systems,” Chemical Engineering Communication, 14, 225 (1982).

9. Karam, H.J., and Bellinger, J.C., “Deformation and Breakup of Liquid Droplets in a Simple Shear Field,” Industrial and Engineering Chemistry Fundamentals, 7, 576 (1968).
10. Tjahjadi, M., Stone, H.A., and Ottino, J.M., “Satellite and Subsatellite formation in Capillary Breakup,” Journal of Fluid Mechanic, 243, 297 (1992).
11. Mighri, F., and Huneault, M.A., “Dispersion Visualization of Model Fluids in a Transparent Coutte Flow Cell,” Journal of Rheology, 45, 783 (2001).
12. Elemans, P.H.M., Bos, H.L., Janssen, J.M.H., and Meijer, H.E.H, “Transient Phenomena in Dispersive Mixing,” Chemical Engineering Science, 48, 267 (1993).
13. Meijer, H.E, Janssen, J.M.H, and Anderson, P.D., “Mixing of Immiscible Liquids,” in Mixing and Compounding of Polymers – Theory and Practice (2nd Ed), Progress in Polymer Processing Series, Carl Hanser, Munich, 2009.
14. Tomotika, S., “Breaking up of a Drop of Viscous Liquid Immersed in Another Viscous Fluid which is Extending at a Uniform Rate,” Proceedings of The Royal Society of London. Series A, Containing Papers of Mathematical and Physical Character, 153, 302 (1936).
15. Mikami, T., Cox, R., and Mason, R.G., “Breakup of Extending Liquid Threads,” International Journal of Multiphase Flow, 2, 113 (1975).
16. Khakhar, D.V., and Ottino, J.M., “Breakup of Liquid Threads in Linear Flow,” International Journal of Multiphase Flow, 13, 71 (1987).
17. Cardinaels, R., Vananroye, A., Van Puyvelde, P., and Moldenaers, P., “Breakup Criteria for Confined Droplet: Effects of Compatibilization and Component Viscoelasticity,” Macromolecular Materials and Engineering, 296, 214 (2011).
18. Van Puyvelde, P., Vananroye, A., and Moldenaers, P., “Review on Morphology of Immiscible Blends in Confined Shear Flow,” Polymer, 49, 5363 (2008).

19. Vananroye, A., Van Puyvelde, P., and Moldenaers, P., "Effect of Confinement on Droplet Breakup in Sheared Emulsions," Langmuir, 22, 3972 (2006).
20. Guido, S., "Shear-Induced Droplet Deformation: Effects of Confined Geometry and Viscoelasticity," Current Opinion in Colloid and Interface Science, 16, 61 (2011).
21. De Bruijn, R. A., "Deformation and Breakup of Drops in Simple Shear Flows," PhD Thesis, Technicshe Universtiteit Eindhoven, Netherlands, (1989).
22. Mashaghi, S., Abbaspourrad, A., Weitz, D. A., and van Oijen, A. M., "Droplet Microfluidics: A Tool for Biology, Chemistry, and Nanotechnology," TrAC - Trends in Analytical Chemistry, 82, 118 (2016).
23. Khorrami, A.M., and Rezai, P., "Oscillating Dispersed-Phase Co-Flow Microfluidic Droplet Generation: Multi-Droplet Size Effect," Biomicrofluidics, 12, 034113 (2018).
24. Ozen, O., Aubry, N., Papageorgiou, D. T., and Petropoulos, P. G., "Monodisperse Drop Formation in Square Microchannels," Physical Review Letters, 96, 144501 (2006).
25. Feng, L., Kawahara, T., Yamanishi, Y., Hagiwara, M., Kosuge, K., and Arai, F., "On-Demand and Size-Controlled Production of Droplets by Magnetically Driven Microtool," Journal of Robotics and Mechatronics, 24, 133 (2012).
26. Zhu, P., Tang, X., and Wang, L., "Droplet Generation in Co-Flow Microfluidic Channels with Vibration," Microfluidics and Nanofluidics, 20, 47 (2016).
27. Schmid, L., and Franke, T., "SAW-Controlled Drop Size for Flow Focusing," Lab on Chip, 13, 1691 (2013).
28. Umbanhowar, P.B., Prasad, V., and Weitz, D.A., "Monodisperse Emulsion Generation via Drop Break Off in a Coflowing Stream," Langmuir, 16, 347 (2000).

29. Utada, A.S., Chu, L.-Y., Fernandez-Nieves, A., Link, D.R., Holtze, C., and Weitz, D.A., "Dripping, Jetting, Drops, and Wetting: The Magic of Microfluidics," MRS Bulletin 32, 702, (2007).
30. Thorsen, T., Roberts, R.W., Arnold, F.H., and Quake, S.R., "Dynamic Pattern Formation in a Vesicle-Generating Microfluidic Device," Physical Review Letters, 86, 4163 (2001).
31. Ushikubo, F.Y., Birribilli, F.S., Oliveira, D.R.B., and Cunha, R.L., "Y- and T-junction Microfluidic Devices: Effect of Fluids and Interface Properties and Operating Conditions," Microfluidics and Nanofluidics, 17, 711 (2014).
32. Chong, Z.Z., Tan, S.H., Gañán-Calvo, A.M., Tor, S.B., Loh, N. H., and Nguyen, N.-T., "Active Droplet Generation in Microfluidics," Lab on Chip 16, 35 (2016).
33. Zhu, P., and Wang, L., "Passive and Active Droplet Generation with Microfluidics: a Review," Lab on Chip, 17, 34 (2017).
34. Saito, T., Kawaguchi, T., and Satoh, I., "Dispersion Control of Immiscible Polymer Blend Using Selective Heating by Infrared Laser Radiation," Journal of Applied Polymer Science, 129, 3606 (2013).
35. Guido, S., and Preziosi, V., "Droplet Deformation Under Confined Poiseuille Flow," Advances in Colloid and Interface Science, 161, 89 (2010).

5. Chapter 5: Conclusion and Outlook for Future Works

5.1.Conclusions

This thesis research focused on investigating the droplet morphology for an immiscible system under the selective radiation method to control droplet dispersion. Both experimental and numerical investigations were carried out to provide an understanding of the droplet deformation and breakup process due to the presence of direct thermal radiation. A generalized model fluid consisted of polybutenes and PDMS silicone oil was proposed as the immiscible fluid system for the experimental work. The visualization of the droplet evolution under selective radiation heating was acquired and compared to the ordinary condition in isothermal ambient room temperature. Finally, a numerical simulation using ANSYS software was employed to estimate the non-isothermal field on the immiscible droplet systems. The combined experimental and numerical simulation works of this thesis research gave the fundamental for the further expansion and application of the selective radiation technique.

In chapter 2, the absorption coefficient for the immiscible systems was acquired by performing the transmissivity measurement for a wide range of light test wavelengths. In the infrared region of 1.5 – 8 μm, polybutenes and PDMS silicone oil showed a fluctuating transmissivity level. Meanwhile, on the shorter wavelength region of 0.4 – 1.1 μm, both of the immiscible fluid components were almost transparent. The transmissivity fluctuation indicates the different levels of the immiscible fluid's absorptivity nature, and this condition gave the guidance for choosing a suitable radiation wavelength source. The polybutenes have a slightly higher absorption coefficient for all tested wavelength ranges than the PDMS silicone oil. The shear viscosity values were acquired from the measurement using a rheometer device. Subsequently, an

empirical fitting approach investigated the temperature dependency nature of the viscosity. The proposed selective radiation heating feasibility was then confirmed based on the model fluid's absorption coefficient and temperature-dependent shear viscosity.

In chapter 3, the experimental investigation for the immiscible droplet system was performed in a counter-rotating Couette apparatus. The shear rate component from the Couette flow was successfully emulated in this Couette apparatus. The droplet deformation at ambient room temperature was consistent with the steady droplet deformation of the immiscible system with viscosity ratio values of more than four. The mean range of the droplet deformation parameter, *Def**, is limited to 0.11 and 0.06 at ambient temperature conditions for an initial viscosity ratio of 4.32 and 17.69. Moreover, no droplet breakup was possible in this condition due to the limiting factor of the viscosity ratio. The restricted droplet deformation can then be outdone by implementing heat irradiation from an infrared laser. For a moderately high viscosity ratio (4.32), the selective radiation effectively enhanced the droplet deformation and even led to the breakup condition, and no droplet retraction was observed at this experimental condition. However, at a higher range of viscosity ratio (17.69), droplet elongation-breakup was also observed even though some droplets showed a retraction behavior after the laser radiation was stopped. The exhaustive droplet visualization provided a clear fundamental of the selective radiation effect for the model immiscible fluid.

In chapter 4, numerical simulation work was carried out using ANSYS software for complementing the experimental work by providing an estimation of the non-isothermal field from the implementation of the radiation heating. The temperature distribution was essential for linking the predicted viscosity ratio modification and droplet breakup criterion. The acquired non-

isothermal field and the subsequent critical capillary number-viscosity ratio interaction suggest that specific adjustment was necessary for the selective radiation heating can be implemented for an immiscible system with a wide range of droplet sizes. A lesser laser intensity level is more suitable for a system with larger droplet size, whereas, for a system with a smaller droplet size, brief heating from the intermediate or higher intensity radiation source is preferable. The breakup mechanism discussion showed that the droplet followed the transient breakup mode rather than an ideal equilibrium mode. A proposed application of selective radiation heating was briefly introduced, the selective radiation technique was suggested for the droplets production of the microfluidic system.

5.2.Outlook for Future Works

A fundamental understanding of selective radiation heating was provided in this thesis research work. The selective radiation method investigation was performed using a generalized model fluid, still categorized as a Newtonian fluid. Many real applications of an immiscible droplet morphology involve fluid components with viscoelastic behavior **[1-3]**. Hence, considering more complex materials with viscoelastic properties should be considered to expand the selective radiation method.

A number of research works showed that droplet confinement reduced Ca_c requirement for the immiscible fluid system with a viscosity ratio value of more than one. Meanwhile, the opposite effect was observed for a viscosity ratio of less than one **[4-7]**. The combined effect of geometry confinement and selective radiation should be investigated if the selective radiation wants to be introduced in the microfluidic application system because many microfluid applications involving geometry confinement of the droplet morphology **[8,9]**.

Another proposed application of selective radiation heating on the microfluid system is enhancing the droplet generation method. The addition of selective radiation heating can accommodate a multi-sized droplet formation from a single production batch. The channel's flow scheme may come in the form of a pressure-driven Poiseuille or an extensional flow. The combination condition of the selective radiation heating effect in mixed channel confinement and the specific Poiseuille flow **[10]** and extensional flow in a confined geometry **[11,12]** should also be considered.

5.3.References

1. Li, H. and Sundararaj, U., "Experimental Investigation of Viscoelastic Drop Deformation in Newtonian Matrix at High Capillary Number Under Simple Shear Flow," Journal of Non-Newtonian Fluid Mechanics, 165, 1219 (2010).
2. Cherdhirankorn, T., Lerdwijitjarud, W., Sirivat, A., and Larson, R.G., "Dynamics of vorticity Stretching and Breakup of Isolated Viscoelastic Droplets in an Immiscible Viscoelastic Matrix," Rheologica Acta, 43, 246 (2004).
3. Van Puyvelde, P. and Moldenaers, P., "Rheology and Morphology Development in Immiscible Polymer Blends," Rheology Review, The British Society of Rheology, 101, (2005).
4. Cardinaels, R., Vananroye, A., Van Puyvelde, P., and Moldenaers, P., "Breakup Criteria for Confined Droplet: Effects of Compatibilization and Component Viscoelasticity," Macromolecular Materials and Engineering, 296, 214 (2011).
5. Van Puyvelde, P., Vananroye, A., and Moldenaers, P., "Review on Morphology of Immiscible Blends in Confined Shear Flow," Polymer, 49, 5363 (2008).

6. Vananroye, A., Van Puyvelde, P., and Moldenaers, P., “Effect of Confinement on Droplet Breakup in Sheared Emulsions,” Langmuir, 22, 3972 (2006).
7. Guido, S., “Shear-Induced Droplet Deformation: Effects of Confined Geometry and Viscoelasticity,” Current Opinion in Colloid and Interface Science, 16, 61 (2011).
8. Christopher, G.F., Bergstein, J., End, N.B., Poon, M., Nguyen, C., and Anna, S.L., “Coalescence and Splitting of Confined Droplets at Microfluidic Junctions,” Lab on Chip, 9, 1102, 2009.
9. Dangla, R., Kayi, S.C., and Baroud, C.N., “Droplet Microfluidics Driven by Gradients of Confinement,” Proceedings of the National Academy of Sciences of the United States of America, 110, 853 (2013).
10. Guido, S., and Preziosi, V., “Droplet Deformation Under Confined Poiseuille Flow,” Advances in Colloid and Interface Science, 161, 89 (2010).
11. Mietus, W.G.P., Matar, O.K., Lawrence, C.J., and Briscoe, B.J., “Droplet Deformation in Confined Shear and Extensional Flow,” Chemical Engineering Science, 57, 1217 (2002).
12. Mulligan, M.K, and Rothstein, J.P., “The Effect of Confinement-Induced Shear on Drop Deformation and Breakup in Microfluidic Extensional Flows,” Physics of Fluids, 23, 022004 (2011).